UNIVERSITY OF CALIFORNIA
SANTA CRUZ

MESOPOROUS INORGANIC MATERIALS FOR THE DESULFURIZATION OF JET FUEL

A dissertation submitted in partial satisfaction
of the requirements for the degree of

DOCTOR OF PHILOSOPHY

In

CHEMISTRY

by

Jessica Marie Palomino

September 2014

The Dissertation of Jessica M. Palomino is approved:

_____
Professor Pradip Mascharak: Chair

_____
Professor Yat Li

_____
Professor Scott Oliver

_____
Tyrus Miller
Vice Provost and Dean of Graduate Studies

Table of Contents

List of Figures

List of Tables

Abstract

Mesoporous Inorganic Materials for the Desulfurization of Jet Fuel

By

Jessica Marie Palomino

A major goal of the U.S. military is to use solid oxide fuel cells (SOFCs) as a power source during military silent watch missions. Fueling these SOFCs with JP-8, the military's primary fuel type, would be ideal. However, the organosulfur compounds present quickly poison the expensive fuel cell and reformer components, drastically limiting the lifetime of the SOFC. Furthermore, current desulfurization technology is unable to produce ultra-low sulfur content JP-8 fuel required for solid oxide fuel cells (SOFCs).

The current desulfurization technique for fossil fuels is hydrodesulfurization, which is a high temperature, high pressure process that must be done at a refinery. While this process is adequate for achieving low sulfur content in lighter fuels such as gasoline, it is ineffective at removing the bulkier organosulfur compounds found in JP-8. Adsorptive desulfurization is a promising alternative to hydrodesulfurization, as it has the potential to be a portable, on-site process performed on JP-8 stocks already in the field without needing additional hydrogen as is the case with hydrodesulfurization. These adsorptive materials are high surface area sorbents with pore sizes large enough to accommodate sulfur contaminants, and typically these are

loaded with d- or f-block metals in ionic, metallic, or oxide form to serve as active sites.

Hierarchical mesoporous monoliths, synthesized using Zeolite Y and Al-SBA-15 with agarose as a templating agent, were explored as possible adsorptive desulfurization materials. Al-SBA-15 monolith was found to be more effective than the Zeolite Y monolith, which is attributed to the difference in pore size between Zeolite Y and Al-SBA-15. However, there was essentially no difference in capacity between the monolith form of Al-SBA-15 and its bulk powder form. Therefore, hierarchical monoliths were not further explored and experiments on bulk Al-SBA-15 were continued.

Three types of SBA-15 were investigated: pure silica SBA-15, aluminoslicate SBA-15 (Al-SBA-15), and aminopropyl-functionalized SBA-15 (APS-SBA-15). Various metal ions were loaded into the frameworks and their loading procedures were evaluated. Ag^+ was found to have the highest adsorption capacity, and loading *via* wet impregnation was beneficial compared to ion exchange procedures. Ultimately, 18 wt.% Ag-Al-SBA-15 was found to have an adsorption capacity of 31.47 mgS/g in JP-8. However, Ag-MCM-41 compared to silver loaded SBA-15 and its derivatives was found to be more effective.

MCM-41, aluminosilicate MCM-41 (Al-MCM-41), and MCM-41 nanoparticles (MSN) were next explored as higher surface area alternatives to SBA-15 and Al-SBA-15. Ag loaded Al-MCM-41 displayed a high desulfurization capacity, but poor reproducibility after regeneration. While silver loaded MCM-41 displayed a

slight decrease in capacity, it had a highly reproducible regenerability of ~ 70%. Silver-loaded MSN displayed a four-fold greater performance towards JP-8 fuel over previously reported sorbents, whereas MCM-41 displayed a three-fold greater capacity than previous reports. Silver-impregnated MSN and MCM-41 were found to have saturation adsorption capacities for JP-8 of 32.6 mgS/g and 25.4 mgS/g, respectively. MSN also displayed a high capacity for the sterically hindered 4,-6-dimethyldibenzothiophenes along with a breakthrough capacity of 0.98 mgS/g at 10ppm$_w$S, which is twice that of other published materials.

In an effort to produce novel sorbents with both high surface areas and active surfaces, we produced a series of silica-zirconia mesoporous materials. Three long-chain primary alkylamines were explored: octylamine, dodecylamine, and hexadecylamine, as well as a variety of Si:Zr ratios. These frameworks were loaded with Ag *via* wet impregnation and tested with model fuels. The optimum material, Ag-DDA-15, produced using dodecylamine and a Si:Zr ratio of 15:1 and 12 wt.% Ag, displayed almost as high of a desulfurization capacity as Ag-MSN, but with a far superior silver efficiency. Ag-DDA-15 also shows better regenerability than Ag-MSN, maintaining 80% of its capacity on the second cycle, compared to 70% with Ag-MSN.

Dedication

To my husband

Rafael Palomino

without your love and support

none of this would have been possible

Acknowledgement

I would like to acknowledge my advisor, Professor Scott R. J. Oliver for giving me the freedom to explore chemistry while providing guidance and insight along the way. I would like to thank my committee members, Professor Pradip Mascharak, Professor Yat Li, and Dr. Stacey Zones for always encouraging me to be a better scientist.

I would like to acknowledge my lab mates for creating an environment of support and collaboration: Dr. David Rogow, Dr. Honghan Fei, Yashar Abdollahian, Kevin Sergo, Howard Han, Jesse Hauser, Ian Colinas, Eaindar Soe, Susan Citrak, and Ana Kareh. Additionally, I would like to thank the exceptional undergraduates who contributed their time and effort to my research: Lisa Staugaard, Chris Miller, Josh Gardner, and Bodhi Canfield. My research would also not have been possible without the help of collaborators: Dat Tran for testing samples with JP-8 and Rob Franks for his help with ICP.

Financial support was provided by DOD ARL, Contract no. W911NF-12-2-0005, and a Dissertation Quarter Sabatical Fellowship.

Chapter 1

Adsorptive Desulfurization of JP-8 Fuel

Abstract

The desulfurization of JP-8 fuel is of particular interest to the U.S. military because of its potential use as a fuel source for solid oxide fuel cells (SOFCs). SOFCs can be used to supply a steady stream of power during military silent watch missions. Adsorptive desulfurization is a promising alternative to hydrodesulfurization, which is unable to remove refractory sulfur compounds to achieve the ultra-low sulfur levels necessary to prevent poisoning of SOFCs. In addition, adsorptive desulfurization could be a portable, on-site process performed on JP-8 stocks already in the field. Herein we review the current status of adsorptive desulfurization specifically performed on JP-8 fuel. Currently, the best performing sorbents are those utilizing high surface area porous frameworks with pore sizes large enough to accommodate sulfur contaminants. Additionally, a variety of metals in ionic, metallic, and oxide form serve as promising active sites within these sorbents.

1.1 Introduction

1.1.1 Environmental and Health Consequences

The U.S. Environmental Protection Agency (EPA) and European Union are continuously imposing more rigorous mandates for the allowable sulfur content in transportation fuel. The EPA's Tier 3 program requires that gasoline will not contain more than 10 ppm sulfur by 2017.[1] Similarly, diesel fuel was capped at 15 ppm sulfur in 2006. Currently, jet fuel, including commercial and military grades, is specified to not exceed 3000 ppm_w S. The driving force behind the EPA's sulfur content mandates are related to health and environmental factors associated with sulfur emissions primarily from ground transportation vehicles. Burning sulfur containing fuel causes the release of sulfur oxide (SO_x) compounds into the environment. SO_2 emissions contribute to acid rain formation, which is particularly harmful to ecosystems.[2, 3] SO_x emissions also contribute to the formation of airborne particulate matter in the atmosphere which poses a threat to the human cardiovascular and respiratory systems.[3-6] It is estimated that the widespread use of ultra-low sulfur jet fuel in aviation could prevent approximately 2300 premature mortalities annually.[7]

1.1.2 Fuel Cell Requirements

Hydrogen fuel cells provide a low emission energy alternative to traditional combustion engines, with reduced SO_x, NO_x, hydrocarbon, and CO_2 release. In addition to being a source of clean energy, fuel cells are also of particular interest to the military for auxiliary power units. Fuel cell power units are doubly advantageous

in that they are nearly silent (compared to conventional onboard generators), and overcome the energy density limitations of conventional battery systems by utilizing much more energy dense JP-8 (Jet Propellant 8) fuel. These auxiliary power units would be especially useful on silent watch missions where conventional generators are too loud. Solid oxide fuel cells (SOFCs) are currently being considered by the military to fill this need.

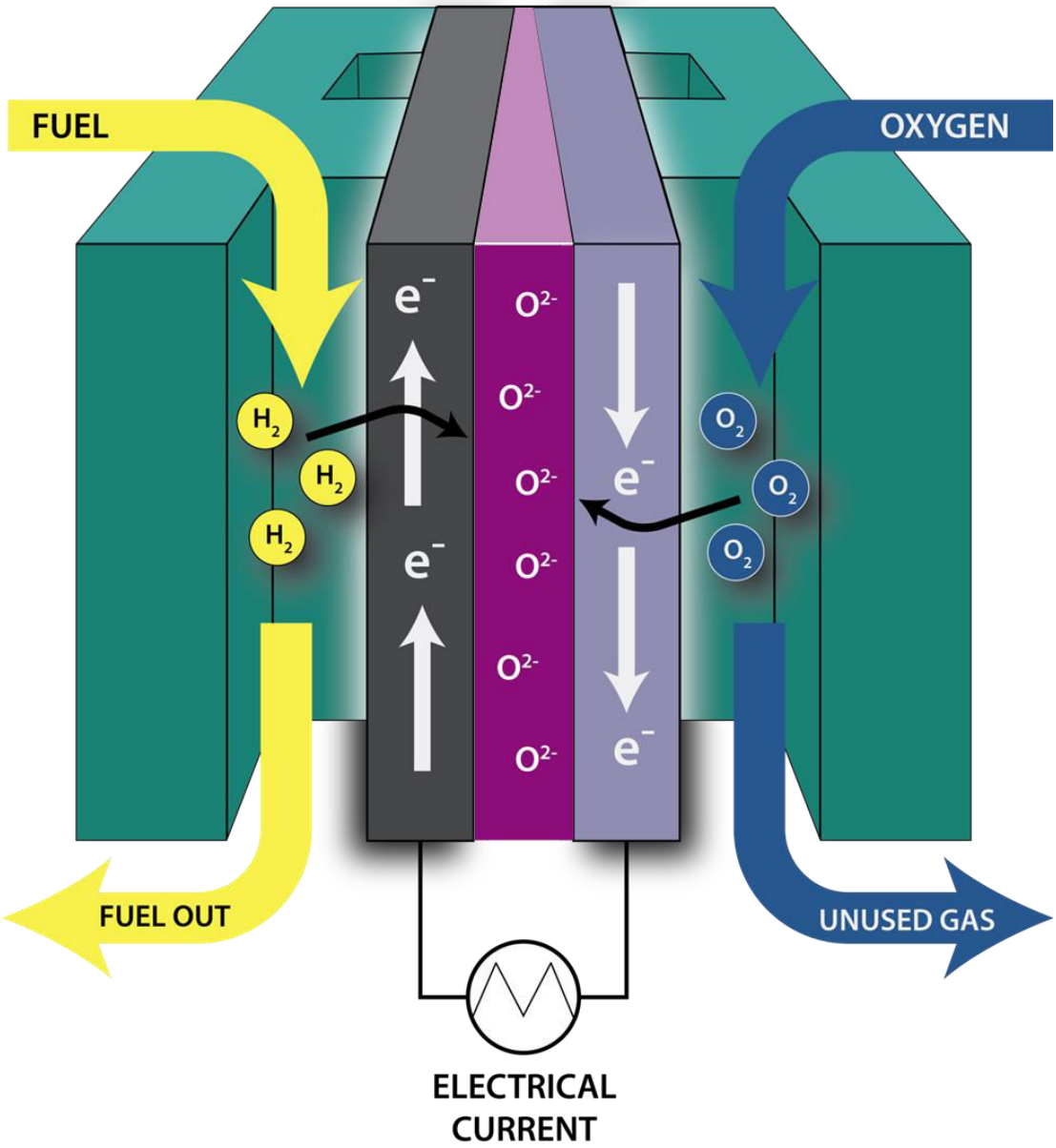

Figure 1.1 General overview of the components of a SOFC and the process for converting fuel into an electrical current. Hydrogen gas is oxidized at the anode (gray) and oxygen is reduced at the cathode (lilac). Oxygen ions are transported across the solid electrolyte (magenta).

SOFCs are of interest because they are energy efficient, have long lifetimes, and can be used with a variety of fuels.[8] Figure 1.1 shows the general configuration of an SOFC. Hydrogen gas (fuel) is supplied to the anode where it is oxidized and

oxygen is supplied to the cathode where it is reduced. The anode is typically composed of nickel dispersed in a porous metal oxide cement.[8] The cathode, which must also be porous, is typically composed of strontium-doped $LaMnO_3$.[8] A solid electrolyte, typically yttria-stabilized zirconia, allows for the oxygen ions to be transported where they can react with hydrogen ions to form water.[8] With the addition of a catalytic partial oxidation (CPOX) reformer, energy dense fuels such as JP-8 can be used as the hydrogen feedstock for SOFCs. The CPOX reformer converts the hydrocarbon chains to hydrogen gas and carbon monoxide with the addition of oxygen and a catalyst, which is made of supported precious metals such as Rh, Pt, or Pd.[9, 10] Sulfur compounds present in the fuel are capable of poisoning the CPOX catalyst by binding to these precious metals, reducing its effectiveness and lifetime. Additionally, sulfur compounds can poison the SOFC itself, binding to the nickel anode and decreasing the number of surface sites available for oxidation. Hu *et al.* have shown that untreated JP-8 (3000 ppm_wS) significantly deactivates the Pd/ZnO catalyst in as little as 3 hours of use.[11] Therefore, in order to keep SOFCs efficient and cost-effective, the fuel source must be desulfurized to as low of a sulfur level as possible.

Table 1.1 shows the electrical efficiency of SOFCs compared to other fuel cells and internal combustion engines. Internal combustion is far less efficient than fuel cells and also produces more harmful emissions. SOFCs are advantageous compared to other fuel cells not only because of their high efficiencies, but their solid construction allows them to be made in various shapes and sizes, and their

components are reasonably affordable. However, they do require high operating temperatures typically around 800 ^{o}C.[12]

Table 1.1 Approximate lower heating value (LHV) electrical efficiencies of different fuel cells compared to an internal combustion engine[12, 13]

Fuel Source	Electrical Efficiency
Solid Oxide Fuel Cell	45-65%
Molten Carbonate Fuel Cell	45-65%
Phosphoric Acid Fuel Cell	37-42%
Polymer Electrolyte Fuel Cell	35%
Internal Combustion Engine	20-30%

JP-8 is an ideal fuel source for SOFCs, as it is the main fuel source used by the military and typically already on-site for other applications. It is also much safer to ship and store compared to other fossil fuels, and has a high energy density. Table 1.2 shows the energy density of JP-8 compared to other fuels. Its gravimetric energy density is significant compared to compressed hydrogen gas and especially compared to lithium ion batteries. However, the sulfur content can range from the hundreds to several thousand ppm_wS.

Table 1.2 LHV gravimetric and volumetric energy densities of common fuel sources including JP-8 compared to the energy density of lithium ion batteries

Fuel	Energy Density (MJ/L)	Energy Density (MJ/kg)
JP-8[14]	34.5	43.4
Diesel[14]	36.2	42.5
Gasoline[15]	32	44
Hydrogen (liquid)[15]	120	8
Methanol[16]	15.6	19.7
Lithium Ion Battery[17]	N/A	0.6

1.1.3 JP-8 Composition

JP-8, a military grade jet fuel, has been the main fuel used by the US military for the past several decades, replacing its predecessor JP-4 as a much safer alternative.[18] The use of JP-4 in combat situations had directly resulted in causalities due to fires and explosions, prompting the evaluation of a safer fuel. JP-8 has much more favorable vapor pressure and flashpoint compared to JP-4, and is available in considerable quantities. With the exception of the Navy, JP-8 is now used in all branches of the US military and on NATO bases around the world. The Navy uses JP-5 onboard its ships. JP-5 is slightly safer than JP-8, reducing the chance of fire or

explosion while at sea, but it is more expensive so it is not used for naval ground applications or in other branches of the U.S. Military.[18, 19]

JP-8 is a kerosene type fuel, similar in composition to commercial Jet-A fuel, but with additional additives to inhibit icing and corrosion.[20] It consists primarily of a mixture of aliphatic and aromatic hydrocarbons ranging in length from C_9 to C_{16}, including paraffins and naphthalenes.[21] The non-sulfur components of JP-8 are highly variable, as shown by Natelson *et al.* (Table 1.3 and in more detail in Table 1.4).[22]

Table 1.3 General composition of three different samples of JP-8, obtained from Wright-Patterson Air Force Base, determined using a pressurized flow reactor[22]

Composition	**JP-8 Sample 1**	**JP-8 Sample 2**	**JP-8 Sample 3**
Aromatics (vol. %)	16.3	18.1	15.9
Olefin (vol. %)	0.9	1.3	0.7
Naphthalenes (vol. %)	1.0	N/A	N/A
Hydrogen content (mass %)	13.7	13.8	13.9
Total sulfur (mass %)	0.14	0.04	0.07

Table 1.4 Detailed composition of one sample of JP-8 determined using a pressurized flow reactor[22]

Class	JP-8 Sample 3 (vol.%)
Paraffins (n- and i-)	57.2
Cycloparaffins	17.4
Dicycloparaffins	6.1
Tricycloparaffins	0.6
Alkylbenzenes	13.5
Indans/tetralins	3.4
Indenes	< 0.2
Naphthalene	< 0.2
Naphthalenes	1.7
Acenaphthenes	< 0.2
Acenaphthylenes	< 0.2
Tricyclic aromatics	< 0.2

JP-8 also contains a variety of organosulfur compounds, which vary based on when and where the sample was obtained. Ubanyionwu and coworkers analyzed the JP-8 fuel over time from Fort Belvoir, VA.[20] The summary of their findings are in Table 1.5. They were able to positively identify seven compounds from the sixteen distinct peaks, with the major sulfur contributors being 2,3-dimethylbenzothiophene and 2,3,7-trimethylbenzothiophene (structures shown in Figure 1.2).[20]

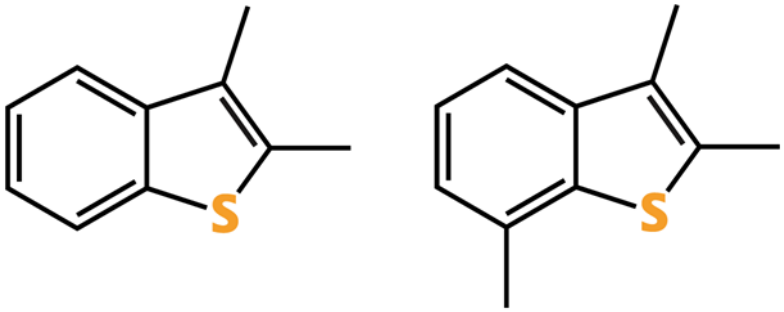

Figure 1.2 The two major sulfur contaminants in JP-8: 2,3-dimethylbenzothiophene (left) and 2,3,7-trimethylbenzothiophene (right).

Table 1.5 Detailed organosulfur content of four different JP-8 samples as determined by GC.[20]

Retention time of peak (min)	Compound assignment	Amount (% of total sulfur concentration)			
		June 2003	Oct. 2004	July 2005	April 2006
< 6.726	unidentified	36.01	32.75	37.1	34.75
6.726	unidentified	1.8	1.69	1.66	1.91
6.789	unidentified	1.4	1.97	1.75	1.73
7.263	2,7-Dimethylbenzothiophene	2.03	2.32	2.93	2.49
7.324	Dimethylbenzothiophene isomers	2.57	2.12	3.02	2.19
7.391	Dimethylbenzothiophene isomers	1.8	1.84	1.99	1.89
7.430	Dimethylbenzothiophene isomers	1.54	1.39	2.52	2.12
7.490	3,5-Dimethylbenzothiophene	1.24	1.39	1.09	1.29
7.534	2,3-Dimethylbenzothiophene	5.36	5.36	5.98	5.39
7.909	Trimethylbenzothiophene isomers	1.68	1.47	1.5	1.51
7.961	2,5,7-Trimethylbenzothiophene	0.96	1.21	1.51	1.1
8.021	Trimethylbenzothiophene isomers	1.22	1.22	2.11	1.92
8.059	Trimethylbenzothiophene isomers	1.68	1.39	1.09	1.34
8.129	2,3,7-Trimethylbenzothiophene	5.72	5.3	3.92	4.11
8.237	2,3,5-Trimethylbenzothiophene/ 2,3,6-Trimethylbenzothiophene	2.35	1.96	2.19	2.61
8.505	unidentified	0.82	0.96	0.72	1.12
8.715	unidentified	1.23	0.9	0.74	0.94
9.998	Dibenzothiophene	0.89	0.77	0.23	0.44
11.11	unidentified	0.74	0.75	0.09	0.2
Total ppm_wS		325	396	1096	648

Materials for desulfurization are often tested on JP-5 in lieu of JP-8. It should be noted that JP-5 is inherently easier to desulfurize than JP-8 due to its lower trimethylbenzothiophene content compared to JP-8. This difference is succinctly demonstrated by Tatarchuk and coworkers. A TiO_2 sorbet loaded with 4 wt.% Ag had more than twice the adsorption capacity when tested in JP-5 compared to JP-8. Further, the sorbent was able to achieve sub 10 ppm_wS levels in JP-5 but not JP-8.[23]

1.1.4 Current Desulfurization Method – Hydrodesulfurization

Currently, fossil fuels are desulfurized through the process of hydrodesulfurization (HDS). As shown in Figure 1.3, hydrogen gas activates the catalyst, typically unsupported solid MoS_2, creating a coordinatively unsaturated site. The sulfur atom on the organosulfur compound is able to attach to this coordinatively unsaturated site resulting in the removal of a sulfide and hydrogenation.[24]

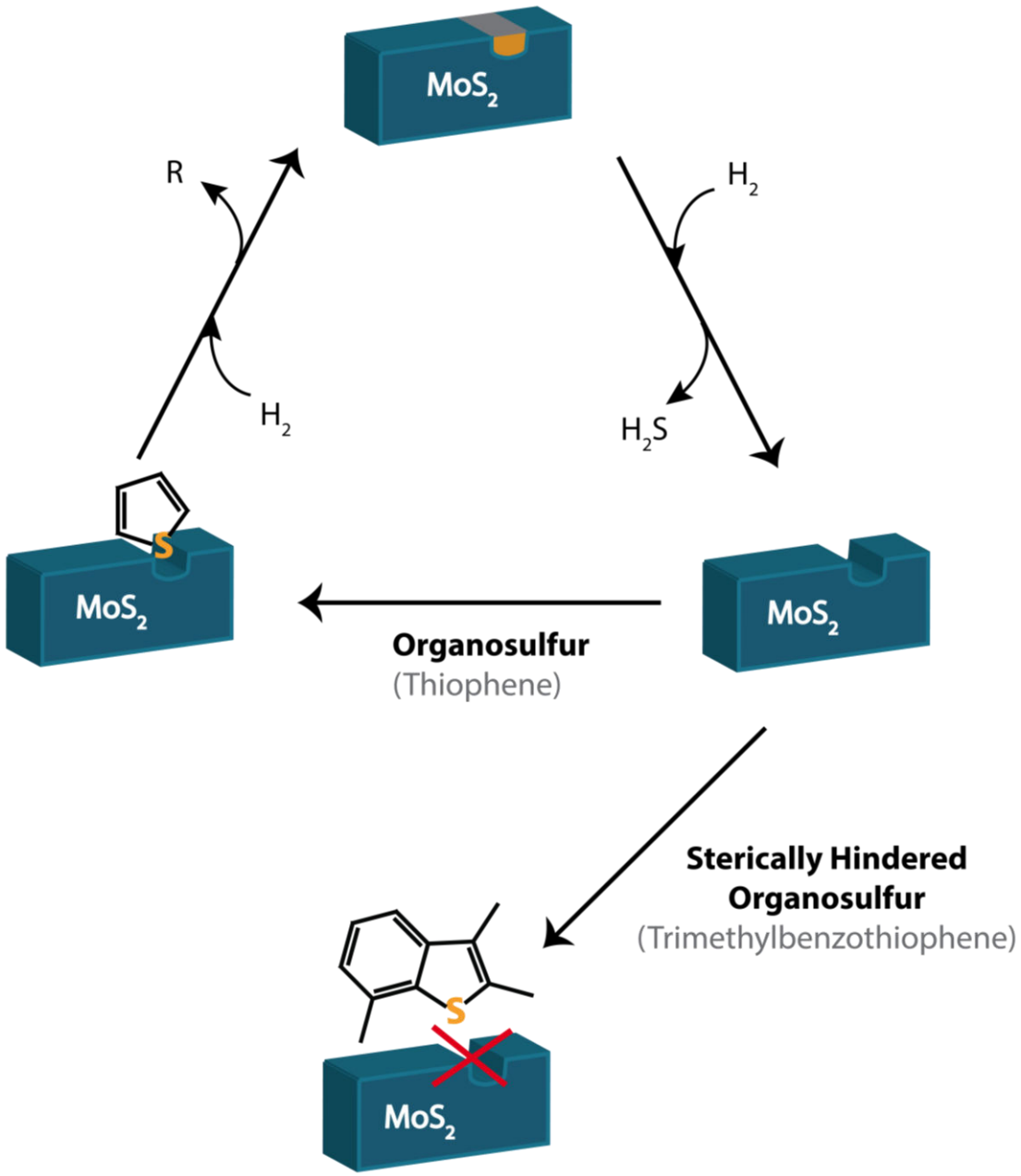

Figure 1.3 The general process for hydrodesulfurization. The MoS_2 catalyst (teal) reacts with hydrogen to create a sulfur vacancy where the sulfur of a nonsterically hindered organosulfur compound can bind (shown as thiophene). Upon addition of more hydrogen, the hydrogeneation occurs releasing a hydrocarbon (in the case of thiophene, butane could be released). And as more hydrogen is added the catalyst releases H_2S again, allowing the catalyst to be reused. A sterically hindered organosulfur compound, however, (shown as trimethylbenzothiophene, bottom of the figure) cannot bind to the sulfur vacancy and therefore cannot be reduced.

This process is highly effective for lighter fuels such as gasoline, where the EPA limit can be easily reached. Heavier fuels that contain larger organosulfur compounds such as methylted benzothiophenes and dibenzothiophenes (Figure 1.3), however, cannot be desulfurized by this process. If the sulfur in the compound is sterically hindered, it will be unable to bind to the catalyst and thus will remain in the fuel. These remaining sulfur compounds are known as refractory sulfur compounds because they remain in the fuel despite the HDS process.

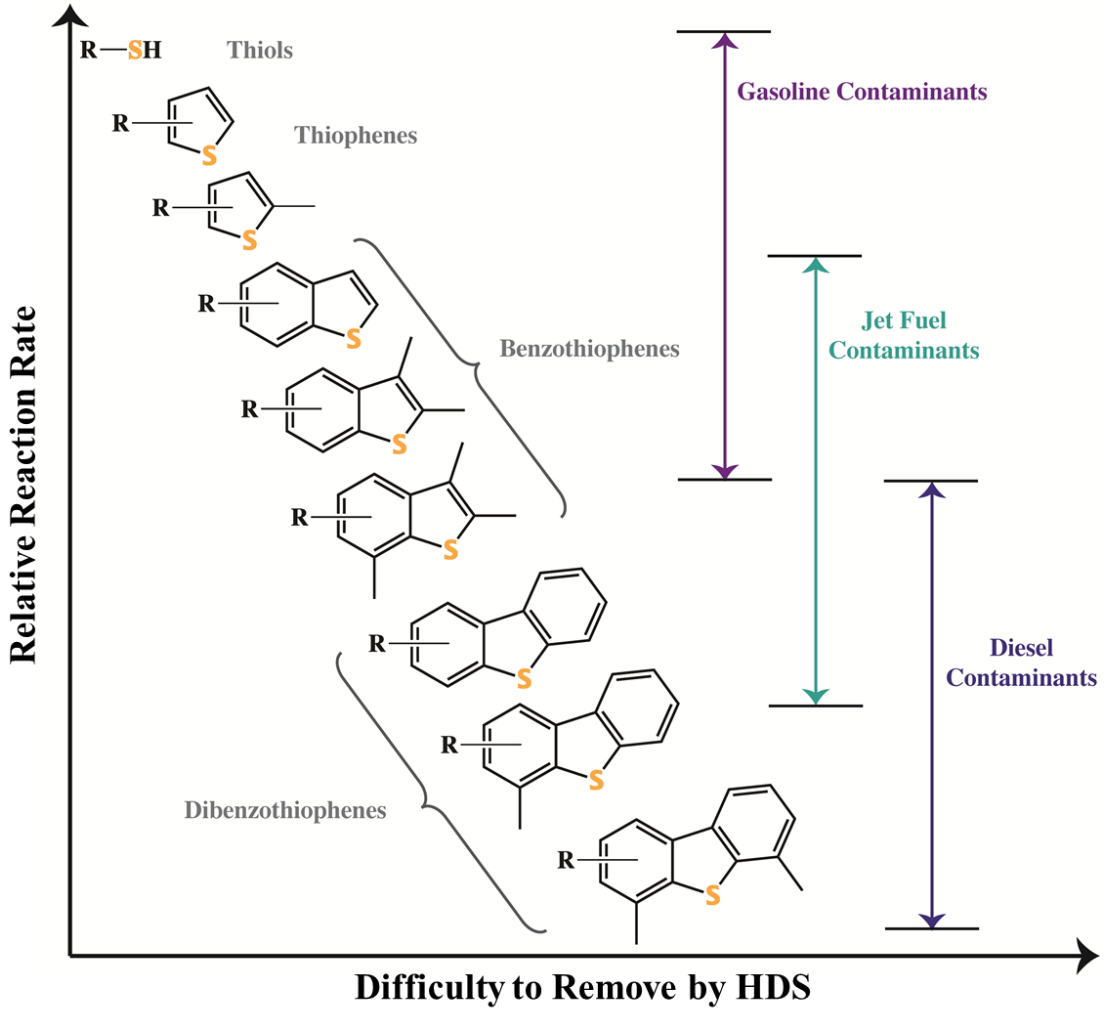

Figure 1.4 The common types of organosulfur compounds found in fossil fuels, categorized by their difficulty to be removed *via* hydrodesulfurization.

JP-8 is rich in methylated benzothiophenes and thus HDS is not an effective method of desulfurization for JP-8. Figure 1.4 shows the relative effectiveness of desulfurization towards a variety of organosulfur compounds found in fuels. As the organosulfur compounds become larger and more methylated, the sulfur atom becomes less likely to attach to the HDS catalyst. There are other drawbacks of HDS, including non-selective hydrogenation which lowers the octane level of the fuel and

the use of hydrogen, resulting in an overall poor hydrogen economy. In addition, HDS must be performed at a refinery as it is a high pressure, high temperature process. Ideally, fuels for use in SOFCs would be capable of desulfurization to specification onsite and under ambient or near-ambient conditions, as the entire stocks of JP-8 used by the military do not need to be desulfurized to the standards required by SOFCs (sub 1 ppm_wS).

1.2 Current Research Directions and Adsorptive Desulfurization Frameworks

A variety of desulfurization techniques are being explored to address the sulfur content in fossil fuels, including JP-8. Advances are being researched in hydrodesulfurization and other higher temperature catalytic processes to try and achieve lower sulfur content in JP-8,[25, 26] though would not be a viable portable process. Low temperature oxidative catalytic desulfurization processes are also being explored,[27-30] including some involving the assistance of sonication.[31-33] Additional more exotic techniques of desulfurization have been explored on other transportation and model fuels. These less traditional techniques include extraction using ionic liquids[34-38] and biodesulfurization[39-42] which utilizes bacteria. These techniques, while effective, are not as portable as adsorptive desulfurization, which is ideal for field applications.

This review will focus on adsorptive techniques, as this process has both yielded promising results and is likely the most viable for onsite applications of

SOFCs in the military. Herein we will limit our scope to techniques employed on JP-8 and light JP-8 (light refers to a lighter fraction or cut of fuel obtained by distillation) as: (i) it is the primary fuel used by the military, and (ii) because it is more difficult to desulfurize than other military fuels, namely JP-5. Therefore, any techniques proven useful on JP-8 will be effective on other grades of jet fuel.

There are several key qualities that are ubiquitous among desulfurization frameworks. Namely, they tend to be porous in nature to afford for very high specific surface areas, creating a significant amount of area for adsorption within a small volume. They are typically composed of low cost materials, usually metal oxides. They are usually loaded with metal active sites for enhanced adsorption, in either metallic, ionic, or oxide form. The frameworks can have unique surface properties, such as surface acidity or ligand functionalization, that help in the dispersion of the active sites or actually aid in the adsorption process. And lastly, these sorbents must be capable of regeneration for them to be applicable for usage by the military.

1.2.1 Nanoporous Zeolites

Zeolites have been used as sorbents for a myriad of applications; their high surface area, pore size, and framework charge make them an attractive option. Their negatively charged framework allows them to easily be loaded with transition metal ions, making them a candidate for adsorptive desulfurization.

1.2.1 (a) Zeolites for Desulfurization

Zeolites loaded with a variety of metals have been explored for the desulfurization of fossil fuels.[43-50] Yang and coworkers investigated Cu^+ (obtained by reduction of Cu^{2+} exchanged Zeolite Y) and Ag^+ exchanged Zeolite Y.[45, 51] Cu^+/Zeolite Y can achieve sub 1 ppm_wS for commercial diesel and can be successfully regenerated thermally to retain 95% of its capacity. The same material can be solvent regenerated with dimethylformamide or carbon tetrachloride, both yielding essentially 100% regeneration.[51] Higher performance was found for Cu^+ compared to Ag^+ exchanged zeolites.[45, 51] However, Cu^+ is less stable than Cu^{2+}, so to obtain Cu^+/Zeolite Y, Zeolite Y exchanged with Cu^{2+} must be reduced by heating to 450 ^oC in helium for 18 hours.[51] Further zeolite testing by the same group showed that desulfurization performance follows $Cu^+ > Ni^+ > Zn^{2+}$, which agreed with their molecular orbital calculations.[43] Cu^+ vapor phase ion exchanged Zeolite Y was explored for desulfurization of a commercial jet fuel with a similar composition to JP-8.[50] Using fixed bed experiments, they achieved a saturated adsorption capacity of 23.2 mgS/g for commercial jet fuel (original sulfur content: 364 ppm_wS).[50]

1.2.1 (b) Effect of Extraframework Metal on Desulfurization of JP-8

Song and coworkers tested a variety of transition metal loaded zeolites, shown in Table 1.6, with JP-8 fuel (750 ppm_wS) at 80 ^oC.[44]

Table 1.6 Loading composition, measured using ICPES, and adsorption capacities in JP-8 (750 ppm_wS) at 80 ^oC[44]

Sorbent	Metal Loading (wt.%)	Adsorption Capacity (mgS/g)
Ni^{2+}/Zeolite Y	1.3	2.0
Cu^{2+}/Zeolite Y	8.9	0.3
Zn^{2+}/Zeolite Y	Not Determined	0
Ce^{3+}/Zeolite Y	21.8	2.7
Pd^{2+}/Zeolite Y	0.7	2.6
H+/Zeolite Y	N/A	1.3

Ce^{3+} and Pd^{2+} are particularly useful in the removal of organosulfur compounds. The Pd^{2+} exchanged zeolite, however, displays much better efficiency: it gave a nearly identical absorption capacity to Ce^{3+} with significantly less metal loading.[44] The authors attribute this efficiency to the possible location of Pd^{2+} in accessible alpha supercages, whereas most of the Ce^{3+} may be in the inaccessible small beta cages of the zeolite (Figure 1.5).[44] They also attribute the higher efficiency of Pd^{2+} to its ability to form π-complexes, whereas Ce^{3+} likely only forms direct S-M interactions.[44] They explored other variables such as desulfurization temperature. With the Ce^{3+} exchanged zeolite, the capacity decreased when adsorption studies were performed at 120 ^oC.[44] Overall, Pd^{2+} could make for a more affordable choice for desulfurization, even though it is more expensive than cerium: only a small amount of

palladium is needed compared to cerium to achieve essentially the same adsorption capacity.

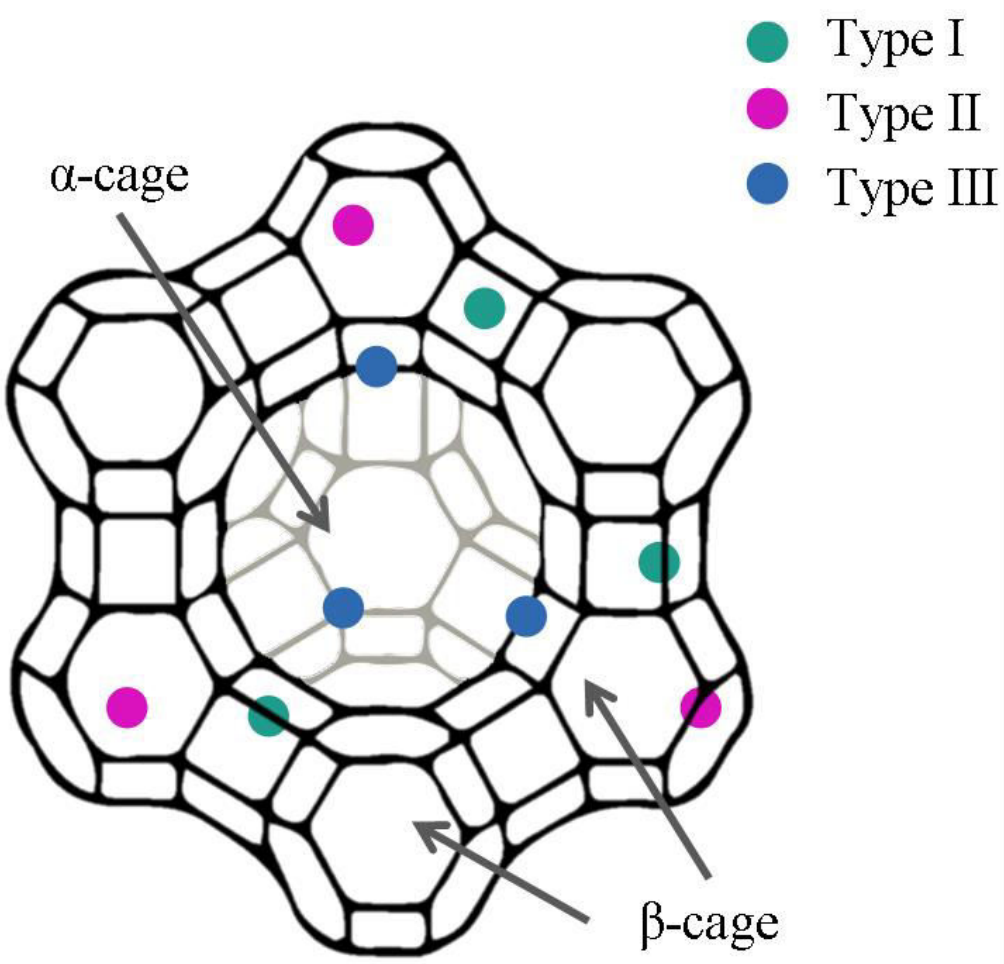

Figure 1.5 The location of different types of ions within zeolite Y.

1.2.1 (c) Effect of Loading Procedure on Desulfurization

Song and coworkers also compared two versions of Ce^{3+} Zeolite Y, one calcined after exchange and one uncalcined, and found the former has a higher

adsorption capacity. This was attributed to the calcined sample containing more Ce^{4+} which could have a more polarizing effect on the organosulfur compounds.[44] Ion-exchanged Zeolite Y also performed better than Zeolite Y loaded with 30 wt.% Ce *via* wet impregnation, which they attributed to less dispersion and possibility of crystallized ceria reducing the porosity.[44] Under the various conditions and metals explored, the lowest sulfur content obtained for 750 ppm_wS JP-8 was only approximately 200 ppm_wS.[44]

Using light fractioned JP-8 and further exploring metal loaded zeolites, they were able to achieve sub ppm_wS fuel.[52] The optimized adsorbent was Zeolite Y that had been ion exchanged for nickel three times followed by reduction by heating to 600ºC in hydrogen for 4-5 hours.[52] Again, they saw that ion exchange was superior to wet impregnated samples.[52] They also found benefits of having K^+ as a co-cation, attributing this to the ability of K^+ to improve reduction of Ni^{2+} and improve distribution and prevent crystal clusters.[52] It is also thought that the metallic nickel is capable of forming direct S-M bonding, whereas unreduced forms mainly π-complex which is less selective, as there are a variety of aromatics in jet fuel.[52]

1.2.1 (d) Framework Properties

Model fuel studies and molecular modeling performed with benzothiophene and dibenzothiophene on Zeolite Y reveal that benzothiophene is just small enough at ~7 Å free diameter to fit into the ~8 Å pore free aperture of Zeolite Y.[53] While Zeolite Y provides a high surface area framework for adsorption, it is likely that the larger di-

and tri-methylbenzothiophenes are incapable of making their way into the porous framework. This explains the above phenomenon seen by Song and coworkers, where exchanged zeolites were only able to achieve sub ppm_wS levels for light fraction JP-8, which would not contain the larger more methylated benzothiophenes. Ultimately, this size exclusion is responsible for the lower adsorption capacities of zeolites compared to the frameworks mentioned hereafter. Overall, zeolites are an effective framework for removing small organosulfurcompounds, but their pore size excludes them from being effective for use on heavier fuels like JP-8.

1.2.2 Silica Frameworks

1.2.2 (a) Silica Frameworks for Desulfurization

Silica has been widely explored for adsorptive desulfurization in general, with a focus on mesoporous silica including MCM-41 (a hexagonal array of 1D pores, typically ~2-4 nm in diameter), SBA-15 (analogous to MCM-41 with ~4.5-30 nm pore diameter), and silica gel.[54-58] Mesoporous silica is of interest because of its very high specific surface area. MCM-41 or SBA-15 frameworks loaded with metal ions or metal oxides have been tested for adsorptive desulfurization with JP-5. The results are summarized in Table 1.7.

Table 1.7 MCM-41 and SBA-15 based sorbents tested with JP-5 fuels, listed by saturation adsorption capacity

Framework	Metal	Metal Loading (mmol/g)	Surface Area (m^2/g)	Breakthrough Capacity (mgS/g) at 50 ppm_wS	Saturation Capacity (mgS/g)
SBA-15[56]	Pd^{2+}	2.6	358	32.1	38.5[c]
MCM-41[58]	Ag^{+}	2.21	490	15.7*	32.1[d]
SBA-15[58]	Ag^{+}	1.77	408	10.3*	29.2[d]
SBA-15[56]	Cu^{+}	5.1	411	19.9	25.7[c]
MCM-41[56]	Pd^{2+}	3.1	502	10.9	16.0[c]
MCM-41[56]	Cu^{+}	5.7	456	7.7	14.4[c]
MCM-41[59]	Cu_2O[a]	6.3	490	9.9	12.8[c]
MCM-41[59]	Cu_2O[b]	6.3	523	5.1	10.3[c]
SBA-15[59]	Cu_2O[a]	4.7	400	5.1	9.6[c]

[a]Calcined at 700 ^oC; [b]Calcined at 550 ^oC; [c]Tested with JP-5 light 841 ppm_wS; [d]Tested on JP-5 1172 ppm_wS. *Breakthrough capacity at 10 ppm_wS.

Cu^{+} and Pd^{2+} loaded MCM-41 and SBA-15 were prepared by activation at 550 ^oC (helium was used for MCM-41, air for SBA-15) followed by spontaneous monolayer dispersion, which entails mixing the metal halide and framework and heating at a high temperature under helium for 24 hours.[56] Ag^{+} loading was achieved

through wet impregnation, and cuprous oxide loading was achieved by wet impregnation followed by autoreduction in helium.[58, 59] The general procedure for synthesizing these mesoporous frameworks is shown in Figure 1.6.

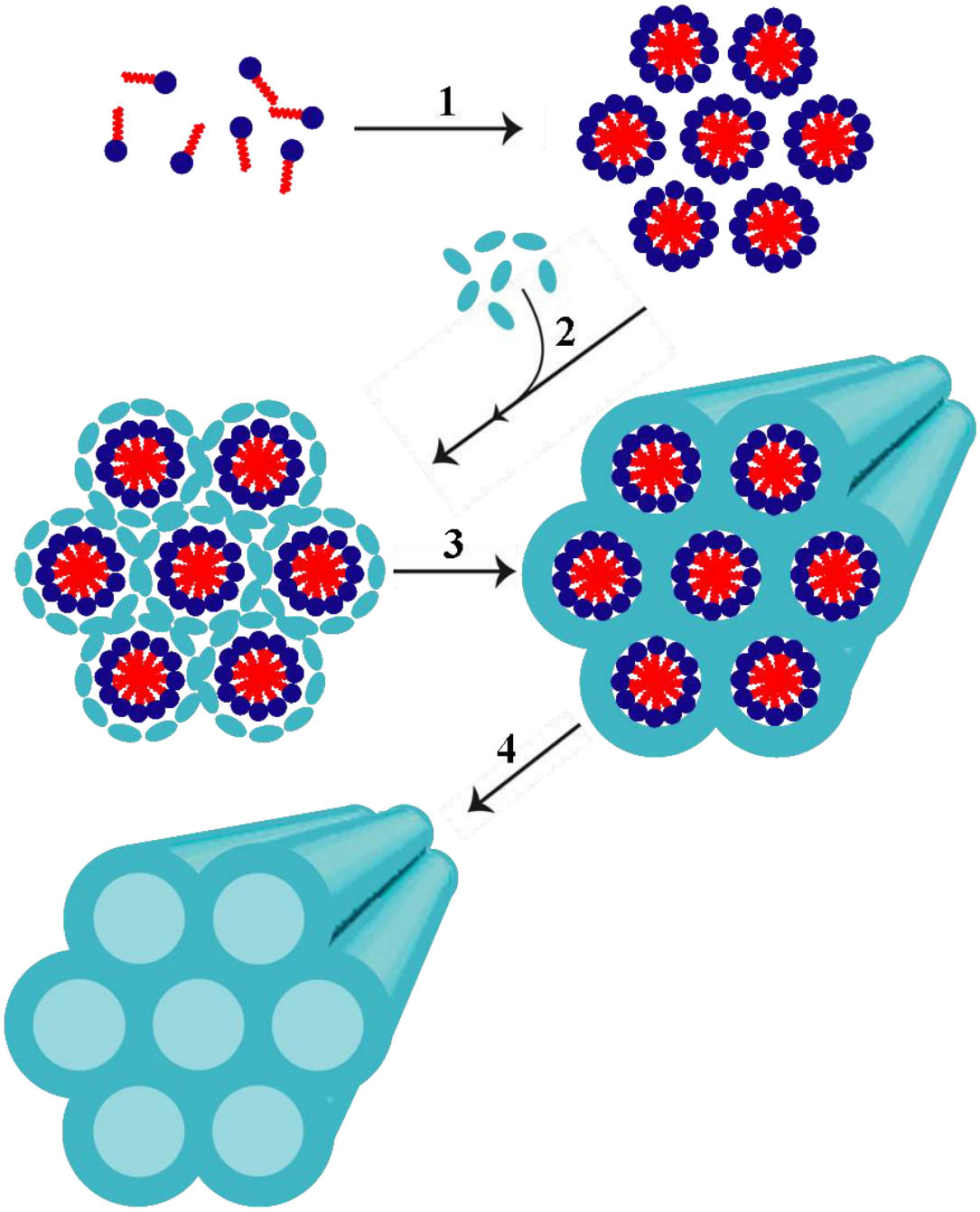

Figure 1.6 The general synthetic method for producing mesoporous silica frameworks. Typically includes the self assembly of a surfactant (1) followed by the addition of a silica precursor (2). This precursor condenses around the surfactant (3) and the surfactant can then be removed typically *via* reflux or calcination (4) to yield the mesoporous silica framework.

The comparison between Cu^{+} and Pd^{2+} revealed that Pd^{2+} is superior because it has greater breakthrough and saturation capacities while being loaded with less metal than the Cu^{+} samples.[56] The authors attributed this to the higher selectivity of Pd^{2+} because it forms a stronger π-complexation than Cu^{+}. Pd^{2+} SBA-15 outperformed Pd^{2+} MCM-41, in spite of only being loaded with 84% the amount of Pd^{2+}.[56] The higher performance is attributed to the larger pore size of SBA-15, approximately double that of MCM-41, which better allows for diffusion within the pores.[56] The authors did not specify, however, the effect of atmosphere (air for MCM-41; helium for SBA-15) on the results. The best sorbent from the group Pd^{2+}/SBA-15 was regenerated *via* benzene solvent regeneration at 70 ^{o}C and retained only approximately half of its saturation adsorption capacity.[56]

The comparison of Ag^{+}/MCM-41 and Ag^{+}/SBA-15 revealed that in this case MCM-41 performed better than SBA-15, which conflicts with the results seen with Pd^{2+} loaded frameworks.[58] The authors contribute this reverse trend to the higher surface area of MCM-41 while loaded as well as a higher silver content.[58] Comparison of the ratios of adsorbed sulfur to silver reveal similar results between the two frameworks, furthering the idea that any difference in pore size, if greater than that of the sulfur containing molecules, do not affect adsorption.[58] Ag^{+}/MCM-41 was thermally regenerated in air to maintain only 50% of its saturation capacity on both the second and third cycle.[58]

The desulfurization results of cuprous oxide supported on MCM-41 and SBA-15 confirm the results that the larger pore size and volume of SBA-15 is not beneficial; rather, the higher surface area of MCM-41 makes it a better framework.[59] Reduction temperature was also explored, revealing that reduction at 700 ^{o}C is more effective than 550 ^{o}C, resulting in more conversion to Cu_2O and therefore a greater adsorption capacity.[59] Thermal regeneration was also employed on these materials, resulting in 100% regeneration.[59]

Overall, these studies reveal the superior performance of free transition metal ions compared to transition metal oxides when it comes to both saturation capacity and breakthrough capacity. SBA-15 loaded with 5.1 mmol/g Cu^+ has almost three times the saturation capacity and four times the breakthrough capacity of SBA-15 loaded with almost an equivalent amount of Cu_2O. The metal oxides are more successful, however, at regeneration. This regenerability can be attributed to the oxide layer being bound to the surface through more covalent interactions, whereas the molecular metal ions are more weakly interacting with the surface. Additionally, the process of regenerating the metal ion materials may produce a metal oxide, which explains the initial loss of capacity for Ag^+/MCM-41 when thermally regenerated (conversion from metallic ion to oxide) followed by maintaining its capacity when regenerated a second time. Between the metal ions tested, Pd^{2+} is likely the best, followed by Ag^+ and Cu^+, although testing of all three under the same conditions need to be studied.

1.2.2 (b) Silica Frameworks for the Desulfurization of JP-8

In addition to the highly ordered mesoporous silica frameworks of MCM-41 and SBA-15, silica gel is also a viable option as it is porous, low cost, and readily available. Song and coworkers studied a silica gel loaded with 5.0 wt.% of an undisclosed metal compound prepared by an undisclosed procedure.[60] They report GC chromatographs of diesel fuel before and after treatment, demonstrating a reduction in the sulfur compounds present.[60] They do not quantify the reduction, however, and simply state that similar results were obtained with JP-8.[60] The authors did perform theoretical molecular orbital calculations on thiophene, benzothiophene and dibenzothiophene. These calculations revealed that the highest occupied molecular orbital for these compounds is located mostly on the sulfur atom. This location suggests that direct interaction between the sulfur and certain metal species is possible. The two known coordination geometries between thiophene and a metal species are shown in Figure 1.7.

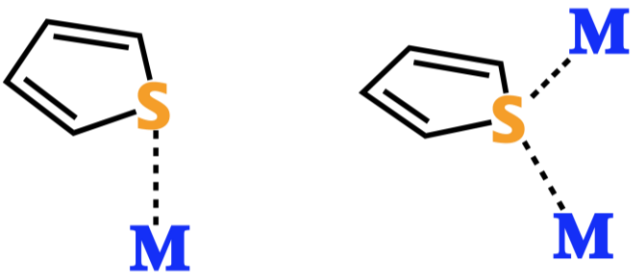

Figure 1.7 Coordination geometries involving direct interaction between the sulfur of a thiophene and a metal atom.

These direct interactions are important because they can result in selective removal of organosulfur compounds from jet fuel, which is rich in non-sulfur aromatics, as previously shown in Tables 1.3 and 1.4. While this very early study does not provide much insight into the sorbent itself, it does show the promise of adsorptive desulfurization as a method for obtaining ultra-low sulfur jet fuel.

1.2.3 Aluminosilicates

Aluminosilicates are attractive options for sorbents over silicates because they can easily be synthesized into high surface area frameworks and, much like zeolites, they possess a negatively charged framework.

1.2.3 (a) Silica Compared to Aluminosilicates for Desulfurization

Along with zeolites, other aluminosilicates have been explored as adsorptive desulfurization frameworks[61, 62] and as catalytic desulfurization frameworks.[63-65] To elucidate the desulfurization effects of the addition of aluminum into silica frameworks, Wang and coworkers created a series of SBA-15 materials with varying degrees of aluminum content.[62] The SBA-15 and alumina containing SBA-15 (AS-X, where AS stands for aluminosilicate SBA-15 and X is the mass percentage of aluminum) were synthesized according to traditional methods using Pluronic P123, a triblock copolymer $HO(CH_2CH_2O)_{20}(CH_2CH(CH_3)O)_{70}(CH_2CH_2O)_{20}H$, as the templating agent, and aluminum was incorporated post synthetically using wet impregnation.[62] Samples were loaded with copper *via* spontaneous monolayer

dispersion.[62] Fuel tests were performed with a model fuel of thiophene in isooctane (564 ppm_wS).

A comparison between copper loaded pure silica SBA-15 and AS-10, shown in Table 1.8, revealed that AS-10 has greater adsorption capacity despite its decreased surface area. This increased capacity for AS-10 is attributed to the higher dispersion of copper compared to the pure silica framework.[62] This study shows the overall potential advantage of aluminosilicate over silicate as a framework for desulfurization.

Table 1.8 Surface area, loading content, and desulfurization adsorption capacities of SBA-15 and aluminosilcate SBA-15. AS-X represents SBA-15 where X is the mass percentage of aluminum

Framework	Unloaded Surface Area (m^2/g)	Loaded Surface Area (m^2/g)	Loading amount Cu^+ (mmol/g)	Adsorption Capacity (mgS/g)
SBA-15	816	547	3.8	5.35
AS-5	650	440	3.9	Not Reported
AS-10	603	366	3.7	7.70
AS-20	442	251	3.8	Not Reported

1.2.3 (b) Aluminosilicates applied to JP-8

Song and coworkers loaded a $SiO_2{-}Al_2O_3$ framework with 55 wt.% metallic nickel prepared by wet impregnation followed by pre-reduction at 500 ^oC in hydrogen

gas and passivation with hexane.[66] The authors explored a variety of column dimensions and tested with JP-8, and a light fraction of JP-8, to optimize the use of this sorbent with the goal of an adsorption capacity of 10 mgS/g.[66] For actual JP-8 they were able to get a 30 ppm_wS breakthrough capacity of 6 mgS/g, whereas the light JP-8 had a breakthrough capacity of 16 mgS/g.[66] This paper demonstrated the possibility of fractioning before performing adsorptive desulfurization to reach lower sulfur levels.[66] Importantly, they showed that even with unfractioned actual JP-8 they were able to obtain sub 30 ppm_wS levels, which is an important step towards the ultimate goal of sub 1 ppm_wS levels for SOFC applications.[66] Also, they demonstrated the possibility of using metallic metal for desulfurization, rather than metal ions or metal oxides. No regeneration was reported, however, for this material.

1.2.4 Functionalized Silica Frameworks

Functionalizing the surface of silica, which is not normally very active, allows for the creation of active sites. These active sites are either those of the attached ligands themselves or those formed by attaching a binding site, typically a metal ion, to the ligand. The latter is more beneficial than loading native silica with metal ions because it allows for better dispersion of the metal ion as well as an efficient system for anchoring the metal ion to the framework. Figure 1.8 shows the general process for adding ligand functionalization to a silica surface to create a site for metal binding and ultimately an adsorptive desulfurization site.

1.2.4 (a) Functionalized Silica Frameworks for Model Fuel Desulfurization

Ligand functionalized silica has been used for adsorptive desulfurization from liquid fuels,[67, 68] gas phase fuels,[69] and for oxidative desulfurization.[70-74] Recently, Song and coworkers functionalized MCM-41 with aminopropyl groups (using 3-aminopropyltrimethoxysilane followed by Cu^{2+} loading, in a synthetic method similar to that shown in Figure 1.8) and the material showed promising results in the desulfurization of a light model fuel.[67] Metal ions anchored by the ligand groups were more efficient at removing the sulfur compounds than just MCM-41 loaded with Cu^{2+}. The ligand modified version removed approximately 1.8 mgS/mmol Cu whereas the ligand-free version removed approximately 0.7 mgS/mmol Cu.[67] The authors attributed this increase to the ligand's ability to better distribute the adsorption sites (Cu^{2+}).[67] But the ligand-free version had its copper as an oxide compared to Cu^{2+} in the ligand version, which could also account for the difference in efficiency. As seen in the previously mentioned study with MCM-41 and SBA-15, copper oxide materials have lower adsorption capacities than copper ion containing frameworks.

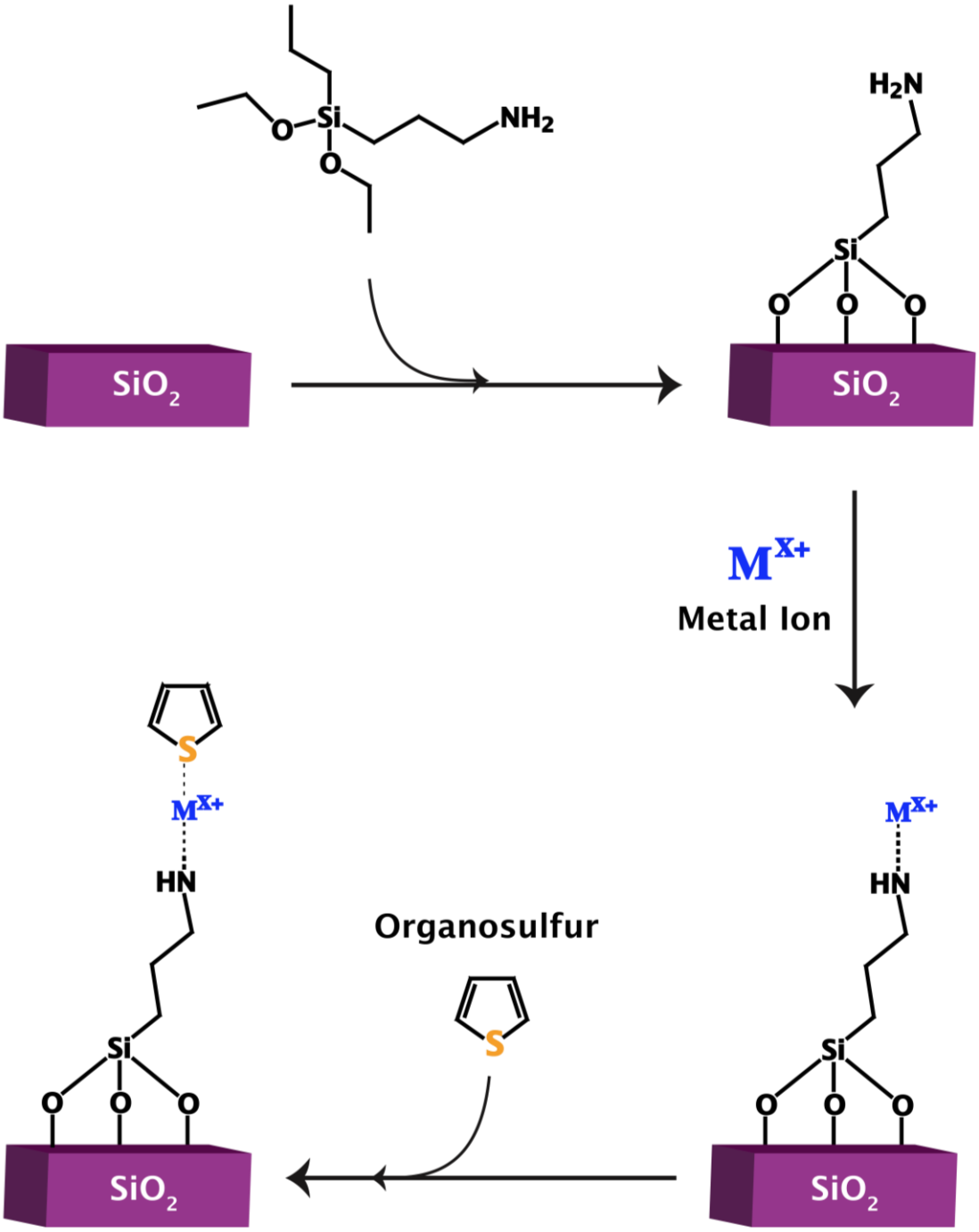

Figure 1.8. The general functionalization and metal loading of silica for sulfur adsorption.

1.2.4 (b) Functionalized Silica Frameworks for JP-8 Desulfurization

Tran *et al.* explored ligand functionalized silica frameworks loaded with gold ions (Au^+/SiO_2) and compared it to silica loaded with gold nanoparticles ($AuNP/SiO_2$) for the desulfurization of JP-8 (430 ppm_wS).[68] The synthesis followed the general method shown in Figure 1.8. The framework was prepared by functionalizing silica gel with an average pore size of 100 Å using 3-aminopropyltriethoxysilane, followed by a 2-3 hour exchange with 5 mM $HAuCl_4$.[68] Gold nanoparticles were also synthesized using $HAuCl_4$, sodium citrate, and sodium borohydride followed by a pH adjustment to 5 before addition of silica.[68] After several hours of stirring, the material was isolated, dried, and calcined.[68] The characterization of Au^+/SiO_2 and $AuNP/SiO_2$ is summarized in Table 1.9.

Table 1.9 Adsorbent properties and Au^+/SiO_2 adsorption capacity at room temperature[68]

Framework	Au wt.%	Surface Area (m^2/g)	Adsorption Capacity (mgS/g)
Au^+/SiO_2	6.6	264.2	5.7 mgS/g
$AuNP/SiO_2$	0.06	361.6	

Au^+/SiO_2 has an adsorption capacity of 5.7 mgS/g at room temperature, and 6.3 mgS/g at 80 ^oC.[68] Column studies reveal that Au^+/SiO_2 initially removes 80% of sulfur content from the JP-8, then dropping to about 70% after two milliliters have been processed.[68] This represents an initial outlet sulfur concentration of

approximately 80-90 ppm_wS.[68] Column studies comparing room temperature and 80 ^oC with Au^+/SiO_2 reveal similar initial sulfur removal for the first few milliliters of processed fuel, but 80 ^oC extends the amount of fuel that can be processed with 70% sulfur removal.[68] The $AuNP/SiO_2$ material is saturated much more quickly. It has a similar initial removal, but quickly drops to approximately 30% sulfur removal before two milliliters have been processed.[68] Solvent regeneration was performed using isooctane on Au^+/SiO_2 and demonstrated essentially 100% regeneration on the second cycle, showing no appreciable loss of adsorption.[68]

Further studies would be needed to explore the difference between gold ions and nanoparticles, as the materials did not contain the same loading content. The regeneration of Au^+/SiO_2 is very encouraging, and if the material could reach a deeper level of desulfurization then this could be a promising material. The use of ligand functionalization appears to be an effective way of maintaining adsorption properties over multiple cycles, likely preventing the loss of metal during regeneration.

1.2.5 Titania

1.2.5 (a) Titania for Desulfurization of JP-8

TiO_2 (commercial available catalyst carrier, anatase phase with a surface area of 150 m^2/g) loaded with 4 wt.% Ag was found to have a saturation capacity of 2.9 mgS/g with JP-8 (630 ppm_wS) compared to a saturation capacity of 6.3 mgS/g for JP-5 (1172 ppm_wS).[23] Breakthrough capacities for JP-5 and light JP-5 were obtained at a 10 ppm_wS level, whereas sub 10 ppm_wS concentrations were not achievable for JP-

8.[23] The latter is attributed to the trimethylbenzothiophenes that are prevalent in JP-8 and were unable to be removed, but are not present in JP-5.[23] The regenerability of this material was reported for use with JP-5; it was able to maintain its breakthrough for 10 cycles following thermal regeneration in air.[23] The authors decided on TiO_2 as a framework after also investigating γ-Al_2O_3 and SiO_2 as supports for silver.[23] For 10 ppm_wS breakthrough capacity, the 4 wt.% Ag loaded supports ranked $SiO_2 < TiO_2 < \gamma$-Al_2O_3 and for saturation adsorption capacity ranked $TiO_2 < \gamma$-$Al_2O_3 < SiO_2$.[23] These results didn't directly point to TiO_2 being the best support, but further testing showed that TiO_2 was the best support in terms of silver dispersion and thermal stability.[23] TiO_2 has been recognized as a stable support for silver in previous research.[75] Once TiO_2 was determined to be worthwhile, the researchers further investigated the effects of surface area and determined that of the three TiO_2 frameworks tested, the highest surface area material was best.[23] Silver loading was also optimized and found that highly dispersed silver is preferred.[23]

1.2.5 (b) Titania Surface Properties for Desulfurization

Titania is an attractive option for desulfurization frameworks due to its low cost and availability, it has been used primarily loaded with silver for adsorptive desulfurization.[23, 76-81] Density functional theory has been used to better understand the interactions that organosulfur compounds have with the surface of titania. Song and coworkers studied the interaction between thiophene and the (001) surface of anatase phase TiO_2 (Figure 1.9) and found that on perfect anatase, the strongest

adsorption occurs between the sulfur and the titanium cation.[79] For oxygen poor surfaces, the sulfur can occupy an oxygen vacancy on the surface and interact with two neighboring titaniums.[79] For an oxygen rich surface, they calculated that the primary interaction is between the extra oxygen atoms, and no longer with the titanium.[79] Overall, the oxygen rich environment has the largest calculated affinity for thiophene.[79] These findings have yet to be followed up with experimental data.

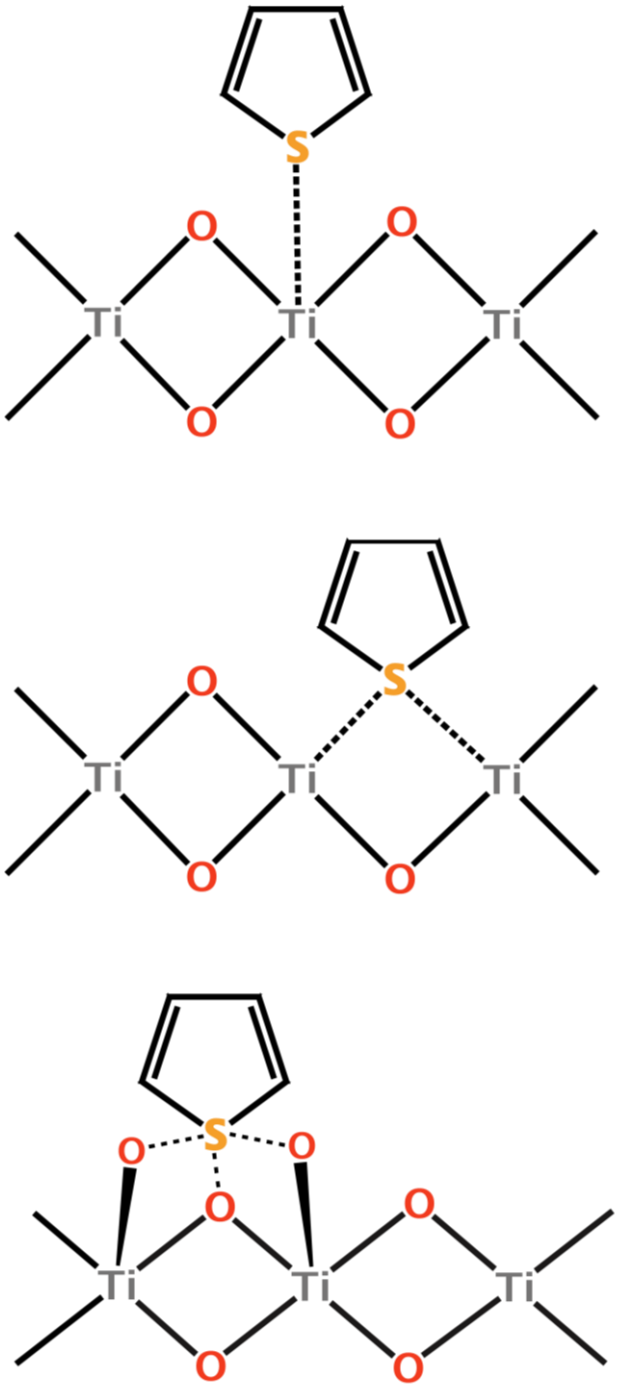

Figure 1.9 Representation of different binding configurations of thiophene on: anatase TiO_2 (top); oxygen poor anatase TiO_2 (middle); oxygen rich anatase TiO_2 (bottom).

1.2.6 Titania Supported on Metal Oxides

More common than pure titania are adsorbents made from either mixed metal titanium oxide or titania supported on other metal oxides.[82-87] In addition to the extensive research on titania dispersed on alumina and silica, which will be discussed below, titania is often mixed with ceria for desulfurization. Ceria is used because it can help lead to oxygen rich sites which have been shown to be effective for adsorptive desulfurization, as shown in Figure 1.9.[82]

1.2.6 (a) Titania Supported on Metal Oxides for Desulfurization of JP-8

Tatarchuk and coworkers prepared a variety of metal oxide supports and performed 48 hour saturation capacity experiments with JP-8.[86] The following Table 1.10 shows the capacities and surface areas using JP-5 fuel.[86] The authors tried three different titania precursors: titanium isopropoxide, titanium (IV) chloride, and titanyl oxide sulfate.[86] These precursors were loaded onto a gamma-Al_2O_3 support *via* incipient wetness impregnation followed by calcination in air.[86] Titanium isopropoxide produced the best results, likely due to the ease of hydrolysis of this precursor thus giving a larger amount of titania dispersed on the surface.[86] Titania loading was also examined, and it was found that Ti:Al = 1:4.4 was an optimal balance between high titania content without starting to block pores and reduce the surface area of the gamma-Al_2O_3 support.[86] Silver loading tests revealed that the optimum loading is between 8 and 12 wt.%, as a balance of providing adsorption sites without starting to block pores and reduce available surface area.[86] Thermal

regeneration was performed on 12 wt.% Ag/TiO_x-Al_2O_3 and the adsorption for JP-5 remained relatively constant over 5 cycles.[86] This is consistent with the thermal regeneration data previously seen with other metal oxide loaded frameworks.

Table 1.10 Surface area and desulfurization results from Tatarchuk and coworkers summarized using JP-5 (1172 ppm_wS)[86]

Framework	BET Surface Area m^2/g	BET Surface Area m^2/g with 4 wt.% Ag	Adsoprtion Capacity mgS/g	Adsoprtion Capacity with 4 wt.% Ag mgS/g	Breakthrough 10 ppm_wS
TiO2	154		2.81	5.65	0.79
Al_2O_3	267		2.77		
SiO_2	319		2.67		
Y-zeolite	660		2.35		
TiO_x–Al_2O_3 (Ti:Al = 1:4.4)	237	222	3.32	10.55	0.90
TiO_x–SiO_2 (Ti:Si = 1:3.9)	304	263	2.98	7.36	0.67
TiO_x–Al_2O_3 (Ti:Al = 1:4.4) (10% Ag)[88]				8.01	0.38

4 wt.% Ag/TiO_x-Al_2O_3 (Ti:Al = 1:4.4) had a 10 ppm_wS breakthrough capacity of 0.12 mgS/g with JP-8 (630 ppm_wS) compared to a breakthrough capacity of 0.90 mg/S with JP-5 (1172 ppm_wS). The saturation adsorption capacity is 6.11 mgS/g for

JP-8 compared to 10.11 mgS/g for JP-5.[86] These adsorption capacities highlight the relative difference in desulfurization level between JP-5 and the more difficult JP-8.

1.2.6 (b) Titania Supported on Metal Oxides: Mechanistic Studies

Further investigation of TiO_x-Al_2O_3 prove that 10 wt.% is the optimal silver loading.[88] Comparisons using model fuels with 10 wt.% Ag/TiO_x-Al_2O_3 show that the presence of non-sulfur containing aromatics decreases the number of available adsorption sites by binding to them. In a competitive binding study between benzene and benzothiophene, benzene occupied 18% of the adsorption sites typically held by benzothiophene.[88] A comparison between 10 wt.% Ag/TiO_x-Al_2O_3 and TiO_x-Al_2O_3 shows that the presence of benzene decreases the capacity of the silver loaded framework, indicating the silver sites are the principle sites for π-complexation with aromatics.[88] IR was used to help determine the adsorption pathways. These studies showed that surface hydroxyl acidic sites were capable of initiating ring opening reactions on adsorbed thiophene and its derivatives to produce aliphatic-like compounds.[88] Additional studies revealed that the surface acid sites interacted with the silver to aid with dispersion.[87] In addition, the Brønsted acid sites were capable of adsorbing thiophene, making a direct interaction with the sulfur, while the silver sites (in the form of silver oxide) are capable of π-interaction with both sulfur containing and non-sulfur containing aromatics.[87]

1.3 Conclusions

The outlook for adsorptive desulfurization being a viable method to desulfurize JP-8 to the levels required by SOFCs looks very promising. Materials have demonstrated the ability to obtain JP-8 in very low ppm_wS concentration, at least in small quantities. Some of the materials have proven themselves regenerable, in several cases even reaching 100% regenerability. Going forward, there are certain qualities that lend themselves to effective JP-8 desulfurization adsorbents. Noble metals, including silver, gold, and palladium, seem to be the most promising active sites for future JP-8 adsorptive desulfurization. Framework pore size needs to be larger than trimethyldibenzothiophene species, though there is no benefit in pore sizes that are significantly larger (i.e. MCM-41 has sufficient mesoporosity, SBA-15 sized macropores are unnecessary). In addition, framework properties (metal oxide surface chemistry or ligand functionalization) that allow for highly dispersed metal species typically allow for greater desulfurization capabilities. Thermal regeneration works best when the material is loaded with a metal oxide, but this method can result in the release of sulfur compounds into the atmosphere. Solvent regeneration can isolate the organosulfur contaminants, preventing further pollution. Solvent regeneration can be used on organic functionalized materials and avoids both the oxidation of metal ions and the need for an inert atmosphere.

1.4 References

1. Control of Air Pollution From Motor Vehicles: Tier 3 Motor Vehicle Emission and Fuel Standards. In Agency, U. S. E. P., Ed. Federal Register: 2013; Vol. 78.

2. Smith, S. J.; van Aardenne, J.; Klimont, Z.; Andres, R. J.; Volke, A.; Delgado Arias, S., Anthropogenic sulfur dioxide emissions: 1850-2005. *Atmos. Chem. Phys.* **2011,** 11, (3), 1101-1116.

3. Small, K. A.; Kazimi, C., On the Costs of Air Pollution from Motor Vehicles. *Journal of Transport Economics and Policy* **1995,** 29, (1), 7-32.

4. Löndahl, J.; Swietlicki, E.; Lindgren, E.; Loft, S., Aerosol exposure versus aerosol cooling of climate: what is the optimal emission reduction strategy for human health? *Atmos. Chem. Phys.* **2010,** 10, (19), 9441-9449.

5. Barrett, S. R. H.; Britter, R. E.; Waitz, I. A., Global Mortality Attributable to Aircraft Cruise Emissions. *Environmental Science & Technology* **2010,** 44, (19), 7736-7742.

6. Woody, M.; Haeng Baek, B.; Adelman, Z.; Omary, M.; Fat Lam, Y.; Jason West, J.; Arunachalam, S., An assessment of Aviation's contribution to current and future fine particulate matter in the United States. *Atmospheric Environment* **2011,** 45, (20), 3424-3433.

7. Barrett, S. R. H.; Yim, S. H. L.; Gilmore, C. K.; Murray, L. T.; Kuhn, S. R.; Tai, A. P. K.; Yantosca, R. M.; Byun, D. W.; Ngan, F.; Li, X.; Levy, J. I.; Ashok, A.; Koo, J.; Wong, H. M.; Dessens, O.; Balasubramanian, S.; Fleming, G. G.; Pearlson, M. N.; Wollersheim, C.; Malina, R.; Arunachalam, S.; Binkowski, F. S.; Leibensperger, E. M.; Jacob, D. J.; Hileman, J. I.; Waitz, I. A., Public Health, Climate, and Economic Impacts of Desulfurizing Jet Fuel. *Environmental Science & Technology* **2012,** 46, (8), 4275-4282.

8. Ormerod, R. M., Solid oxide fuel cells. *Chemical Society Reviews* **2003,** 32, (1), 17-28.

9. Kee, R. J.; Zhu, H.; Goodwin, D. G., Solid-oxide fuel cells with hydrocarbon fuels. *Proceedings of the Combustion Institute* **2005,** 30, (2), 2379-2404.

10. Cheekatamarla, P. K.; Finnerty, C. M., Synthesis gas production via catalytic partial oxidation reforming of liquid fuels. *International Journal of Hydrogen Energy* **2008,** 33, (19), 5012-5019.

11. Hu, J.; Wang, Y.; VanderWiel, D.; Chin, C.; Palo, D.; Rozmiarek, R.; Dagle, R.; Cao, J.; Holladay, J.; Baker, E., Fuel processing for portable power applications. *Chemical Engineering Journal* **2003,** 93, (1), 55-60.

12. *Fuel Cell Handbook*. 7 ed.; U.S. Department of Energy, Office of Fossil Energy, Washington, DC: 2004.

13. Hernández, L.; Kafarov, V., Use of bioethanol for sustainable electrical energy production. *International Journal of Hydrogen Energy* **2009,** 34, (16), 7041-7050.

14. Johnson, G.; Hunter, G. *How to Deal with Fuel Found in Theater: AVL Cypress-Cylinder Pressure Based Combustion Control for Consistent Performance with Varying Fuel Properties*; DTIC Document: 2012.

15. Satyapal, S.; Petrovic, J.; Read, C.; Thomas, G.; Ordaz, G., The U.S. Department of Energy's National Hydrogen Storage Project: Progress towards meeting hydrogen-powered vehicle requirements. *Catalysis Today* **2007,** 120, (3-4), 246-256.

16. Campanari, S.; Manzolini, G.; Garcia de la Iglesia, F., Energy analysis of electric vehicles using batteries or fuel cells through well-to-wheel driving cycle simulations. *Journal of Power Sources* **2009,** 186, (2), 464-477.

17. Gomez, A.; Berry, J. J.; Roychoudhury, S.; Coriton, B.; Huth, J., From jet fuel to electric power using a mesoscale, efficient Stirling cycle. *Proceedings of the Combustion Institute* **2007,** 31, (2), 3251-3259.

18. Smith, B. L.; Bruno, T. J., Composition-Explicit Distillation Curves of Aviation Fuel JP-8 and a Coal-Based Jet Fuel. *Energy & Fuels* **2007,** 21, (5), 2853-2862.

19. Beery, G. T.; Clodfelter, R. G.; Gandee, G. W.; Spear, D. M.; Wight, D. C. *Assessment of JP-8 as a Replacement Fuel for the Air Force Standard Jet Fuel JP-4. Part I. Assessment of JP-8/JP-4 Fuel in Noncombat Environment*; Air Force Aero Propulsion Laboratory Wright-Patterson Air Force Base, Ohio: 1975.

20. Lee, I. C.; Ubanyionwu, H. C., Determination of sulfur contaminants in military jet fuels. *Fuel* **2008,** 87, (3), 312-318.

21. *Toxicological Profile for JP-5 and JP-8*; U.S. Department of Health and Human Services, Public Health Service Agency for Toxic Substances and Disease Registry, Division of Toxicology/Toxicology Information Branch, Atlanta, GA 1998.

22. Natelson, R. H.; Kurman, M. S.; Cernansky, N. P.; Miller, D. L., Experimental investigation of surrogates for jet and diesel fuels. *Fuel* **2008,** 87, (10-11), 2339-2342.

23. Nair, S.; Tatarchuk, B. J., Supported silver adsorbents for selective removal of sulfur species from hydrocarbon fuels. *Fuel* **2010,** 89, (11), 3218-3225.

24. Ma, X.; Schobert, H. H., Molecular simulation on hydrodesulfurization of thiophenic compounds over MoS2 using ZINDO. *Journal of Molecular Catalysis A: Chemical* **2000,** 160, (2), 409-427.

25. Huang, X.; King, D. L., Gas-Phase Hydrodesulfurization of JP-8 Light Fraction Using Steam Reformate. *Industrial & Engineering Chemistry Research* **2006,** 45, (21), 7050-7056.

26. Huang, X.; King, D. A.; Zheng, F.; Stenkamp, V. S.; TeGrotenhuis, W. E.; Roberts, B. Q.; King, D. L., Hydrodesulfurization of JP-8 fuel and its microchannel distillate using steam reformate. *Catalysis Today* **2008,** 136, (3-4), 291-300.

27. Strohm, J. J.; Zheng, J.; Song, C., Low-temperature steam reforming of jet fuel in the absence and presence of sulfur over Rh and Rh-Ni catalysts for fuel cells. *Journal of Catalysis* **2006,** 238, (2), 309-320.

28. Ma, X.; Zhou, A.; Song, C., A novel method for oxidative desulfurization of liquid hydrocarbon fuels based on catalytic oxidation using molecular oxygen coupled with selective adsorption. *Catalysis Today* **2007,** 123, (1-4), 276-284.

29. Sundararaman, R.; Ma, X.; Song, C., Oxidative Desulfurization of Jet and Diesel Fuels Using Hydroperoxide Generated in Situ by Catalytic Air Oxidation. *Industrial & Engineering Chemistry Research* 49, (12), 5561-5568.

30. Timko, M. T.; Schmois, E.; Patwardhan, P.; Kida, Y.; Class, C. A.; Green, W. H.; Nelson, R. K.; Reddy, C. M., Response of Different Types of Sulfur Compounds to Oxidative Desulfurization of Jet Fuel. *Energy & Fuels* **2014,** 28, (5), 2977-2983.

31. Wan, M.-W.; Yen, T.-F., Enhance efficiency of tetraoctylammonium fluoride applied to ultrasound-assisted oxidative desulfurization (UAOD) process. *Applied Catalysis A: General* **2007,** 319, (0), 237-245.

32. Etemadi, O.; Yen, T. F., Selective Adsorption in Ultrasound-Assisted Oxidative Desulfurization Process for Fuel Cell Reformer Applications. *Energy & Fuels* **2007,** 21, (4), 2250-2257.

33. Gonzalez, L. A.; Kracke, P.; Green, W. H.; Tester, J. W.; Shafer, L. M.; Timko, M. T., Oxidative Desulfurization of Middle-Distillate Fuels Using Activated Carbon and Power Ultrasound. *Energy & Fuels* **2012,** 26, (8), 5164-5176.

34. Bosmann, A.; Datsevich, L.; Jess, A.; Lauter, A.; Schmitz, C.; Wasserscheid, P., Deep desulfurization of diesel fuel by extraction with ionic liquids. *Chemical Communications* **2001**, (23), 2494-2495.

35. Zhang, S.; Zhang, Q.; Zhang, Z. C., Extractive Desulfurization and Denitrogenation of Fuels Using Ionic Liquids. *Industrial & Engineering Chemistry Research* **2003,** 43, (2), 614-622.

36. Wasserscheid, P.; Jess, A., Deep desulfurization of oil refinery streams by extraction with ionic liquids. *Green Chemistry* **2004,** 6, (7), 316-322.

37. Jiang, X.; Nie, Y.; Li, C.; Wang, Z., Imidazolium-based alkylphosphate ionic liquids - A potential solvent for extractive desulfurization of fuel. *Fuel* **2008,** 87, (1), 79-84.

38. Rodríguez-Cabo, B.; Rodríguez, H.; Rodil, E.; Arce, A.; Soto, A., Extractive and oxidative-extractive desulfurization of fuels with ionic liquids. *Fuel* **2014,** 117, Part A, (0), 882-889.

39. Maghsoudi, S.; Vossoughi, M.; Kheirolomoom, A.; Tanaka, E.; Katoh, S., Biodesulfurization of hydrocarbons and diesel fuels by Rhodococcus sp. strain P32C1. *Biochemical Engineering Journal* **2001,** 8, (2), 151-156.

40. Chang, J. H.; Chang, Y. K.; Ryu, H. W.; Chang, H. N., Desulfurization of light gas oil in immobilized-cell systems of Gordona sp. CYKS1 and Nocardia sp. CYKS2. *FEMS Microbiology Letters* **2000,** 182, (2), 309-312.

41. Rhee, S.-K.; Chang, J. H.; Chang, Y. K.; Chang, H. N., Desulfurization of dibenzothiophene and diesel oils by a newly isolated Gordona strain, CYKS1. In Am Soc Microbiol: 1998; Vol. 64, pp 2327-2331.

42. Alejandro Dinamarca, M.; Orellana, L.; Aguirre, J.; Baeza, P.; Espinoza, G.; Canales, C.; Ojeda, J., Biodesulfurization of dibenzothiophene and gas oil using a bioreactor containing a catalytic bed with Rhodococcus rhodochrous immobilized on silica. *Biotechnology Letters* **2014**, 1-4.

43. Hernández-Maldonado, A. J.; Yang, F. H.; Qi, G.; Yang, R. T., Desulfurization of transportation fuels by π-complexation sorbents: Cu(I)-, Ni(II)-, and Zn(II)-zeolites. *Applied Catalysis B: Environmental* **2005,** 56, (1-2), 111-126.

44. Velu, S.; Ma, X.; Song, C., Selective Adsorption for Removing Sulfur from Jet Fuel over Zeolite-Based Adsorbents. *Industrial & Engineering Chemistry Research* **2003,** 42, (21), 5293-5304.

45. Yang, R. T.; Hernández-Maldonado, A. J.; Yang, F. H., Desulfurization of Transportation Fuels with Zeolites Under Ambient Conditions. *Science* **2003,** 301, (5629), 79-81.

46. Hernández-Maldonado, A. J.; Yang, R. T., Desulfurization of Diesel Fuels by Adsorption via π-Complexation with Vapor-Phase Exchanged Cu(I)−Y Zeolites. *Journal of the American Chemical Society* **2004,** 126, (4), 992-993.

47. Hernández-Maldonado , A. J.; Yang, R. T., Desulfurization of Diesel Fuels by Adsorption via π-Complexation with Vapor-Phase Exchanged Cu(I)-Y Zeolites. *Journal of the American Chemical Society* **2004,** 126, (4), 992-993.

48. Bhandari, V. M.; Hyun Ko, C.; Geun Park, J.; Han, S.-S.; Cho, S.-H.; Kim, J.-N., Desulfurization of diesel using ion-exchanged zeolites. *Chemical Engineering Science* **2006,** 61, (8), 2599-2608.

49. Hernández-Maldonado , A. J.; Yang, R. T., Desulfurization of Diesel Fuels via pi-Complexation with Nickel(II)-Exchanged X- and Y-Zeolites. *Industrial & Engineering Chemistry Research* **2004,** 43, (4), 1081-1089.

50. Hernández-Maldonado , A. J.; Yang, R. T.; Cannella, W., Desulfurization of Commercial Jet Fuels by Adsorption via π-Complexation with Vapor Phase Ion Exchanged Cu(I)-Y Zeolites. *Industrial & Engineering Chemistry Research* **2004,** 43, (19), 6142-6149.

51. Hernández-Maldonado, A. J.; Yang, R. T., Desulfurization of Liquid Fuels by Adsorption via π Complexation with Cu(I)−Y and Ag−Y Zeolites. *Industrial & Engineering Chemistry Research* **2003,** 42, (1), 123-129.

52. Velu, S.; Song, C.; Engelhard, M. H.; Chin, Y.-H., Adsorptive Removal of Organic Sulfur Compounds from Jet Fuel over K-Exchanged NiY Zeolites Prepared by Impregnation and Ion Exchange. *Industrial & Engineering Chemistry Research* **2005,** 44, (15), 5740-5749.

53. Xiao, J.; Li, Z.; Liu, B.; Xia, Q.; Yu, M., Adsorption of Benzothiophene and Dibenzothiophene on Ion-Impregnated Activated Carbons and Ion-Exchanged Y Zeolites. *Energy & Fuels* **2008,** 22, (6), 3858-3863.

54. Kwon, J.-M.; Moon, J.-H.; Bae, Y.-S.; Lee, D.-G.; Sohn, H.-C.; Lee, C.-H., Adsorptive Desulfurization and Denitrogenation of Refinery Fuels Using Mesoporous Silica Adsorbents. *ChemSusChem* **2008,** 1, (4), 307-309.

55. McKinley, S. G.; Angelici, R. J., Deep desulfurization by selective adsorption of dibenzothiophenes on Ag^+/SBA-15 and Ag^+/SiO_2. *Chemical Communications* **2003**, (20), 2620-2621.

56. Wang, Y.; Yang, R. T.; Heinzel, J. M., Desulfurization of jet fuel by π-complexation adsorption with metal halides supported on MCM-41 and SBA-15 mesoporous materials. *Chemical Engineering Science* **2008,** 63, (2), 356-365.

57. Wang, Y.; Yang, R. T.; Heinzel, J. M., Desulfurization of Jet Fuel JP-5 Light Fraction by MCM-41 and SBA-15 Supported Cuprous Oxide for Fuel Cell Applications. *Industrial & Engineering Chemistry Research* **2008,** 48, (1), 142-147.

58. Chen, H.; Wang, Y.; Yang, F. H.; Yang, R. T., Desulfurization of high-sulfur jet fuel by mesoporous π-complexation adsorbents. *Chemical Engineering Science* **2009,** 64, (24), 5240-5246.

59. Wang, Y.; Yang, R. T.; Heinzel, J. M., Desulfurization of Jet Fuel JP-5 Light Fraction by MCM-41 and SBA-15 Supported Cuprous Oxide for Fuel Cell Applications. *Industrial & Engineering Chemistry Research* **2009,** 48, (1), 142-147.

60. Ma, X.; Sun, L.; Song, C., A new approach to deep desulfurization of gasoline, diesel fuel and jet fuel by selective adsorption for ultra-clean fuels and for fuel cell applications. *Catalysis Today* **2002,** 77, (1-2), 107-116.

61. Li, W.; Liu, Q.; Xing, J.; Gao, H.; Xiong, X.; Li, Y.; Li, X.; Liu, H., High-efficiency desulfurization by adsorption with mesoporous aluminosilicates. *AIChE Journal* **2007,** 53, (12), 3263-3268.

62. He, G.-S.; Sun, L.-B.; Song, X.-L.; Liu, X.-Q.; Yin, Y.; Wang, Y.-C., Adjusting Host Properties to Promote Cuprous Chloride Dispersion and Adsorptive Desulfurization Sites Formation on SBA-15. *Energy & Fuels* **2011,** 25, (8), 3506-3513.

63. Turaga, U. T.; Song, C., MCM-41-supported Co-Mo catalysts for deep hydrodesulfurization of light cycle oil. *Catalysis Today* **2003,** 86, (1-4), 129-140.

64. Li, W.; Tang, H.; Zhang, T.; Li, Q.; Xing, J.; Liu, H., Ultra-deep desulfurization adsorbents for hydrotreated diesel with magnetic mesoporous aluminosilicates. *AIChE Journal* **2010,** 56, (5), 1391-1396.

65. Wang, G.; Wen, Y.; Fan, J.; Xu, C.; Gao, J., Reactive Characteristics and Adsorption Heat of Ni/ZnO–SiO2–Al2O3 Adsorbent by Reactive Adsorption Desulfurization. *Industrial & Engineering Chemistry Research* **2011,** 50, (22), 12449-12459.

66. Velu, S.; Ma, X.; Song, C.; Namazian, M.; Sethuraman, S.; Venkataraman, G., Desulfurization of JP-8 Jet Fuel by Selective Adsorption over a Ni-based Adsorbent for Micro Solid Oxide Fuel Cells. *Energy & Fuels* **2005,** 19, (3), 1116-1125.

67. Song, L.; Bu, T.; Zhu, L.; Zhou, Y.; Xiang, Y.; Xia, D., Synthesis of Organically-Inorganically Functionalized MCM-41 for Adsorptive Desulfurization of C4 Hydrocarbons. *The Journal of Physical Chemistry C* **2014,** 118, (18), 9468-9476.

68. Tran, D. T.; Dunbar, Z. W.; Chu, D., Regenerable sulfur adsorbent for liquid phase JP-8 fuel using gold/silica based materials. *International Journal of Hydrogen Energy* **2012,** 37, (13), 10430-10434.

69. Tailor, R.; Ahmadalinezhad, A.; Sayari, A., Selective removal of SO2 over tertiary amine-containing materials. *Chemical Engineering Journal* **2014,** 240, (0), 462-468.

70. Chen, Y.; Zhao, S.; Song, Y.-F., An efficient heterogeneous catalyst based on highly dispersed $Na_7H_2LaW_{10}O_{36}\cdot 32H_2O$ nanoparticles on mesoporous silica for deep desulfurization. *Applied Catalysis A: General* **2013,** 466, (0), 307-314.

71. Zheng, H.; Sun, Z.; Chen, X.; Zhao, Q.; Wang, X.; Jiang, Z., A micro reaction-controlled phase-transfer catalyst for oxidative desulfurization based on polyoxometalate modified silica. *Applied Catalysis A: General* **2013,** 467, (0), 26-32.

72. Zhu, M.; Luo, G.; Kang, L.; Dai, B., Novel catalyst by immobilizing a phosphotungstic acid on polymer brushes and its application in oxidative desulfurization. *RSC Advances* **2014,** 4, (32), 16769-16776.

73. Wei, X.; Husson, S. M.; Mello, M.; Chinn, D., Removal of Branched Dibenzothiophenes from Hydrocarbon Mixtures via Charge Transfer Complexes with a TAPA-Functionalized Adsorbent. *Industrial & Engineering Chemistry Research* **2008,** 47, (13), 4448-4454.

74. Luo, G.; Kang, L.; Zhu, M.; Dai, B., Highly active phosphotungstic acid immobilized on amino functionalized MCM-41 for the oxidesulfurization of dibenzothiophene. *Fuel Processing Technology* **2014,** 118, (0), 20-27.

75. Seyedmonir, S. R.; Strohmayer, D. E.; Guskey, G. J.; Geoffroy, G. L.; Vannice, M. A., Characterization of supported silver catalysts: III. Effects of support, pretreatment, and gaseous environment on the dispersion of Ag. In Elsevier: 1985; Vol. 93, pp 288-302.

76. Nair, S.; Tatarchuk, B., Characteristics of sulfur removal by silver-titania adsorbents at ambient conditions. *Adsorption* **2011,** 17, (4), 663-673.

77. Samokhvalov, A.; Duin, E. C.; Nair, S.; Bowman, M.; Davis, Z.; Tatarchuk, B. J., Study of the Surface Chemical Reactions of Thiophene with Ag/Titania by the Complementary Temperature-Programmed Electron Spin Resonance, Temperature-Programmed Desorption, and X-ray Photoelectron Spectroscopy: Adsorption, Desorption, and Sorbent Regeneration Mechanisms. *The Journal of Physical Chemistry C* **2010,** 114, (9), 4075-4085.

78. Sitamraju, S.; Janik, M.; Song, C., Selectivity of Adsorption of Thiophene and its Derivatives on Titania Anatase Surfaces: A Density Functional Theory Study. *Topics in Catalysis* **2012,** 55, (5-6), 229-242.

79. Guo, J.; Watanabe, S.; Janik, M. J.; Ma, X.; Song, C., Density functional theory study on adsorption of thiophene on TiO2 anatase (0 0 1) surfaces. *Catalysis Today* **2010,** 149, (1-2), 218-223.

80. Webster, E. R.; Park, A.; Stratton, M. B.; Park, V. C.; Mosier, A. M.; Shine, R. S.; Benz, L., Adsorption of Dibenzothiophene and Fluorene on TiO2(110) and Supported Ag Clusters. *Energy & Fuels* **2013,** 27, (11), 6575-6580.

81. Wang, X.-j.; Li, F.-t.; Liu, J.-x.; Kou, C.-g.; Zhao, Y.; Hao, Y.-j.; Zhao, D., Preparation of TiO2 in Ionic Liquid via Microwave Radiation and in Situ Photocatalytic Oxidative Desulfurization of Diesel Oil. *Energy & Fuels* **2012,** 26, (11), 6777-6782.

82. Xiao, J.; Wang, X.; Fujii, M.; Yang, Q.; Song, C., A novel approach for ultra-deep adsorptive desulfurization of diesel fuel over TiO2–CeO2/MCM-48 under ambient conditions. *AIChE Journal* **2013,** 59, (5), 1441-1445.

83. Xiao, J.; Sitamraju, S.; Chen, Y.; Janik, M.; Song, C., Air-Promoted Adsorptive Desulfurization over Ti0.9Ce0.1O2 Mixed Oxides from Diesel Fuel under Ambient Conditions. *ChemCatChem* **2013,** 5, (12), 3582-3586.

84. Yan, X.-M.; Mei, P.; Xiong, L.; Gao, L.; Yang, Q.; Gong, L., Mesoporous titania-silica-polyoxometalate nanocomposite materials for catalytic oxidation desulfurization of fuel oil. *Catalysis Science & Technology* **2013,** 3, (8), 1985-1992.

85. Xiao, J.; Wang, X.; Chen, Y.; Fujii, M.; Song, C., Ultra-Deep Adsorptive Desulfurization of Light-Irradiated Diesel Fuel over Supported TiO2-CeO2 Adsorbents. *Industrial & Engineering Chemistry Research* **2013,** 52, (45), 15746-15755.

86. Shahadat Hussain, A. H. M.; Tatarchuk, B. J., Adsorptive desulfurization of jet and diesel fuels using $Ag/TiO_x–Al_2O_3$ and $Ag/TiO_x–SiO_2$ adsorbents. *Fuel* **2013,** 107, 465-473.

87. Shahadat Hussain, A. H. M.; Tatarchuk, B. J., Mechanism of hydrocarbon fuel desulfurization using Ag/TiO2-Al2O3 adsorbent. *Fuel Processing Technology* **2014,** 126, (0), 233-242.

88. Hussain, A. H. M. S.; Yang, H.; Tatarchuk, B. J., Investigation of Organosulfur Adsorption Pathways from Liquid Fuels onto Ag/TiO_x-Al_2O_3 Adsorbents at Ambient Conditions. *Energy & Fuels* **2013,** 27, (8), 4353-4362.

Chapter 2

Agarose Templated Hierarchical Mesoporous Monoliths for Adsorptive Desulfurization

Abstract

Hierarchical mesoporous materials are of interest for a variety of applications, such as battery matreials and biomaterials, due to their high surface area and tunable pore size. These qualities make them potential sorbents for desulfurization of JP-8, which requires organosulfur removal prior to use as a feedstock for solid oxide fuel cells. Hierarchical mesoporous monoliths were synthesized using Zeolite Y and Al-SBA-15 with agarose as a templating agent. Al-SBA-15 monolith is more effective than Zeolite Y monolith towards JP-8, which is attributed to the pore size of Zeolite Y being too small to accommodate the organosulfur compounds found in JP-8. However, there is no increase in efficacy between Al-SBA-15 monolith and Al-SBA-15 bulk powder for this application.

2.1 Introduction

Hierarchical porous materials have multiple levels of pore sizes: larger sized pore channels leading to smaller sized pore channels (similar to the human vascular system with larger veins leading to smaller capillaries). These materials are sought after for a variety of applications including the obvious adsorption[1, 2] and catalysis[3, 4], and also more exotic applications such as tissue engineering[5, 6] and electronics[7, 8]. These materials can be made out of organic materials[9, 10] or inorganic materials including titania[11], silica[12], or zeolites[3, 13]. Their tunable porosity and surface area paired with different surface chemistries based on their precursors, these materials can be used for highly varied applications. Polymer based materials heiracrical porous materials show promise for applications including pollution remediation. A hierachical porous sponge made of polyurethane and polysiloxane has been reported as cleanup material for oil spills in the ocean.[1] This low-cost material can be reused in excess of 300 cycles, while showing excellent oil removing performance.[1] Hierachical porous materials can also mimic biological tissue. Bioactive glass foam can be produced with a similar hierarchical structure to bone, and can be tailored to meet tissue regeneration needs.[5] Due to their extensive potential applications, advances made in the synthesis of hierarchical porous material can benefit many fields of research.

The synthesis techniques range from one-pot syntheses both with and without templating agents, and can include post-synthetic modifications. We will focus on the use of organic templating agents, particularly agarose, to form porous networks.

Figure 2.1 shows how, with the addition of water and heat, the polymer chains of agarose can form hydrogels. These polymer networks are the perfect inverse to a porous framework, and thus have been exploited to make solid porous monoliths.

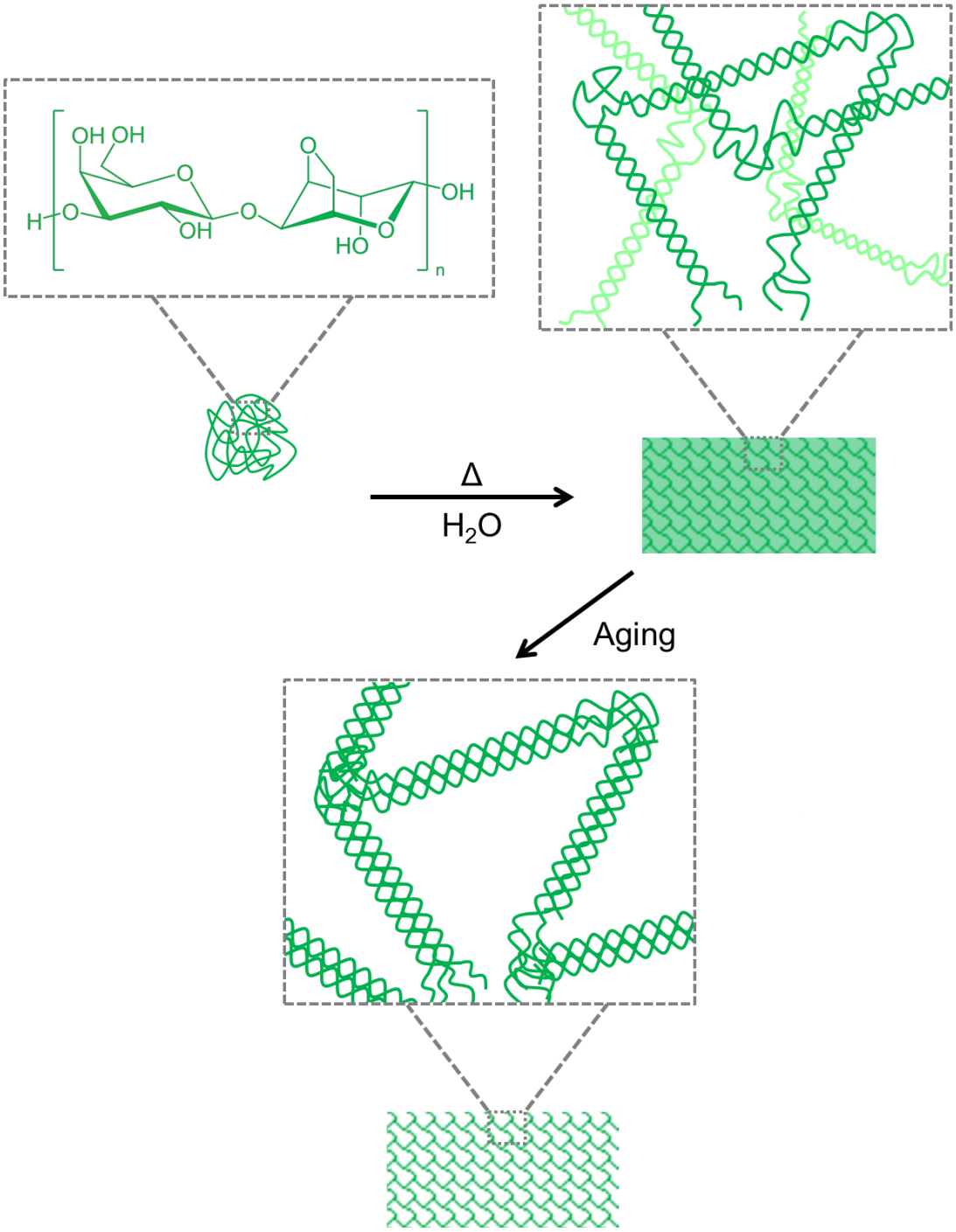

Figure 2.1 The formation of an agarose hydrogel using agarose polymer, water, and heat. The agarose polymer distributes throughout the water into an amorphous hydrogel network.

Research groups, including ours, have utilized agarose hydrogels to construct inorganic porous monoliths.[14-17] As shown in Figure 2.2, the hydrogel is typically exchanged in a non-aqueous solvent such as ethanol (typically by first soaking in a 50:50 water:organic solvent solution) before being placed in a metal oxide precursor. This precursor can be a variety of metal alkoxides, including tetraethyl orthosilicate and titanium isopropoxide. The gel is then transferred to either pure water or water with a catalyst to achieve a solid metal oxide monolith that contains the organic agarose network. The agarose network can then be removed chemically, with solvents such as DMSO, or thermally, leaving behind a solid monolith with pores in the spaces once occupied by the agarose network. The porosity can easily be tuned by adjusting the level of agarose in the initial gel.

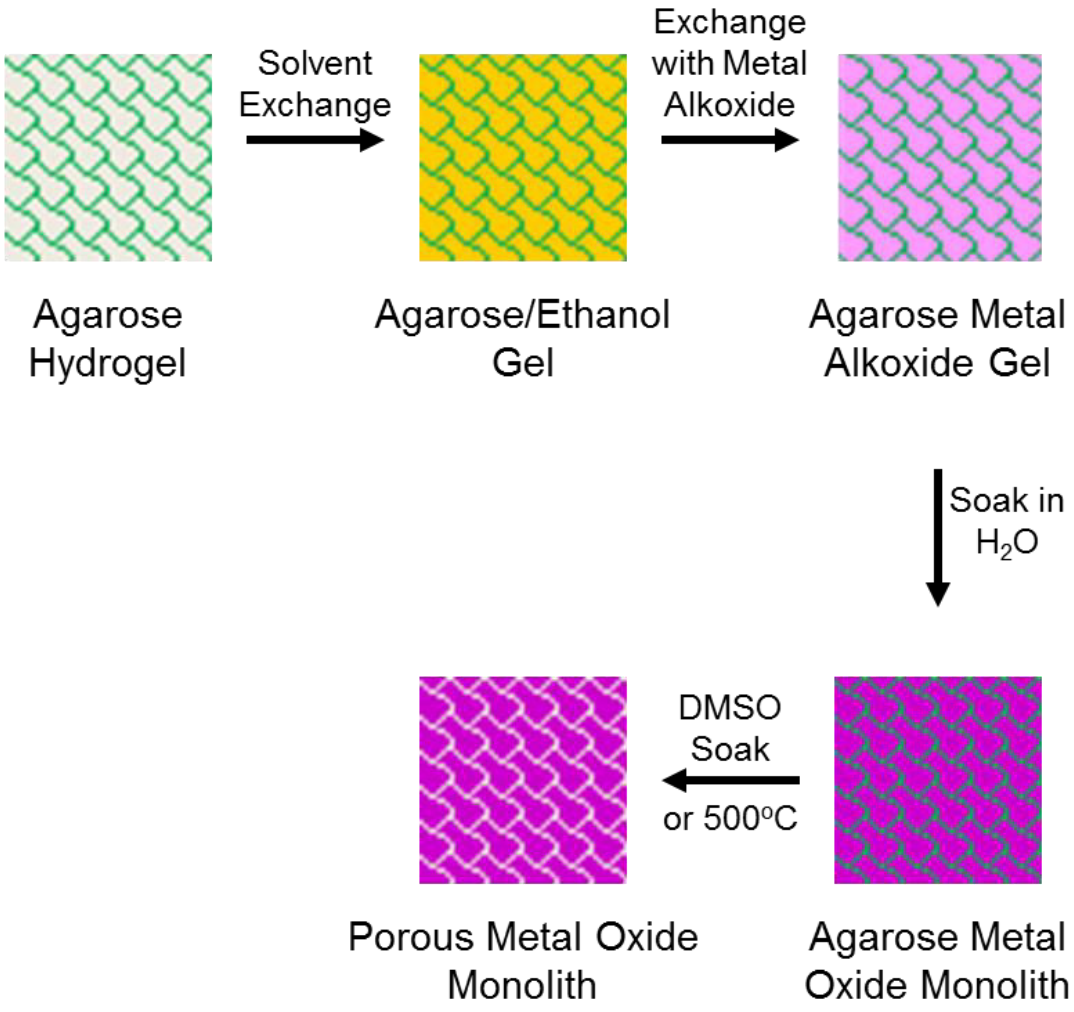

Figure 2.2 Synthetic procedure to produce porous metal oxide monoliths using agarose as a templating agent.

These agarose templated materials have been applied to several applications, particularly by Caruso and coworkers. The majority of reports have been for photocatalytic materials.[18, 19] Porous TiO_2 containing gold nanoparticles demonstrated photocatalytic activity, making it a potential material for environmental remidation.[18] Adsorption properties have also been explore, porous zirconium titanium mixed oxide pellets were found to have a high capacity and adsorption rate for the adsorption of

vanadate (a model species).[17] These templated materials have also shown promise as electrodes for dye-sensitized solar cells.[20]

Herein, we will describe the first use of agarose gel to make hierarchical mesoporous monoliths. Instead of using metal oxide precursors to fill the gel, gels were filled with bulk porous powders of either Zeolite Y or Al-SBA-15 during the initial agarose gel formation. Calcination at a high enough temperature to sinter the powder together resulted in a hierarchical porous monolith: larger pores left by the agarose lead to smaller pores where the walls are either Zeolite Y or Al-SBA-15. These materials were tested for their capacity as adsorptive desulfurization materials. Ideally, using these hierarchical porous materials will allow for larger organosulfur contaminants to be trapped in the large pore formed by the agarose network, whereas smaller contaminates will travel into the pores of the SBA-15 or Zeolite Y and be trapped. Hierarchical porous materials have yet to be used for desulfurization. However, SBA-15 and Zeolite Y have shown promising results for this application.[21, 22]

2.2 Experimental

2.2.1 Materials

All chemicals were used as received without further purification. Tetraethylorthosilicate (TEOS), agarose, and aluminum isopropoxide were all obtained from Acros Organics. HCl was obtained from Fisher Scientific, silver nitrate was obtained through MP Biomedicals, 200 proof ethanol from Decon Labs, poly (ethylene glycol)-block-poly(propylene glycol)-block-poly(ethylene glycol) with a feed ratio of 20:70:20 of EO:PO:EO (Pluronic P123) from Sigma-Aldrich, and Zeolite Y from Zeolyst.

2.2.2 Zeolite Y Monoliths and Silver Loading

Two methods were used to prepare silver loaded Zeolite Y monoliths. The first involves creating a monolith and then exchanging with silver (labeled Zeolite Y Monolith-PSE, PSE for post-synthesis exchange). The second uses Zeolite Y already exchanged with silver as the wall material (labeled Zeolite Y Monolith-IE, IE for initial exchange). Zeolite Y monolith-PSE was prepared by mixing 24.5 g doubly distilled deionized water, 0.50 g agarose, and 3.2 g Zeolite Y in a covered beaker with gentle heating and magnetic stirring. Once the agarose dissolved, the solution was cast in a plastic petri dish resulting in a gel slightly less than 1 cm thick. Once the gel cooled to room temperature it was cut with a razor into approximately 1 cm cubes. These cubes were allowed to dehydrate at room temperature for at least 24 hours. Once dried, the cubes were calcined at 500, 700, or 800^{o}C for 6 hours with a 1^{o}C/min

ramp rate. After calcination, the cubes were further cut into smaller pieces before being exchanged in a 0.3 mM silver nitrate solution for 24 hours, rinsed with doubly distilled deionized water, and repeated for a total of two exchanges and rinses. Zeolite Y monolith-IE was prepared according to an identical method; the Zeolite Y powder, however, was exchanged twice in a silver nitrate solution before the creation of the monolith.

2.2.3 Al-SBA-15 Monolith Synthesis

The Al-SBA-15 Monolith was made according to the same overall procedure as Zeolite Y Monolith-PSE except the following amounts were used to make the initial gel: 0.35 g uncalcined Al-SBA-15 (synthetic procedure found in Chapter 3), 0.31 g agarose, and 14.74 g doubly distilled deionized water. It was calcined at 750^{o}C for 6 hours with a 1^{o}C/min ramp rate. The exchange procedure was identical to Zeolite Y Monolith-PSE.

2.2.4 Characterization

Powder X-Ray Diffraction (PXRD) was performed on a Rigaku MiniFlex+ X-ray diffractometer with Cu Kα radiation. Samples were analyzed from 1.5º to 10º (2θ) with a step size of 0.01º and scan rate of 1^{o} per minute. BET surface area of the samples was measured by physical adsorption of N_2 at 77 K using a Micromeritics physisorption analyzer (TriStar II 3020 v1.03). Adsorption/desorption isotherm measurements were collected in the relative pressure range (P/P_o) from 0.01 to 1.00.

2.2.5 JP-8 fuel test

Prior to all JP-8 and model fuel testing, the adsorbents were heated under vacuum at 110 °C overnight to remove trapped gas or water. For column tests (breakthrough and regeneration), the prepared materials were packed in a Chrom Tech column (4.6 mm ID, 50 mm length). JP-8 fuel was pumped at 0.5 mL/min into the column using a Shimadzu HPLC pump. Column and 24-hour batch (beaker) test experiments were analyzed for total sulfur concentration using a UV total sulfur analyzer (multi EA 3100, Analytikjena) with a detection limit of 45 ppb. Typical batch test experiments were done with ~ 2.8 g of sorbent in ~ 5.5 g of JP-8, whereas column experiments were done with ~ 0.18 g of sorbent.

2.3 Results and Discussion

2.3.1 Synthesis and Characterization

The general synthetic procedure for the Zeolite Y and Al-SBA-15 containing monoliths are shown in Figure 2.3.

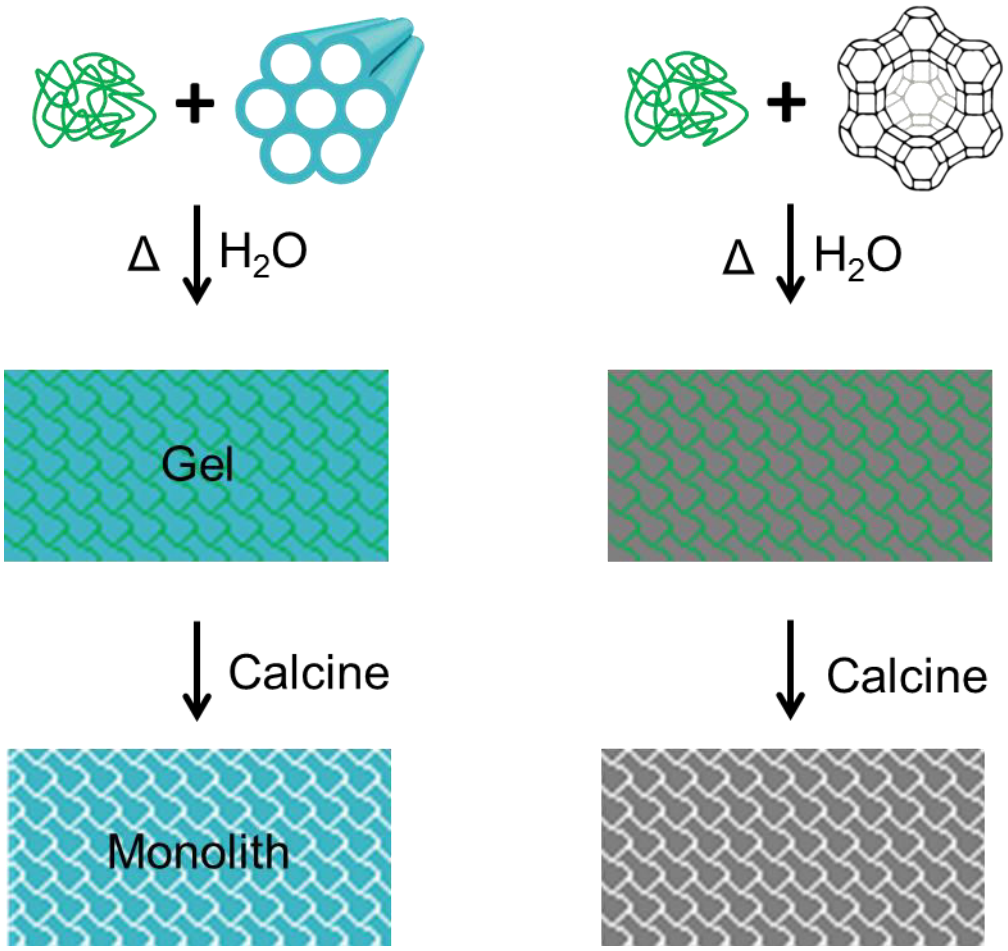

Figure 2.3 The synthetic procedure of creating hierarchical mesoporous monoliths. The porous powders (Zeolite Y or Al-SBA-15) are combined with water and agarose, heated to form a gel, cast and dried, followed by calcination at a high enough temperature to sinter the powder together.

The calcination temperature was important to control in order to yield solid monoliths instead of powders. Low temperatures did not allow for sintering of the

particles together, whereas too high of temperatures will eventually cause a collapse of the pore system in the Zeolite Y or Al-SBA-15. Figure 2.4 shows the difference in stability between calcining a sample at 500^{o}C and 700^{o}C.

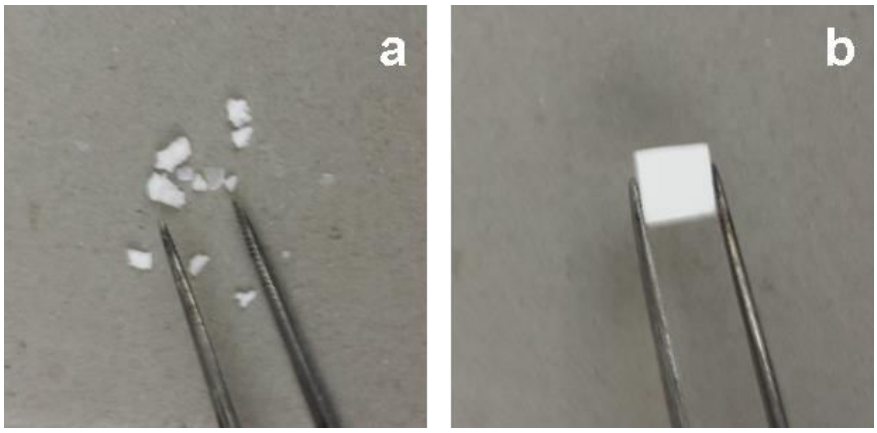

Figure 2.4 Zeolite Y Monolith calcined at 500^{o}C (a) and at 700^{o}C (b), actual size shown.

PXRD was used to confirm that the nanoporous Zeolite Y structure did not collapse during calcination. Figure 2.5 shows only a slight decrease in overall crystallinity as the intensity of the peaks decreases at 800^{o}C. Overall, the Zeolite Y structure stays intact. The pore size of Al-SBA-15 is too large to confirm through typical PXRD analysis ((100) is below 1.5^{o}).

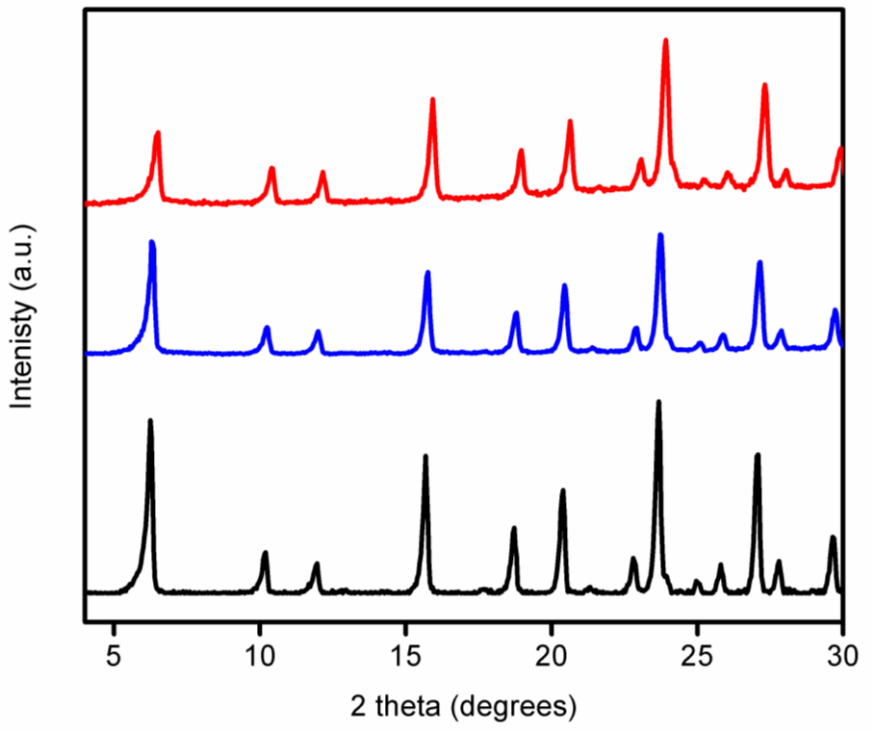

Figure 2.5 PXRD analysis of Zeolite Y (black) after calcination at 700°C (blue) and at 800°C (red).

2.3.2 Fuel Testing

Silver exchanged zeolites and SBA-15 have been shown to be effective desulfurization adsorbents.[22, 23] Column studies were performed on Zeolite Y monoliths exchanged with silver. A comparison was performed between the two methods used to prepare silver loaded Zeolite Y monoliths. The first method consists of creating a monolith and then exchanging with silver (labeled Zeolite Y Monolith-PSE, PSE for post-synthesis exchange). The second uses Zeolite Y already exchanged with silver (labeled Zeolite Y Monolith-IE, IE for initial exchange). As shown in Figures 2.6 and 2.7, Zeolite Y Monolith-PSE performed better than Zeolite Y

Monolith-IE. It did not fully saturate until it processed 20 mL of fuel, compared to just 5 mL of fuel for the pre-exchanged monolith. Furthermore, the Zeolite Y Monolith-PSE had approximately three times the adsorption capacity compared to Zeolite Y Monolith-IE. We attribute this to Zeolite Y Monolith-PSE containing most of its silver as Ag^+, where Zeolite Y Monolith-IE likely contains mostly silver oxide. The process of heating the silver ions in the Zeolite Y Monolith-IE in air at temperatures in excess of 500^{o}C would convert them to silver oxide. Similar materials impregnated with silver salts have shown conversion to silver oxide under these conditions.[24-26] Additionally, the Zeolite Y Monolith-PSE contains more surfaces for the Ag^+ to be adsorbed onto: inside the Zeolite Y and inside the pores created by the agarose template. This could lead to an increase in Ag^+ sites, allowing for greater sulfur adsorption.

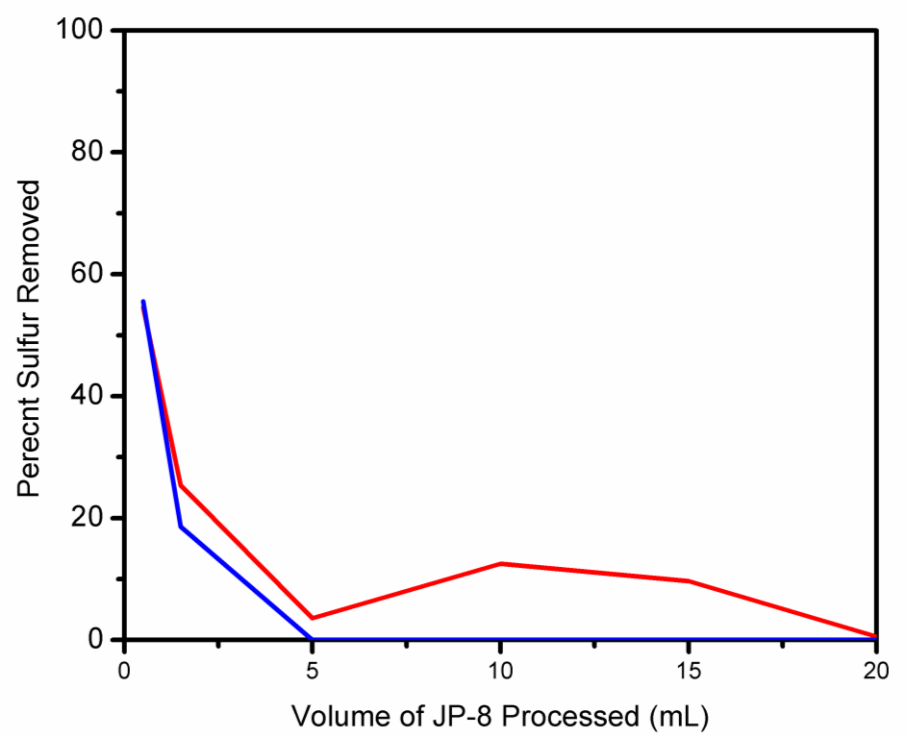

Figure 2.6 Column study of Zeolite Y Monolith-PSE (red) and Zeolite Y Monolith-IE (blue). The study was performed with JP-8 fuel, showing the percent sulfur removed from the fuel.

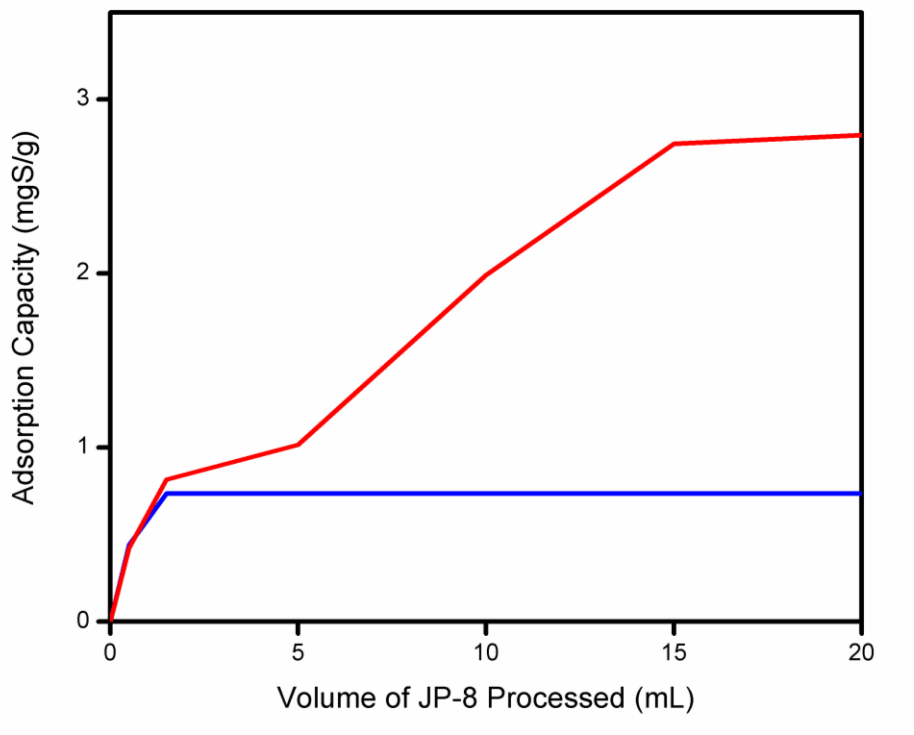

Figure 2.7 Column study of Zeolite Y Monolith-PSE (red) and Zeolite Y Monolith-IE (blue). Study done with JP-8 fuel, displaying the difference in adsorption capacity.

While this study did provide insight into the effectiveness of different silver exchange procedures, the overall sulfur adsorption of these materials is subpar. For both monoliths, the initial outlet fuel concentration was ~ 270 ppm_wS, far from the sub 1ppm_wS desired for fuel cell applications. It has been shown the pore size of Zeolite Y is too small to accommodate the larger sulfur contaminants found in jet fuels.[27] The goal for these monoliths was that the larger organosulfur molecules would be adsorbed in the larger pores created by the agarose, and that the smaller contaminants would be trapped in the Zeolite Y pores. However, based on these fuel tests, it can be concluded that Zeolite Y monoliths are not effective adsorptive

desulfurization adsorbents. Due to these results, unloaded Zeolite Y monoliths and bulk silver-exchanged Zeolite Y were not tested.

To address the small pore size issue of Zeolite Y, Al-SBA-15 monoliths were prepared. These monoliths were exchanged with silver post-monolith synthesis, as this was shown more effective than with the Zeolite Y monoliths. This monolith, along with Al-SBA-15 bulk powder, were exchanged with silver under the same conditions, and then compared using a batch 24-hour fuel test with JP-8 (Table 2.1). The Al-SBA-15 monolith was superior to the Zeolite Y monolith, with nearly double the adsorption capacity. However, the monolith and bulk versions of Al-SBA-15 have essentially identical adsorption capacities, showing that there is no practical advantage to using the monolith form for the application. Bulk Al-SBA-15 will be further explored in Chapter 3.

Table 2.1 24-hour batch fuel tests results with JP-8

Sample	Final JP-8 Concentration (ppm_wS)	Adsorption Capacity (mgS/g)
Ag-Al-SBA-15	197.98	5.11
Ag-Al-SBA-15 monolith	190.74	5.12

2.4 Conclusions

Hierarchical mesoporous monoliths can be formed using Zeolite Y or Al-SBA-15 as precursors, and agarose as a templating agent. Calcination temperatures above 500^{o}C are necessary to form a mechanically stable monolith. It is advantageous to exchange these monoliths post-synthetically with silver for adsorptive desulfurization applications. Al-SBA-15 monolith is twice as effective as Zeolite Y monolith as a sorbent. This is attributed to the pore size of Zeolite Y being too small to accommodate all of the contaminants found in JP-8. However, there was no advantage seen in using Al-SBA-15 monolith over the bulk powder version. Therefore, no further exploration will be performed on monoliths, but Al-SBA-15 will undergo further testing in Chapter 3.

2.5 References

1. Zhu, Q.; Chu, Y.; Wang, Z.; Chen, N.; Lin, L.; Liu, F.; Pan, Q., Robust superhydrophobic polyurethane sponge as a highly reusable oil-absorption material. *Journal of Materials Chemistry* **2013,** 1, (17), 5386-5393.

2. Yu, J.; Zhang, L.; Cheng, B.; Su, Y., Hydrothermal preparation and photocatalytic activity of hierarchically sponge-like macro-/mesoporous titania. *The Journal of Physical Chemistry C* **2007,** 111, (28), 10582-10589.

3. Perez-Ramirez, J.; Christensen, C. H.; Egeblad, K.; Christensen, C. H.; Groen, J. C., Hierarchical zeolites: enhanced utilisation of microporous crystals in catalysis by advances in materials design. *Chemical Society Reviews* **2008,** 37, (11), 2530-2542.

4. Parlett, C. M. A.; Wilson, K.; Lee, A. F., Hierarchical porous materials: catalytic applications. *Chemical Society Reviews* **2013,** 42, (9), 3876-3893.

5. Jones, J. R.; Lee, P. D.; Hench, L. L., Hierarchical porous materials for tissue engineering. *Philosophical Transactions of the Royal Society A: Mathematical, Physical and Engineering Sciences* **2006,** 364, (1838), 263-281.

6. Sanchez, C. m.; Arribart, H.; Guille, M. M. G., Biomimetism and bioinspiration as tools for the design of innovative materials and systems. *Nature Materials* **2005,** 4, (4), 277-288.

7. Wang, D.-W.; Li, F.; Cheng, H.-M., Hierarchical porous nickel oxide and carbon as electrode materials for asymmetric supercapacitor. *Journal of Power Sources* **2008,** 185, (2), 1563-1568.

8. Xia, K.; Gao, Q.; Jiang, J.; Hu, J., Hierarchical porous carbons with controlled micropores and mesopores for supercapacitor electrode materials. *Carbon* **2008,** 46, (13), 1718-1726.

9. Fan, L. Z.; Hu, Y. S.; Maier, J.; Adelhelm, P.; Smarsly, B.; Antonietti, M., High electroactivity of polyaniline in supercapacitors by using a hierarchically porous carbon monolith as a support. *Advanced Functional Materials* **2007,** 17, (16), 3083-3087.

10. Wang, D.-W.; Li, F.; Liu, M.; Lu, G. Q.; Cheng, H.-M., 3D Aperiodic Hierarchical Porous Graphitic Carbon Material for High-Rate Electrochemical Capacitive Energy Storage. *Angewandte Chemie* **2008,** 47, (2), 373-376.

11. Zhang, L.; Jimmy, C. Y., A sonochemical approach to hierarchical porous titania spheres with enhanced photocatalytic activity. *Chemical Communications* **2003**, (16), 2078-2079.

12. Sen, T.; Tiddy, G. J. T.; Casci, J. L.; Anderson, M. W., One-Pot Synthesis of Hierarchically Ordered Porous-Silica Materials with Three Orders of Length Scale. *Angewandte Chemie* **2003,** 115, (38), 4797-4801.

13. Wang, Y.; Tang, Y.; Dong, A.; Wang, X.; Ren, N.; Gao, Z., Zeolitization of diatomite to prepare hierarchical porous zeolite materials through a vapor-phase transport process. *Journal of Materials Chemistry* **2002,** 12, (6), 1812-1818.

14. Fan, X.; Fei, H.; Demaree, D. H.; Brennan, D. P.; St. John, J. M.; Oliver, S. R. J., Polymer gel templating of free-standing inorganic monoliths for photocatalysis. *Langmuir* **2009,** 25, (10), 5835-5839.

15. Drisko, G. L.; Wang, X.; Caruso, R. A., Strong silica monoliths with large mesopores prepared using agarose gel templates. *Langmuir* **2011,** 27, (6), 2124-2127.

16. Zhou, J.; Zhou, J.; Zhou, M.; Caruso, R. A., Agarose template for the fabrication of macroporous metal oxide structures. *Langmuir* **2006,** 22, (7), 3332-3336.

17. Drisko, G. L.; Luca, V.; Sizgek, E.; Scales, N.; Caruso, R. A., Template synthesis and adsorption properties of hierarchically porous zirconium titanium oxides. *Langmuir* **2009,** 25, (9), 5286-5293.

18. Wang, X.; Mitchell, D. R. G.; Prince, K.; Atanacio, A. J.; Caruso, R. A., Gold Nanoparticle Incorporation into Porous Titania Networks Using an Agarose Gel Templating Technique for Photocatalytic Applications. *Chemistry of Materials* **2008,** 20, (12), 3917-3926.

19. Huang; Zhou; Cheng, Y.-B.; Caruso, R. A., Al-Containing Porous Titanium Dioxide Networks: Sol-Gel Synthesis within Agarose Gel Template and Photocatalytic Activity. *Chemistry of Materials* **2006,** 18, (25), 5835-5839.

20. Huang, F.; Li, Q.; Thorogood, G. J.; Cheng, Y.-B.; Caruso, R. A., Zn-doped TiO2 electrodes in dye-sensitized solar cells for enhanced photocurrent. *Journal of Materials Chemistry* **2012,** 22, (33), 17128-17132.

21. Yang, R. T.; Hernández-Maldonado, A. J.; Yang, F. H., Desulfurization of Transportation Fuels with Zeolites Under Ambient Conditions. *Science* **2003,** 301, (5629), 79-81.

22. Hernández-Maldonado, A. J.; Yang, R. T., Desulfurization of Liquid Fuels by Adsorption via π Complexation with Cu(I)−Y and Ag−Y Zeolites. *Industrial & Engineering Chemistry Research* **2003,** 42, (1), 123-129.

23. McKinley, S. G.; Angelici, R. J., Deep desulfurization by selective adsorption of dibenzothiophenes on Ag^{+}/SBA-15 and Ag^{+}/SiO_2. *Chemical Communications* **2003**, (20), 2620-2621.

24. Seker, E.; Cavataio, J.; Gulari, E.; Lorpongpaiboon, P.; Osuwan, S., Nitric oxide reduction by propene over silver/alumina and silver-gold/alumina catalysts: effect of preparation methods. *Applied Catalysis A: General* **1999,** 183, (1), 121-134.

25. Zeng, D.; Yang, J.; Wang, J.; Xu, J.; Yang, Y.; Ye, C.; Deng, F., Solid-state NMR studies of methanol-to-aromatics reaction over silver exchanged HZSM-5 zeolite. *Microporous and Mesoporous Materials* **2007,** 98, (1-3), 214-219.

26. Abu-Zied, B. M.; Schwieger, W.; Unger, A., Nitrous oxide decomposition over transition metal exchanged ZSM-5 zeolites prepared by the solid-state ion-exchange method. *Applied Catalysis B: Environmental* **2008,** 84, (1-2), 277-288.

27. Xiao, J.; Li, Z.; Liu, B.; Xia, Q.; Yu, M., Adsorption of Benzothiophene and Dibenzothiophene on Ion-Impregnated Activated Carbons and Ion-Exchanged Y Zeolites. *Energy & Fuels* **2008,** 22, (6), 3858-3863.

Chapter 3

SBA-15 and its Derivatives as Frameworks for Adsorptive Desulfurization

Abstract

SBA-15 is a high surface area framework with a pore size large enough to accommodate organosulfur contaminants found in fossil fuels. SBA-15, aluminosilicate SBA-15 (Al-SBA-15), and aminopropyl-functionalized SBA-15 (APS-SBA-15) were explored for the desulfurization of real and model fuels. Ag^{+}, Ce^{3+}, and Ni^{2+} were explored to determine the best metal ion for desulfurization, as well as different methods for loading the frameworks with these metals, including wet impregnation and ion exchange. Ag^{+} was found to have the highest desulfurization capacity, which can be increased when wet impregnation is used compared to ion exchange procedures. Ultimately, 18 wt.% Ag-Al-SBA-15 was the best performing material and was found to have an adsorption capacity of 31.47 mgS/g in JP-8 (725.9 ppm_wS).

3.1 Introduction

SBA-15 was first reported in 1998 by Stucky and coworkers as a mesoporous silica material with a hexagonal array of pores, similar in structure to MCM-41, but with pore sizes ranging from 46Å to 300Å.[1] MCM-41 is typically synthesized using ionic surfactants, such as CTAB, as a structure directing agent. This is in contrast to SBA-15, which uses a non-ionic triblock copolymer as a templating agent, as shown in Figure 3.1.

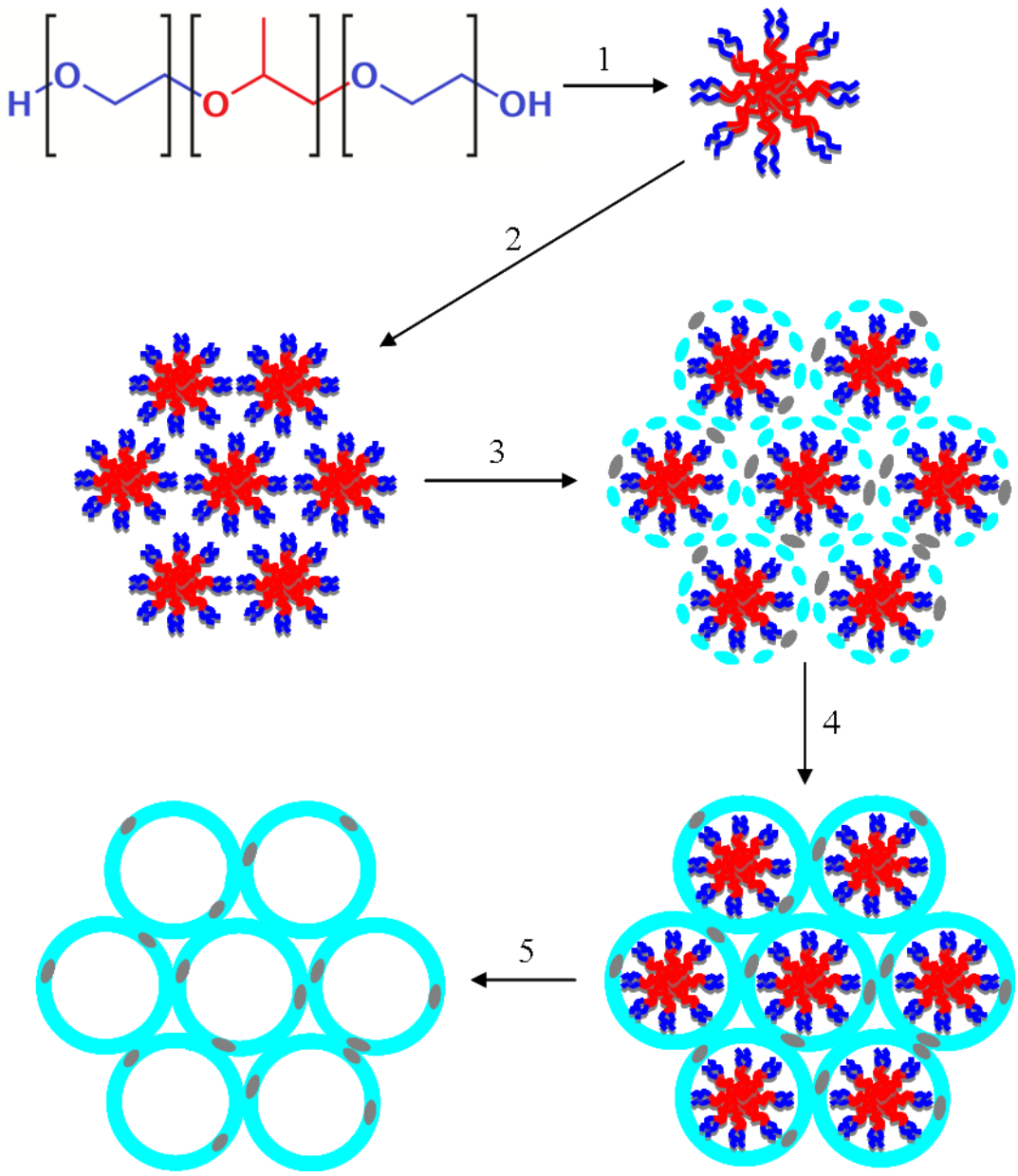

Figure 3.1 General schematic of the production of Al-SBA-15. Pluronic P123 forms micelles (1) in solution, which can pack in a hexagonal array (2). TEOS (aqua) and aluminum isopropoxide (gray) surround the micelles (3), and condense to form a solid structure (4). The P123 can then be removed through solvent extraction or calcination (5).

SBA-15 and its derivatives have been explored for a variety of applications including drug delivery[2-5], water remediation[6, 7], and catalysis[8-10]. SBA-15's tunable

pore size and high surface area make it an ideal framework for adsorptive desulfurization.

Several model fuel studies have been performed using SBA-15. Silver loaded SBA-15 was found to be an effective adsorbent for model fuels.[11] SBA-15 with a 52.3 Å average pore diameter was loaded with 28.4 wt.% Ag^+ and found to remove over 80% of the sulfur from both a model fuel of dibenzothiophene in decane, and 4,5-dimethyldibenzothiophene in decane.[11] Cu^+ loaded SBA-15 and Al-SBA-15 have been tested on model fuels of thiophene in isooctane.[12] It was found that Cu^+/SBA-15 has an adsorption capacity of 5.35 mgS/g and Cu^+/Al-SBA-15 has a capacity of 7.70 mgS/g when both are loaded with ~ 24 wt.% Cu^+.[12]

SBA-15 has also been explored for use with real fuels. Wang *et al.* explored $PdCl_2$/SBA-15 and CuCl/SBA-15 as desulfurization adsorbents for a light fraction of JP-5 with an initial sulfur content of 841 ppm_wS.[13] They found that CuCl/SBA-15 and $PdCl_2$/SBA-15 have saturation adsorption capacities of 25.7 mgS/g and 38.5 mgS/g respectively.[13] They also examined the efficiency of the metal. CuCl/SBA-15 adsorbed 0.09 molS/molCu and $PdCl_2$/SBA-15 adsorbed 0.35 molS/molPd, showing that Pd is much more efficiently used.[13] Thermal and solvent regeneration were also explored. Thermal regeneration of $PdCl_2$/SBA-15 using helium recovered only 7% of its initial capacity, whereas solvent regeneration with benzene recovered 48%.[13] They explained the heightened ability of benzene to regenerate the material by the ability of benzene to form π-complexes with Pd^{2+}, effectively displacing the bound organosulfur compounds.[13] The same group also explored SBA-15 loaded with Cu_2O.

However, this framework yielded a significantly lower capacity of 9.6 mgS/g with the same fuel.[14]

Herein, we report the use of SBA-15 and two of its derivatives: aluminosilicate SBA-15 (Al-SBA-15) and aminopropyl-functionalized SBA-15 (APS-SBA-15) as adsorptive desulfurization frameworks. The loading with three different metals are explored: Ag, Ce, and Ni, as are several different loading procedures and post loading modifications. Model fuel and JP-8 tests are reported along with solvent regeneration data.

3.2 Experimental Section

3.2.1 Materials

All chemicals were used as received without further purification. Tetraethylorthosilicate (TEOS), dibenzothiophene (DBT), 3-aminopropyltriethoxysilane (APS), and aluminum isopropoxide were all obtained from Acros Organics. HCl and $Ni(NO_3)_2 \cdot 6H_2O$ were obtained from Fisher Scientific. Silver nitrate was obtained through MP Biomedicals, 200 proof ethanol from Decon Labs, poly(ethylene glycol)-block-poly(propylene glycol)-block-poly(ethylene glycol) with a feed ratio of 20:70:20 of EO:PO:EO (Pluronic P123) from Sigma-Aldrich, and $Ce(NO_3)_3 \cdot 6H_2O$ from Spectrum.

3.2.2 SBA-15 and Al-SBA-15 Synthesis

Synthetic methods were modified from existing methods.[15] 4 g of Pluronic P123 was added to 30 g of doubly distilled deionized water. A solution of 1.68 g concentrated HCl diluted to 70 g with doubly distilled deionized water was added to the Pluronic solution and stirred until the Pluronic was completely dissolved. For SBA-15, 9 g of TEOS was added in a quick dropwise fashion to the stirring solution and allowed to stir for 24 hours at room temperature. For Al-SBA-15, 2.94 g aluminum isopropoxide and 9 g of TEOS was added in a quick dropwise fashion to the stirring solution and allowed to stir for 24 hours at room temperature. The solution was then transferred to a Teflon bottle and statically aged at 100°C for 24 hours. The solution was filtered and rinsed with copious amounts of doubly distilled

deionized water, followed by soxlet extraction with ethanol overnight. The product was then calcined at 550°C for 8 hours with a 1°C/min ramp rate.

3.2.3 Aminopropyl Fuctionalization of SBA-15

The functionalization procedure was based on existing methods.[16] 1.33 g aminopropyltriethoxy silane was added to 22.6 g of 200 proof ethanol. The solution was stirred for 10 minutes prior to the addition of 0.37 g of SBA-15. After 2 hours of stirring, the solution was filtered and rinsed with ethanol. The APS-SBA-15 product was dried at 100°C under vacuum.

3.2.4 Metal Loading *via* Exchange

SBA-15, Al-SBA-15, or APS-SBA-15 was added to a 0.2 M solution of $Ni(NO_3)_2 \cdot 6H_2O$, $Ce(NO_3)_3 \cdot 6H_2O$ or $AgNO_3$ in doubly distilled deionized water overnight with stirring The solution was either kept at room temperature or 70°C (as noted in results). Post-exchange thermal treatment consisting of calcination at 550°C for 8 hours with a 1°C/min ramp rate was performed on some samples, as noted.

3.2.5 Metal Loading *via* Wet Impregnation

The desired amount of $AgNO_3$ was dissolved in a minimal (less than 1 mL) amount of doubly distilled deionized water. This solution was added dropwise to the framework until wet. The framework was then dried under vacuum at 110°C. This

process was repeated until all of the desired metal solution was loaded onto the framework.

3.2.6 Characterization

BET surface area of the samples was measured by physical adsorption of N_2 at 77 K using a Micromeritics TriStar II (TriStar II 3020 v1.03). Adsorption/desorption isotherm measurements were collected in the relative pressure range P/P_o from 0.01 to 1.00.

3.2.7 Model and Real Fuel Tests

Prior to all JP-8 and model fuel testing, the adsorbents were heated under vacuum at 110 °C overnight to remove trapped gas or water. All model fuel tests were performed using dibenzothiophene in dodecane, with concentrations denoted alongside the data. For column tests, the prepared materials were packed in a Chromtech column (4.6 mm ID, 50 mm length). JP-8 fuel was pumped at 0.5 mL/min into the column using a Shimadzu HPLC pump. Column and 24 hour batch (beaker) test experiments were analyzed for total sulfur concentration using a UV total sulfur analyzer (multi EA 3100, Analytikjena) with a detection limit of 45 ppb. Typical JP-8 batch test experiments were done with ~ 0.05 g of sorbent in ~ 5.5 g of JP-8, whereas column experiments were done with ~ 0.2 g of sorbent in the same amount of JP-8. Model fuel batch tests were performed with 20-30 g of fuel per gram

of sorbent and were analyzed by UV-Vis on a Hewlett-Packard Model 8452A spectrophotometer.

3.3 Results and Discussion

3.3.1 Characterization

BET surface area analysis was performed on SBA-15 and Al-SBA-15 revealing surface areas of 723.0 m^2/g and 514.4 m^2/g, respectively. The pore sizes are too large to confirm through typical PXRD analysis ((100) is below 1.5^o). However, using the surface area analysis along with the confirmed synthetic procedures, it is reasonable to expect that the syntheses did result in the production of both SBA-15 and Al-SBA-15. The surface areas are similar to those reported in literature, where SBA-15 prepared with P123 has a typical surface area range between 700-900 m^2/g and Al-SBA-15 with a gel Si:Al ratio of 3:1 typically has a surface area between 300-650 m^2/g.[17-20]

3.3.2 Model Fuel Tests

Silver, nickel, and cerium are all known to be active metals for desulfurization.[21-26] Free Ag^+ in solution is known to make direct S-M bonds with dibenzothiophene,[11] however, molecular orbital calculations show it is capable of forming π-complexes as well.[27] Ce^{3+} is capable of making S-M bonds and π-complexes with organosulfur compounds, such as thiophenes.[28] Ni^{2+} is known to form π-complexes.[29] No studies directly evaluate the effectiveness of these three metals under the same conditions. Al-SBA-15 has negatively charged surface sites, making it ideal for exchanging with positively charged metal ions. Al-SBA-15 was soaked at room temperature in isomolar solutions of all three ions for equal periods of

time prior to desulfurization experiments. After a 30 minute fuel test, it was clear that the order of effectiveness is:

$$Ag^{+} > Ce^{3+} > Ni^{2+}$$

However, all three materials had adsorption capacities below 1 mgS/g, as shown in Table 3.1.

Elevated temperature was explored in an attempt to achieve a higher level of exchange, creating more adsorption sites within the framework. A 70^{o}C exchange compared to room temperature increased the sulfur capacity of the Ag^{+} loaded framework 5-fold, the Ce^{3+} frameworks capacity 6-fold, and the Ni^{2+} 8-fold. The trend, however, remained the same with Ag^{+} outperforming the other two metals, as shown in Table 3.1.

There have been successful reports of thermally treating frameworks following their metal loading, converting the metal ions present into metal oxides.[28, 30, 31] However, for these sorbents, thermal treatment in air resulted in a decrease in adsorption capacity as shown in Table 3.1. The Ag^{+} exchanged material displayed only a 7% loss in capacity, while Ce^{3+} and Ni^{2+} displayed a loss of 37% and 20%, respectively. The silver oxide is much more effective than the other two metal oxides.

Table 3.1 Al-SBA-15 exchanged with Ag^{+}, Ce^{3+}, and Ni^{2+} under various conditions. 30 min fuel test in 625 ppm_wS DBT in dodecane

Metal Salt	Loading Method[a]	Post-exchange Treatment	Adsorption Capacity (mgS/g)
$AgNO_3$	70°C Exchange	N/A	3.99
$AgNO_3$	70°C Exchange	550°C 8 hours in air	3.72
$AgNO_3$	RT Exchange	N/A	0.74
$Ce(NO_3)_3 \cdot 6H_2O$	70°C Exchange	N/A	3.42
$Ce(NO_3)_3 \cdot 6H_2O$	70°C Exchange	550°C 8 hours in air	2.17
$Ce(NO_3)_3 \cdot 6H_2O$	RT Exchange	N/A	0.53
$Ni(NO_3)_2 \cdot 6H_2O$	70°C Exchange	N/A	3.08
$Ni(NO_3)_2 \cdot 6H_2O$	70°C Exchange	550°C 8 hours in air	2.47
$Ni(NO_3)_2 \cdot 6H_2O$	RT Exchange	N/A	0.37

[a]Exchanges performed for 24 hours. RT is room temperature.

In addition to exchange, wet impregnation has been widely used to load metals into adsorptive desulfurization sorbents.[32-35] Wet impregnation provides a convenient technique for loading a very specific amount of metal into a framework, allowing for quick optimization under controlled conditions. Through capillary action, wet impregnation draws the metal into the pores of the framework. Testing the unloaded framework, Figure 3.2, reveals that it removes a similar amount of sulfur

compared to the room temperature exchanged frameworks. Al-SBA-15 loaded with 9 wt.% silver outperforms the 70°C exchanged material, with a capacity of 5.50 mgS/g compared to only 3.99 mgS/g with the exchange. The capacity continues to increase with increased loading, reaching a maximum at 18 wt.% Ag with a capacity of 7.87 mgS/g. With increased loading above 18 wt.%, the capacity begins to decrease with 21 wt.% only adsorbing 6.86 mgS/g. This decrease is likely due to the formation of silver aggregates blocking some of the channels in the material, decreasing the number of available surface sites. This decrease in capacity with increased metal loading has been observed with other desulfurization sorbents.[36]

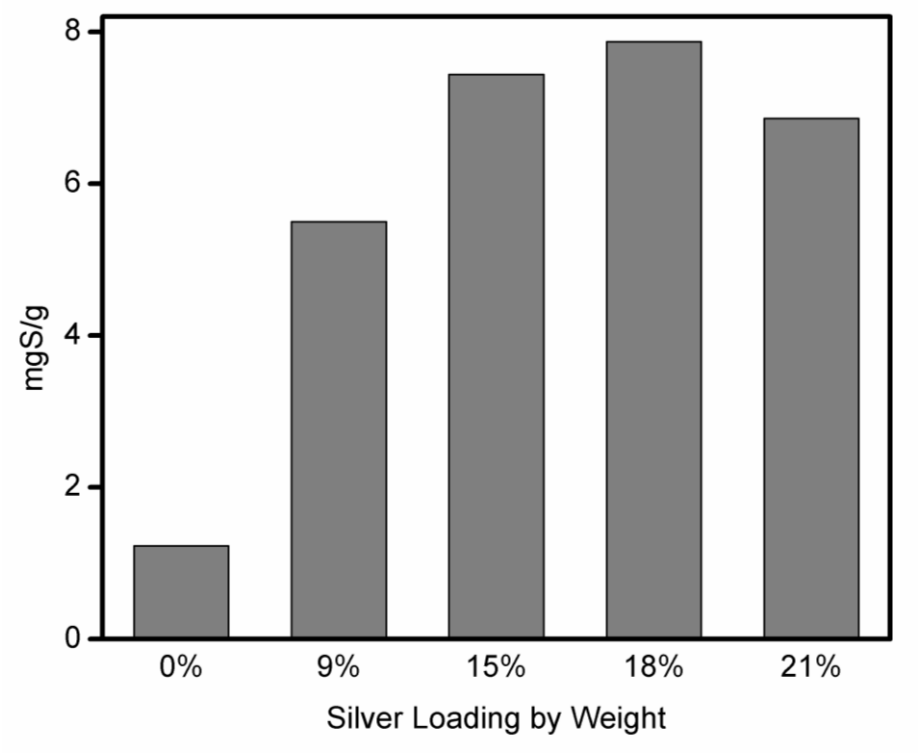

Figure 3.2 30 minute batch fuel tests in 580 ppm_wS DBT in dodecane of Al-SBA-15 wet impregnated with the designated amount of Ag^+.

3.3.3 Regeneration

In order for a desulfurization sorbent to be useful, it must be reusable. Typically, these sorbents are regenerated thermally or by solvent rinsing. Thermal regeneration poses problems as it releases sulfur compounds back into the atmosphere and it must be done under inert atmosphere. Furthermore, the results in Table 3.1 showed that heating in air causes a reduction in adsorption capacity. Solvent regeneration is a simple solution, as it conveniently keeps all the organosulfur compounds confined in liquid form and does not require the equipment set-up of a furnace under increasingly expensive inert atmosphere. The sulfur compounds could easily be separated from the regeneration solvent through distillation, so that the solvent could be reused. Figure 3.3 displays the adsorption capacity over two regeneration cycles. After the first cycle, 93% of the capacity is maintained, and 87% of the original capacity is maintained after the second cycle. This small decrease in capacity is likely due to a small amount of silver being lost from the framework either during the fuel test or the regeneration procedure.

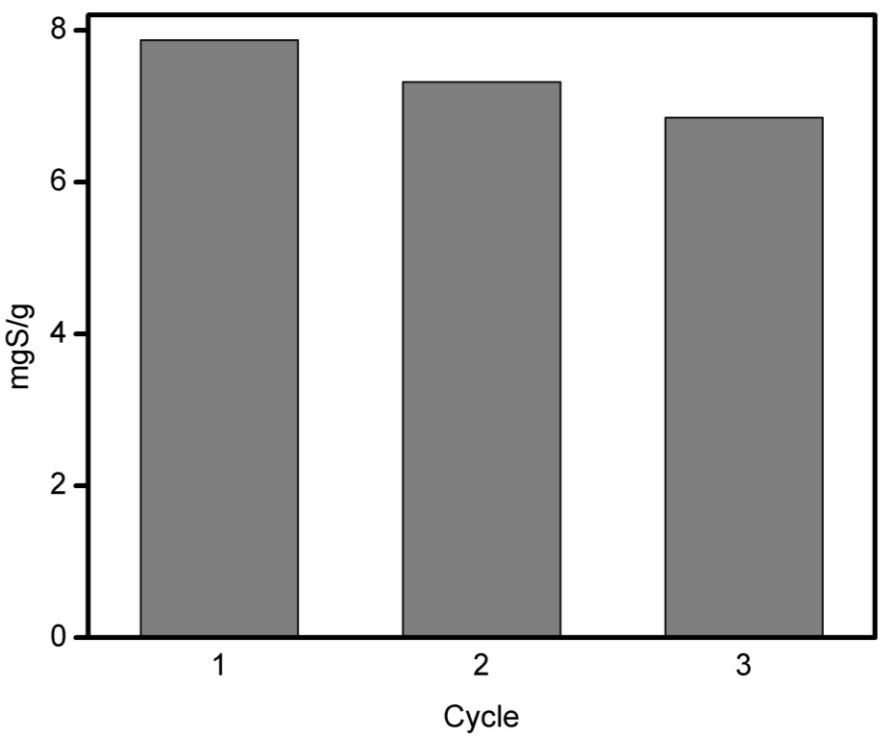

Figure 3.3 Regeneration of Al-SBA-15 loaded with 18 wt.% Ag, regenerated with diethyl ether. Using 580 ppm_wS DBT in dodecane, 30 minute batch testing.

3.3.4 Ligand Functionalization

In addition to impregnation, another technique to improve the metal capacity of a framework over traditional exchange is to functionalize the material with a ligand. Figure 3.4 shows a general schematic of functionalizing SBA-15 with a 3-aminopropyl group, which may allow the metal sites to be more tightly bound to the framework. Table 3.2 shows the adsorption capacities under the same conditions as the non-ligand functionalized Al-SBA-15. The ligand functionalization did increase the adsorption capacity. Increases of 18%, 30%, and 27% were observed with Ag^+,

Ce^{3+}, and Ni^{2+} respectively. While these increases are substantial compared to the original exchange method, they are insignificant when compared to results obtained by the impregnation method.

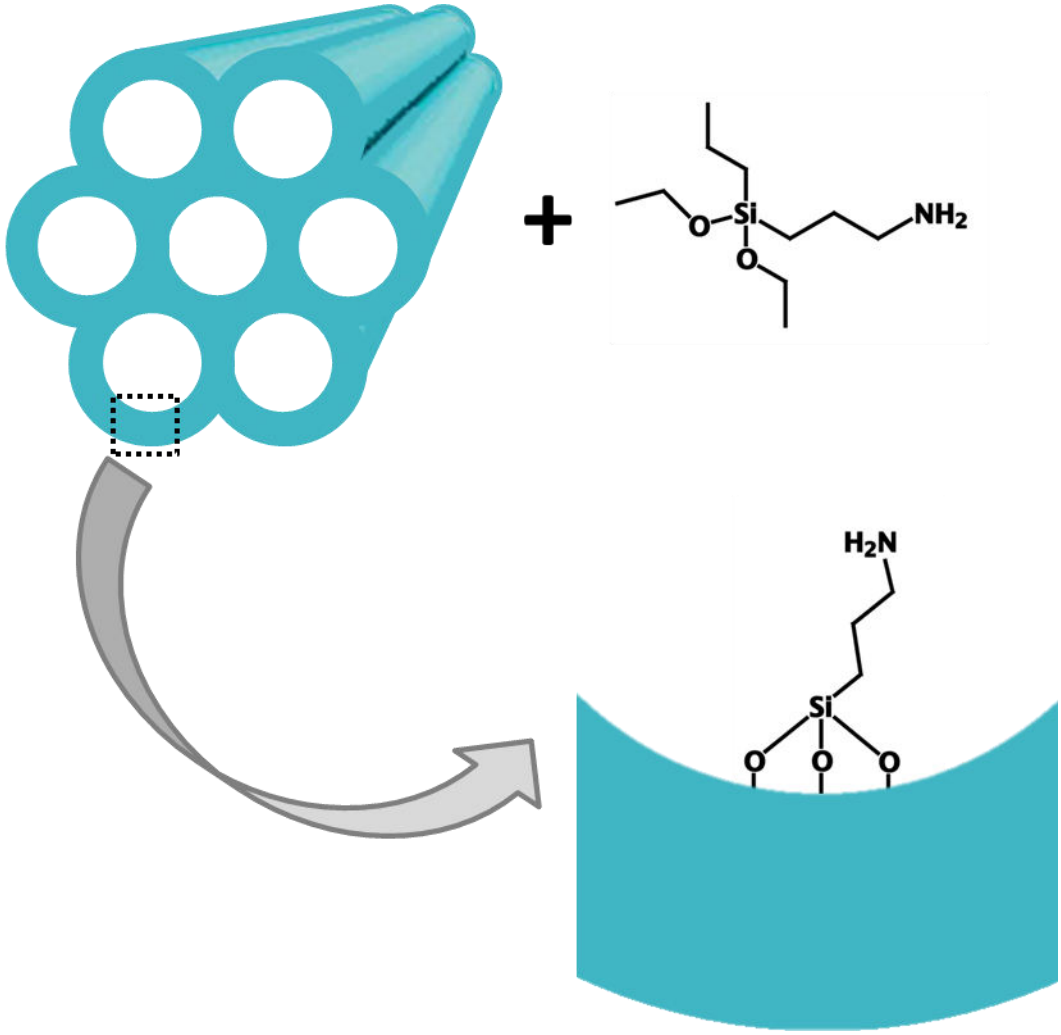

Figure 3.4 Schematic showing the general idea of functionalizing the surface of Si-SBA-15.

Table 3.2 30 minute batch fuel test in 680 ppm_wS DBT in dodecane for APS-SBA-15 following 24-hour 70°C exchange.

Metal Ion	Adsorption Capacity (mg S/g)
Ag^+	4.70
Ce^{3+}	4.48
Ni^{2+}	3.90

3.3.5 JP-8 Testing

As 18 wt.% Ag loaded Al-SBA-15 performed the best in model fuel tests, it along with SBA-15 were selected for testing with real JP-8. SBA-15 was included because although it doesn't have the negative framework charge that Al-SBA-15 contains, it does possess a higher surface area. Materials with high surface area have been shown consistently to make the best adsorptive desulfurization frameworks.[30, 37] As shown in Table 3.3, SBA-15 has a higher surface area, and retains a higher surface area after loading with 18 wt.% Ag.

Both Al-SBA-15 and SBA-15 display similar adsorption capacities before silver loading. After being impregnated, Ag-SBA-15 has a 15% higher adsorption capacity but a 33% higher surface area. This demonstrates that even though the addition of aluminum decreases the surface area, the incorporation of aluminum also plays a role in adsorption. Previously published studies with Al-SBA-15 and SBA-15 loaded with Cu^+ show an increased capacity with Al-SBA-15 which the authors attribute the Cu^+ ions being better distributed in the aluminosilicate framework.[12]

Table 3.3 24-hour batch fuel tests with JP-8 (725.9 ppm_wS), silver loaded containing 18 wt.% Ag

Sample	Final JP-8 Concentration (ppm_wS)	Adsorption Capacity (mgS/g)	Surface Area (m^2/g)
Al-SBA-15	695.6	3.04	514.4
SBA-15	693.8	3.24	723.0
Ag-Al-SBA-15	403.8	31.47	395.3
Ag-SBA-15	347.94	36.31	525.6

Ag-Al-SBA-15 was further studied with real JP-8 in a packed column study, as shown in Figures 3.5 and 3.6. The initial processed fuel passing through the column has 97.2% of its initial sulfur removed, corresponding to a concentration of 20.5 ppm_wS. While this outlet concentration doesn't meet the requirements of sub 1 ppm_wS desired for use with solid oxide fuel cells, it is still a significant advance. Compared with gold loaded silica, whose initial outlet concentration is ~ 45 ppm_wS, this is an improvement.[16]

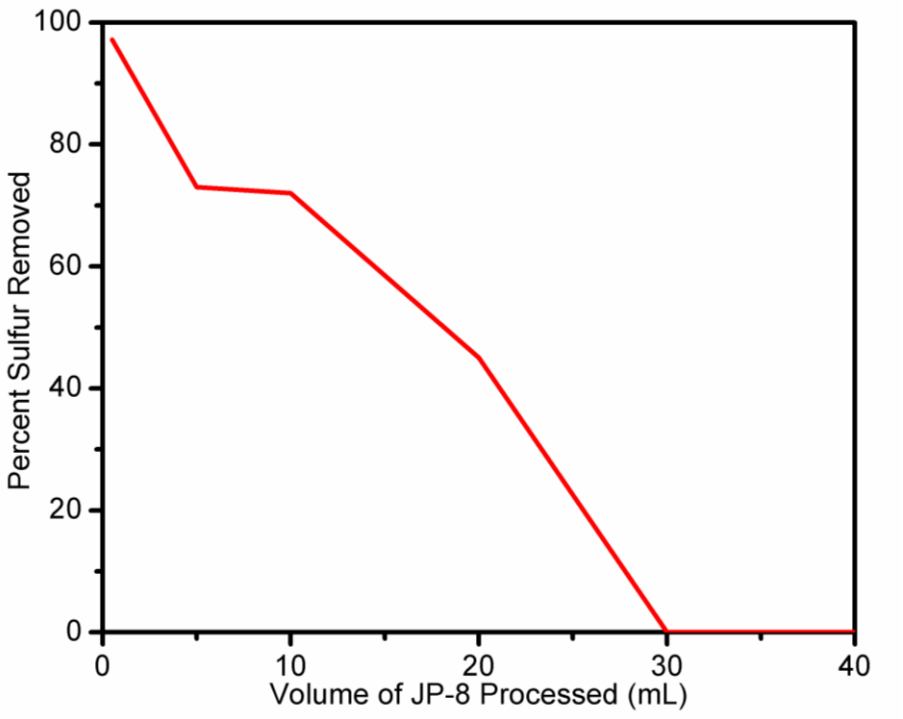

Figure 3.5 Column study of Al-SBA-15 with 18 wt.% Ag in JP-8 (725.9 ppm_wS) as a function of the percent sulfur removed of the effluent after passing through the column.

The column study shows the material is completely saturated after 30 mL of processed fuel. However, the capacity quickly drops off. After 5mL, it removed 73% of the sulfur compounds present, and 45% at 20 mL.

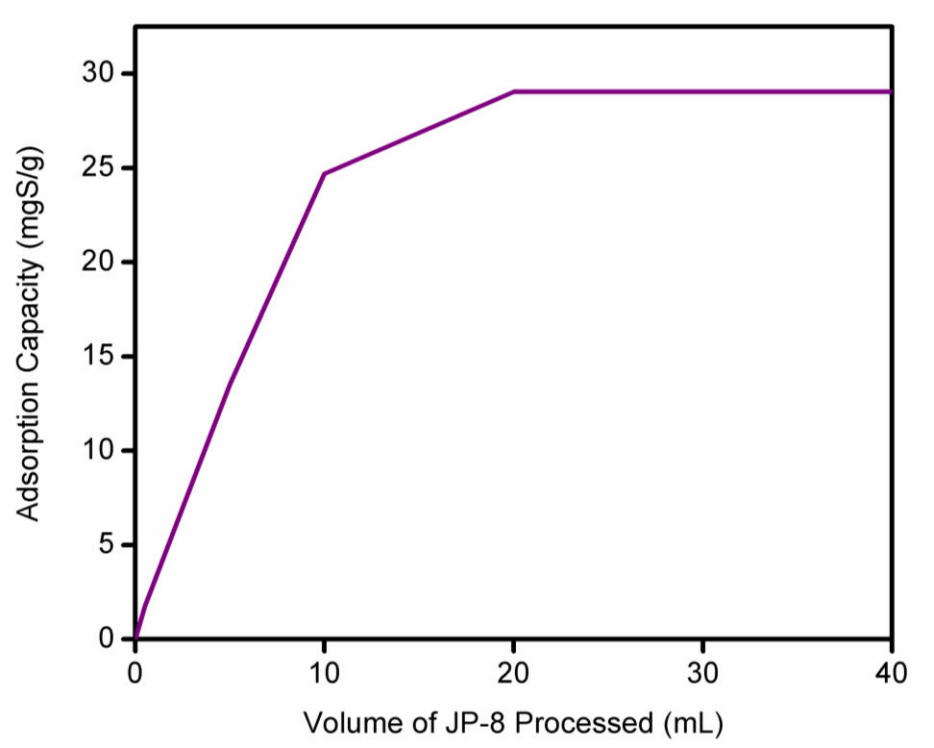

Figure 3.6 Column study of Al-SBA-15 with 18 wt.% Ag in JP-8 (725.9 ppm_wS) as a function of the total adsorption capacity of the sorbent.

A higher silver loading was also explored with JP-8 to see if the adsorption capacity could be increased when using real fuel (Figure 3.7). A dramatic increase in silver loading, 18 wt.% to 66 wt.%, did result in an increase in adsorption capacity to 34.60 mgS/g compared to 31.47 mgS/g. This 10% increase in capacity is marred by the poor silver efficiency. At 18 wt.% the material adsorbs 0.58 molS/molAg, utilizing over half the loaded silver for adsorption, while at 66 wt.% the material adsorbs 0.18 molS/molAg, utilizing only about a fifth of the silver.

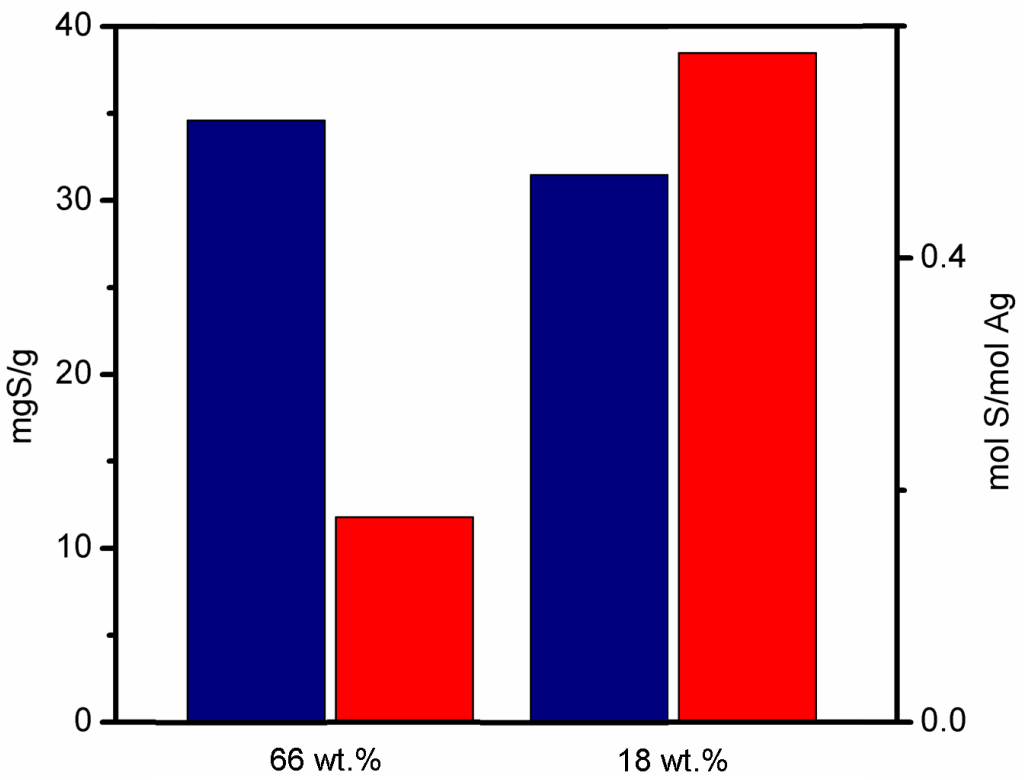

Figure 3.7 Al-SBA-15 24-hour batch test with JP-8 comparing 66 wt.% with 18 wt.% Ag loading. Adsorption capacity in blue and silver efficiency in red.

An initial comparison between Al-SBA-15 and MCM-41 was performed by doing side-by-side 1-hour fuel tests with JP-8. Table 3.4 reveals that when both are loaded with identical amounts of silver nitrate and tested under the same procedure, MCM-41 outperforms Al-SBA-15. The Ag-MCM-41 displays both a higher adsorption capacity and higher silver efficiency. The use of MCM-41 will be further explored in Chapter 4.

Table 3.4 1-hour batch fuel tests with JP-8 (738 ppm_wS), silver loaded containing 18 wt.% Ag

Sample	Unloaded Adsorption Capacity (mgS/g)	Ag Loaded Adsorption Capacity (mgS/g)	Silver Efficiency (molS/molAg)
Al-SBA-15	5.2	29.1	0.54
MCM-41	4.0	34.5	0.64

3.4 Conclusions

The comparison of silver, cerium, and nickel reveal the following trend in adsorption capacity:

$$Ag^{+} > Ce^{3+} > Ni^{2+}$$

The overall performance based on loading procedure of (Al)-SBA-15 is as follows:

Wet impregnation > Aminopropyl functionalization > Exchange

Exchange is best performed at an elevated temperature without post-exchange calcination in air. Overall, 18 wt.% Ag-Al-SBA-15 is a promising desulfurization sorbent for JP-8, capable of reaching 20 ppm_wS levels and with a high silver efficiency of 0.57 molS/molAg. This material outperformed existing published sorbents in terms of overall adsorption capacity. However, it was not capable of achieving a sub 1 ppm_wS level. While SBA-15 and Al-SBA-15 are promising materials for the desulfurization of jet fuel, their pore size is excessively larger than that required to accommodate the contaminants of JP-8. By slightly decreasing the pore size, the surface area can be increased, allowing for a greater adsorption capacity. Analogous in structure, yet with smaller pore size, MCM-41 may be a more effective alternative to investigate.

3.5 References

1. Zhao, D.; Feng, J.; Huo, Q.; Melosh, N.; Fredrickson, G. H.; Chmelka, B. F.; Stucky, G. D., Triblock Copolymer Syntheses of Mesoporous Silica with Periodic 50 to 300 Angstrom Pores. *Science* **1998,** 279, (5350), 548-552.

2. Doadrio, A. L.; Sousa, E. M. B.; Doadrio, J. C.; Pérez Pariente, J.; Izquierdo-Barba, I.; Vallet-Regı, M., Mesoporous SBA-15 HPLC evaluation for controlled gentamicin drug delivery. *Journal of Controlled Release* **2004,** 97, (1), 125-132.

3. Song, S. W.; Hidajat, K.; Kawi, S., Functionalized SBA-15 materials as carriers for controlled drug delivery: influence of surface properties on matrix-drug interactions. *Langmuir* **2005,** 21, (21), 9568-9575.

4. Fagundes, L. B.; Sousa, T. G. F.; Sousa, A.; Silva, V. V.; Sousa, E. M. B., SBA-15-collagen hybrid material for drug delivery applications. *Journal of Non-Crystalline Solids* **2006,** 352, (32-35), 3496-3501.

5. Wang, S., Ordered mesoporous materials for drug delivery. *Microporous and Mesoporous Materials* **2009,** 117, (1-2), 1-9.

6. Mureseanu, M.; Reiss, A.; Stefanescu, I.; David, E.; Parvulescu, V.; Renard, G.; Hulea, V., Modified SBA-15 mesoporous silica for heavy metal ions remediation. *Chemosphere* **2008,** 73, (9), 1499-1504.

7. Da'na, E.; Sayari, A., Adsorption of heavy metals on amine-functionalized SBA-15 prepared by co-condensation: Applications to real water samples. *Desalination* **2012,** 285, 62-67.

8. Wang, X.; Lin, K. S. K.; Chan, J. C. C.; Cheng, S., Direct synthesis and catalytic applications of ordered large pore aminopropyl-functionalized SBA-15 mesoporous materials. *The Journal of Physical Chemistry B* **2005,** 109, (5), 1763-1769.

9. Martínez, A. n.; López, C.; Márquez, F.; Díaz, I., Fischer-Tropsch synthesis of hydrocarbons over mesoporous Co/SBA-15 catalysts: the influence of metal loading, cobalt precursor, and promoters. *Journal of Catalysis* **2003,** 220, (2), 486-499.

10. Rioux, R. M.; Song, H.; Hoefelmeyer, J. D.; Yang, P.; Somorjai, G. A., High-surface-area catalyst design: synthesis, characterization, and reaction studies of platinum nanoparticles in mesoporous SBA-15 silica. *The Journal of Physical Chemistry B* **2005,** 109, (6), 2192-2202.

11. McKinley, S. G.; Angelici, R. J., Deep desulfurization by selective adsorption of dibenzothiophenes on Ag^+/SBA-15 and Ag^+/SiO_2. *Chemical Communications* **2003**, (20), 2620-2621.

12. He, G.-S.; Sun, L.-B.; Song, X.-L.; Liu, X.-Q.; Yin, Y.; Wang, Y.-C., Adjusting Host Properties to Promote Cuprous Chloride Dispersion and Adsorptive Desulfurization Sites Formation on SBA-15. *Energy & Fuels* **2011,** 25, (8), 3506-3513.

13. Wang, Y.; Yang, R. T.; Heinzel, J. M., Desulfurization of jet fuel by π-complexation adsorption with metal halides supported on MCM-41 and SBA-15 mesoporous materials. *Chemical Engineering Science* **2008,** 63, (2), 356-365.

14. Wang, Y.; Yang, R. T.; Heinzel, J. M., Desulfurization of Jet Fuel JP-5 Light Fraction by MCM-41 and SBA-15 Supported Cuprous Oxide for Fuel Cell Applications. *Industrial & Engineering Chemistry Research* **2009,** 48, (1), 142-147.

15. Vinu, A.; Murugesan, V.; Tangermann, O.; Hartmann, M., Adsorption of Cytochrome c on Mesoporous Molecular Sieves: Influence of pH, Pore Diameter, and Aluminum Incorporation. *Chemistry of Materials* **2004,** 16, (16), 3056-3065.

16. Tran, D. T.; Dunbar, Z. W.; Chu, D., Regenerable sulfur adsorbent for liquid phase JP-8 fuel using gold/silica based materials. *International Journal of Hydrogen Energy* **2012,** 37, (13), 10430-10434.

17. Vinu, A.; Murugesan, V.; Böhlmann, W.; Hartmann, M., An Optimized Procedure for the Synthesis of AlSBA-15 with Large Pore Diameter and High Aluminum Content. *The Journal of Physical Chemistry B* **2004,** 108, (31), 11496-11505.

18. Kao, H.-M.; Ting, C.-C.; Chao, S.-W., Post-synthesis alumination of mesoporous silica SBA-15 with high framework aluminum content using ammonium hexafluoroaluminate. *Journal of Molecular Catalysis A: Chemical* **2005,** 235, (1â€“2), 200-208.

19. Li, Y.; Pan, D.; Yu, C.; Fan, Y.; Bao, X., Synthesis and hydrodesulfurization properties of NiW catalyst supported on high-aluminum-content, highly ordered, and hydrothermally stable Al-SBA-15. *Journal of Catalysis* **2012,** 286, 124-136.

20. Dragoi, B.; Dumitriu, E.; Guimon, C.; Auroux, A., Acidic and adsorptive properties of SBA-15 modified by aluminum incorporation. *Microporous and Mesoporous Materials* **2009,** 121, (1-3), 7-17.

21. Xiao, J.; Wang, X.; Fujii, M.; Yang, Q.; Song, C., A novel approach for ultra-deep adsorptive desulfurization of diesel fuel over TiO2–CeO2/MCM-48 under ambient conditions. *AIChE Journal* **2013,** 59, (5), 1441-1445.

22. Wang, G.; Wen, Y.; Fan, J.; Xu, C.; Gao, J., Reactive Characteristics and Adsorption Heat of Ni/ZnO–SiO2–Al2O3 Adsorbent by Reactive Adsorption Desulfurization. *Industrial & Engineering Chemistry Research* **2011,** 50, (22), 12449-12459.

23. Velu, S.; Ma, X.; Song, C.; Namazian, M.; Sethuraman, S.; Venkataraman, G., Desulfurization of JP-8 Jet Fuel by Selective Adsorption over a Ni-based Adsorbent for Micro Solid Oxide Fuel Cells. *Energy & Fuels* **2005,** 19, (3), 1116-1125.

24. Shahadat Hussain, A. H. M.; Tatarchuk, B. J., Mechanism of hydrocarbon fuel desulfurization using Ag/TiO2-Al2O3 adsorbent. *Fuel Processing Technology* **2014,** 126, (0), 233-242.

25. Wang, J.; Xu, F.; Xie, W.-j.; Mei, Z.-j.; Zhang, Q.-z.; Cai, J.; Cai, W.-m., The enhanced adsorption of dibenzothiophene onto cerium/nickel-exchanged zeolite Y. *Journal of Hazardous Materials* **2009,** 163, (2), 538-543.

26. Hernández-Maldonado, A. J.; Yang, R. T., Desulfurization of Diesel Fuels via π-Complexation with Nickel(II)-Exchanged X- and Y-Zeolites. *Industrial & Engineering Chemistry Research* **2004,** 43, (4), 1081-1089.

27. Yang, R. T.; Hernández-Maldonado, A. J.; Yang, F. H., Desulfurization of Transportation Fuels with Zeolites Under Ambient Conditions. *Science* **2003,** 301, (5629), 79-81.

28. Duan, L.; Gao, X.; Meng, X.; Zhang, H.; Wang, Q.; Qin, Y.; Zhang, X.; Song, L., Adsorption, Co-adsorption, and Reactions of Sulfur Compounds, Aromatics, Olefins over Ce-Exchanged Y Zeolite. *The Journal of Physical Chemistry C* **2012,** 116, (49), 25748-25756.

29. Shan, G.; Zhang, H.; Liu, H.; Xing, J., π-Complexation Studied by Fluorescence Technique: Application in Desulfurization of Petroleum Product using Magnetic π-Complexation Sorbents. *Separation Science and Technology* **2005,** 40, (14), 2987-2999.

30. Shahadat Hussain, A. H. M.; Tatarchuk, B. J., Adsorptive desulfurization of jet and diesel fuels using $Ag/TiO_x–Al_2O_3$ and $Ag/TiO_x–SiO_2$ adsorbents. *Fuel* **2013,** 107, 465-473.

31. Xue, M.; Chitrakar, R.; Sakane, K.; Hirotsu, T.; Ooi, K.; Yoshimura, Y.; Toba, M.; Feng, Q., Preparation of cerium-loaded Y-zeolites for removal of organic

sulfur compounds from hydrodesulfurizated gasoline and diesel oil. *Journal of Colloid and Interface Science* **2006,** 298, (2), 535-542.

32. Velu, S.; Song, C.; Engelhard, M. H.; Chin, Y.-H., Adsorptive Removal of Organic Sulfur Compounds from Jet Fuel over K-Exchanged NiY Zeolites Prepared by Impregnation and Ion Exchange. *Industrial & Engineering Chemistry Research* **2005,** 44, (15), 5740-5749.

33. Jeevanandam, P.; Klabunde, K. J.; Tetzler, S. H., Adsorption of thiophenes out of hydrocarbons using metal impregnated nanocrystalline aluminum oxide. *Microporous and Mesoporous Materials* **2005,** 79, (1), 101-110.

34. Kim, J. H.; Ma, X.; Zhou, A.; Song, C., Ultra-deep desulfurization and denitrogenation of diesel fuel by selective adsorption over three different adsorbents: A study on adsorptive selectivity and mechanism. *Catalysis Today* **2006,** 111, 74-83.

35. Xiao, J.; Li, Z.; Liu, B.; Xia, Q.; Yu, M., Adsorption of benzothiophene and dibenzothiophene on ion-impregnated activated carbons and ion-exchanged Y zeolites. *Energy & Fuels* **2008,** 22, (6), 3858-3863.

36. Nair, S.; Tatarchuk, B. J., Supported silver adsorbents for selective removal of sulfur species from hydrocarbon fuels. *Fuel* **2010,** 89, (11), 3218-3225.

37. Liang, C.; Tian, F.; Li, Z.; Feng, Z.; Wei, Z.; Li, C., Preparation and adsorption properties for thiophene of nanostructured W2C on ultrahigh-surface-area carbon materials. *Chemistry of Materials* **2003,** 15, (25), 4846-4853.

Chapter 4

MCM-41 and its Derivatives as Sorbents for the Desulfurization of JP-8

Abstract

Effective adsorbents are needed for the desulfurization of JP-8 fuel to meet the energy needs of the U.S. military. If ultra-low sulfur JP-8 is obtained, it can be used as a fuel source for solid oxide fuel cells. Here, we compare the use of silver loaded MCM-41, aluminosilicate MCM-41 (Al-MCM-41), and MCM-41 nanoparticles (MSN). We report the desulfurization performance of optimally loaded MCM-41, and the first real fuel desulfurization applications of Al-MCM-41 and MSN. Silver-loaded MSN displays a four-fold greater performance towards JP-8 fuel over previously reported sorbents, whereas MCM-41 displays a three-fold greater capacity. Al-MCM-41 displays a high first cycle capacity, but poor reproducibility after regeneration. Silver-impregnated MSN and MCM-41 were found to have saturation adsorption capacities of 32.6 mgS/g and 25.4 mgS/g, respectively. MSN displays a high capacity for the sterically hindered 4,-6-dimethyldibenzothiophenes along with a breakthrough capacity of 0.98 mgS/g at 10ppm$_w$S, which is twice that of previously published materials.

4.1 Introduction

MCM-41, discovered by Mobil researchers in 1992, is a mesoporous silicate material characterized by its hexagonal array of channels whose pore sizes can be tuned based on the synthetic conditions.[1] MCM-41 synthesis typically employs the use of the cationic surfactant cetyltrimtylammonium bromide (CTAB), shown in Figure 4.1, as a templating agent. However, the chain length of this surfactant can be tailored to produce different pore sizes. In addition, swelling agents can be added to the synthesis to increase pore size.[1]

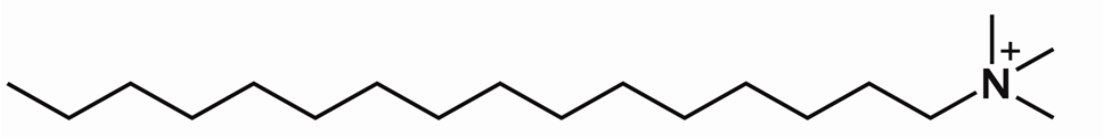

Figure 4.1 Chemical structure of CTAB containing a 16 carbon hydrophobic tail and an ionic head hydrophilic head group.

The high surface area and tunable pore size of MCM-41 has drawn much attention to the material as a potential sorbent for a variety of applications including water remediation.[2-5] Its high surface area also makes it ideal for use as a catalyst support.[6-8] Furthermore, MCM-41 has been explored as a delivery vehicle for theraputics.[9, 10]

MCM-41 has been explored for adsorptive desulfurization with both real and model fuels, and as a support for catalytic desulfurization.[11-13] CuCl/MCM-41 and $PdCl_2$/MCM-41 were tested with JP-5 (841 ppm_wS) and found to have saturation adsorption capacities of 14.4mgS/g and 16.0 mgS/g respectively, which are

noteworthy.[14] Cuprous oxide loaded MCM-41 was also explored, but with disappointing results compared to Cu^{+} when tested with JP-5.[15] Nickel nanoparticle loaded MCM-41 demonstrated the capacity to desulfurize several milliliters of model fuel per gram of sorbent to below 10 ppm_wS.[16] Lanthanum loaded MCM-41 was found to have a high breakthrough capacity of 1.53 mgS/g with diesel fuel.[17] Chen *et al.* tested $AgNO_3$ impregnated MCM-41 for the desulfurization of JP-5 (initial concentration 1172 ppm_wS). Their material displayed a saturation adsorption capacity of 32.1 mgS/g and a breakthrough capacity at 10 ppm_wS of 15.7mgS/g.[18] They were able to solvent regenerate their material to maintain 50% of its original capacity on the second cycle.[18] Overall, the current research points to MCM-41 being a promising framework, witch metal ions being more favorable than the corresponding metal oxide, and silver the most promising metal ion tested to date.

Aluminosilcate MCM-41 has been tested as a possible desulfurization sorbent for model fuels. Meng and coworkers tested aluminosilicate versions of MCM-41 and SBA-15 loaded with Ag^{+}, Ni^{2+}, or Ce^{3+} for the desulfurization of model fuel.[19] However, they neglected to compare the aluminosilicate frameworks to the pure silicate versions, making it impossible to draw conclusions as to whether the alumination was beneficial.

While MCM-41, and to a lesser extent Al-MCM-41, have been explored as desulfurization adsorbents, MCM-41 silica nanoparticles (MSN) have yet to be tested for this application. MSN's small size and high surface area make it ideal for a variety of applications including drug delivery, catalysis, imaging, and sensing.[20-22] These

properties also make them a promising framework for adsorptive desulfurization. Reports of mesoporous silica nanoparticles (not MCM-41 structured) have been used with model fuels. Fe_3O_4 magnetic core mesoporous silica microspheres were reported to desulfurize model fuel, yielding capacities of 4.70 mgS/g after introducing $AgNO_3$.[23]

Ag-MCM-41 has been reported for desulfurization, however, the authors did not report any attempts to optimize the silver loading, or give their reasoning for the amount of silver selected. The derivatives of MCM-41, aluminosilicate (Al-MCM-41) and nanoparticle MCM-41 (MSN), have not been tested with silver as potential desulfurization sorbents. Herein, we elucidate the optimized silver loading for these three frameworks: MCM-41, Al-MCM-41, and MSN, and determine the most promising sorbent for adsorptive desulfurization of JP-8. We also optimize the regeneration procedure, explore the binding mechanism between the organosulfur contaminants and the sorbent, and study the selectivity of organosulfur removal over non-sulfur containing aromatics.

4.2 Experimental

4.2.1 Materials

All chemicals were used as received without further purification. Tetraethylorthosilicate (TEOS), benzothiophene (BT), and dibenzothiophene (DBT) were all obtained from Acros Organics. Sodium hydroxide, aluminum isopropoxide, ammonium hydroxide, and naphthalene (NA) were obtained from Fisher Scientific. Cetyltrimethylammonium bromide (CTAB), diethyl ether, and bulk MCM-41 were obtained from Sigma Aldrich. Silver nitrate was obtained through MP Biomedicals, decane from TCI, 4,6-dimethyldibenzothiophene (DMDBT) from Frontier Scientific, and isopropanol from Ricca Chemical.

4.2.2 Synthesis of Al-MCM-41

High aluminum content MCM-41 was synthesized in a similar manner to that found in literature[24]. 1.4 g of aluminum isopropoxide was dissolved in 21.88 g of isopropanol with magnetic stirring. In a separate beaker, 3.6 g of CTAB was dissolved in 120 g doubly distilled deionized water and 9.24 g ammonium hydroxide. 10.00 g of TEOS was added to the isopropanol solution, stirred, and then added dropwise to CTAB solution over approximately 15 minutes with stirring. The solution was allowed to stir for an additional 30 minutes before static aging overnight at room temperature. The solid was filtered and rinsed with copious amount of doubly distilled deionized water. The material was dried and then calcined at 550^{o}C for 5 hours with a 1°C/min ramp rate.

4.2.3 Synthesis of MSN

MCM-41 nanoparticles (MSN) were synthesized using a method previously published by our lab.[25] A solution containing 1.0 g CTAB, 0.28 g NaOH, and 483.5 g doubly distilled deionized water was stirred at 80 ^{o}C at a rate of 625 rpm. After at least 15 minutes of stirring, 4.58 g TEOS was added dropwise over a two minute period. After two hours of stirring, the beaker was removed from the oil bath and allowed to age at room temperature prior to filtering and rinsing with copious amounts of doubly distilled deionized water. The product was then dried, ground, and calcined at 560 ^{o}C for 4 hours with a ramp rate of 1 ^{o}C/min.

4.2.4 Metal Loading

MCM-41, MSN, and Al-MCM-41 were loaded with the desired amount of silver *via* wet impregnation. Silver nitrate was dissolved in a minimal amount (typically ~ 0.3 g) of water/ethanol solution and added dropwise to the frameworks. Once the samples were wet, they were placed in a 110 ºC vacuum oven to dry. These steps were repeated until the sample had adsorbed all the silver from solution. To achieve 18 wt.% and 20 wt.% Ag, 0.283 g and 0.315 g of $AgNO_3$, respectively, were used per gram of framework material.

4.2.5 Characterization

Powder X-ray Diffraction (PXRD) was performed on a Rigaku SmartLab X-ray diffractometer with Cu Kα radiation. Samples were analyzed from 2º to 80º (2θ) with a step size of 0.01º. BET surface area of the samples was measured by physical adsorption of N_2 at 77 K using a Micromeritics physisorption analyzer (TriStar II 3020 v1.03). Adsorption/desorption isotherm measurements were collected in the relative pressure range (P/P_o) from 0.01 to 1.00. Scanning electron microscopy (SEM) and scanning transmission electron microscopy (STEM) data were collected with a FEI Quanta 3D Dualbeam microscope. Inductively Coupled Plasma (ICP) was collected on a Perkin-Elmer Optima 7000 DV. UV–Vis diffuse reflectance spectra (UV–Vis DRS) were obtained by using a Varian Cary 5000 UV–Vis–NIR spectrophotometer (Harrick Praying Mantis diffuse reflectance cell attachment, Teflon standard).

4.2.6 Fuel Tests

Model fuels were made with n-decane and BT, DBT, DMDBT, or NA as the contaminant, with concentrations as noted. Model fuel batch tests were performed over 1 hour unless otherwise noted. JP-8 batch tests were performed over 24 hours with approximately 40 mg of sorbent in 5g of JP-8. Both column and 24-hour batch (beaker) test experiments were analyzed for total sulfur concentration using a UV total sulfur analyzer (multi EA 3100, Analytikjena) with a detection limit of 45 ppb.

Model fuel test concentrations were determined by UV-Vis on a Hewlett-Packard Model 8452A spectrophotometer. FT-IR data was collected after exposing sorbents to 500 ppm_wS model fuel of DBT in n-decane for 1 hour, rinsing with decane to remove any physisorbed DBT, followed by drying at 110°C under vacuum before forming KBr pellets. Infrared spectra were recorded using a Perkin-Elmer Spectrum-One FT-IR. Selectivity tests were performed using a model fuel composed of decane containing 7.4 mM dibenzothiophene and 7.4 mM naphthalene (Acros Organics for solvent and reagents). Samples were analyzed by gas chromatography (HP 5890 Series II, Restek column Rxi-5HT 30m length, 0.25mm I.D., 0.25μm film thickness) after one hour exposure to the sorbent.

4.3 Results and Discussion

4.3.1 Synthesis and Characterization

Similar synthetic methods were used for both aluminosilicate MCM-41 (Al-MCM-41) and MCM-41 nanoparticles (MSN). Figure 4.2 shows the general synthetic scheme: the templating agent self assembles into micelles where the silicate precursors (or aluminosilicate precursors in the case of Al-MCM-41) condense around them, followed by removal of the templating agent to yield a mesoporous framework. Other than the addition of aluminum, the major synthetic differences between bulk Al-MCM-41 and MSN is the relative solvent concentration and stir speed. Bulk Al-MCM-41 can be produced in a relatively concentrated solution and stir speed does not need to be closely regulated. However, the MSN synthesis requires a very dilute reaction mixture and a highly regulated stir speed, and without both spherical nanoparticles will not be obtained.

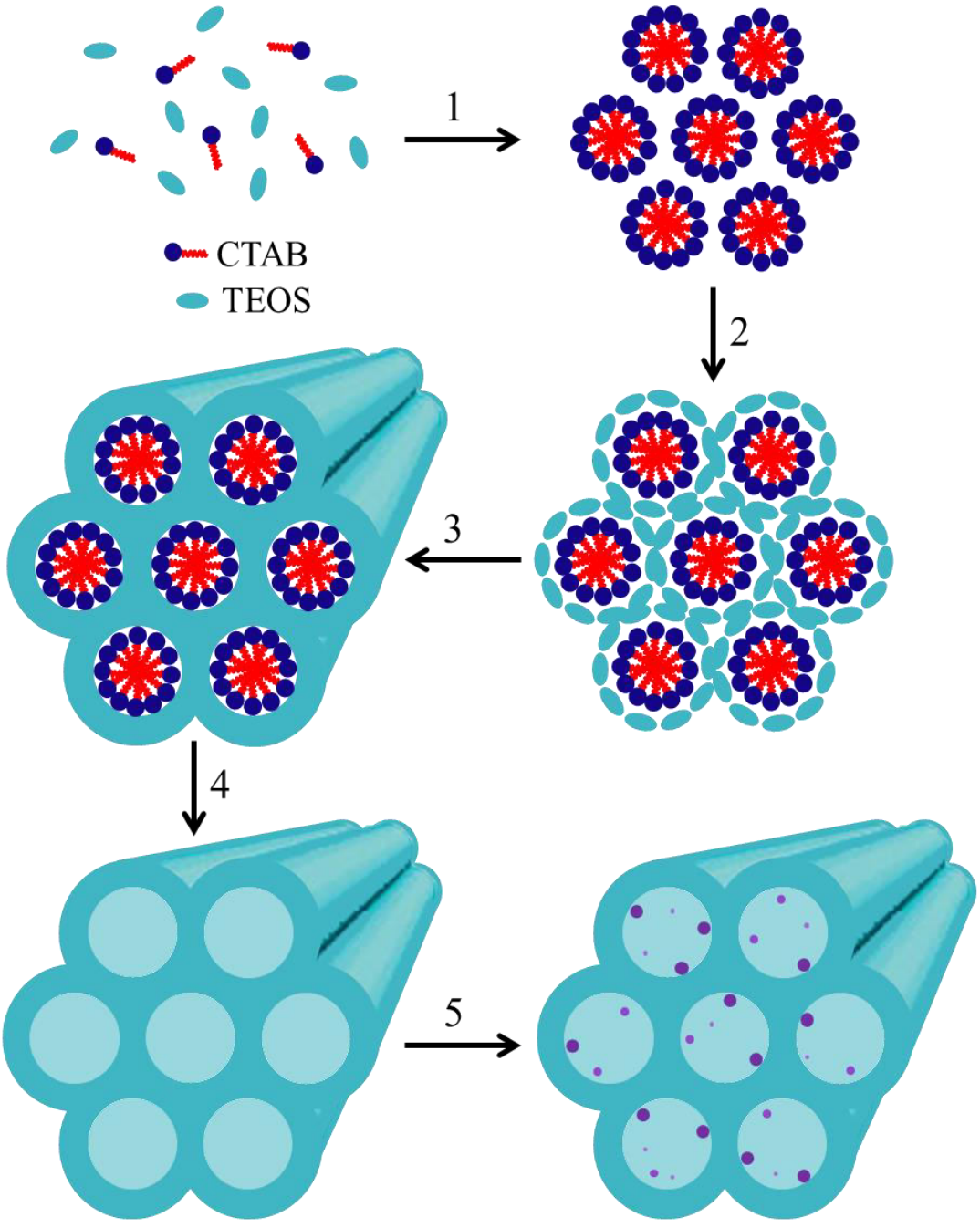

Figure 4.2 Representation of the synthesis of MCM-41. The templating agent, CTAB, self-assembles into hexagonally packed cylindrical micelles (1). These micelles are surrounded by TEOS (2) and go through hydrolysis to form a solid framework (3). The CTAB can then be removed through extraction or calcination (4). The framework is then impregnated with silver (5).

Both synthetic procedures for aluminosilicate MCM-41 (Al-MCM-41) and nanoparticle MCM-41 (MSN) utilized CTAB as the organic templating agent. This resulted in the (100) peak for both to have a similar d-spacing by PXRD analysis, indicating similar pore sizes. The most dramatic difference between the PXRD patterns of MCM-41 (Figure 4.3), MSN (Figure 4.4), and Al-MCM-41 (Figure 4.5) is that for Al-MCM-41 only the (100) peak is present. For both MCM-41 and MSN the (110) and (200) are clearly visible, and the (210) peak is detectable. This indicates the MSN synthesis and commercial MCM-41 have more long-range order than the Al-MCM-41 material. It is common to see this occur as the Si:Al ratio is decreased in aluminosilicate MCM-41, as does the overall intensity of the PXRD peaks, and the (110), (200), and (210) peaks can be completely absent.[26, 27]

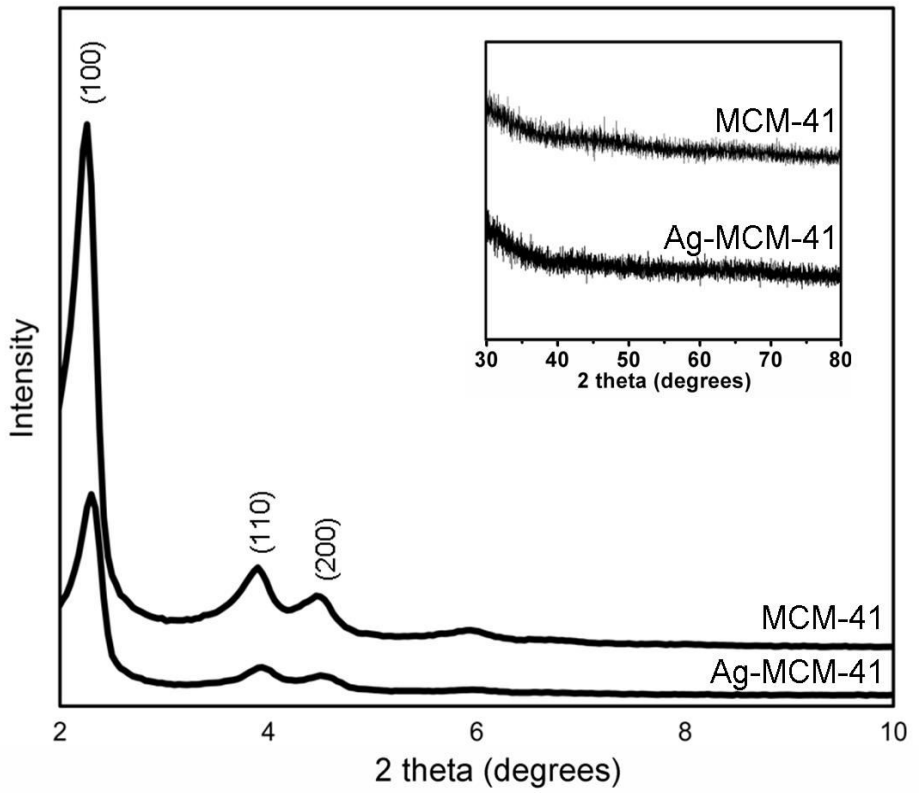

Figure 4.3 PXRD of bulk powder MCM-41 and Ag-MCM-41 which is loaded with 18 wt.% Ag. Inset: lacks higher angle peaks, indicating silver is well dispersed.

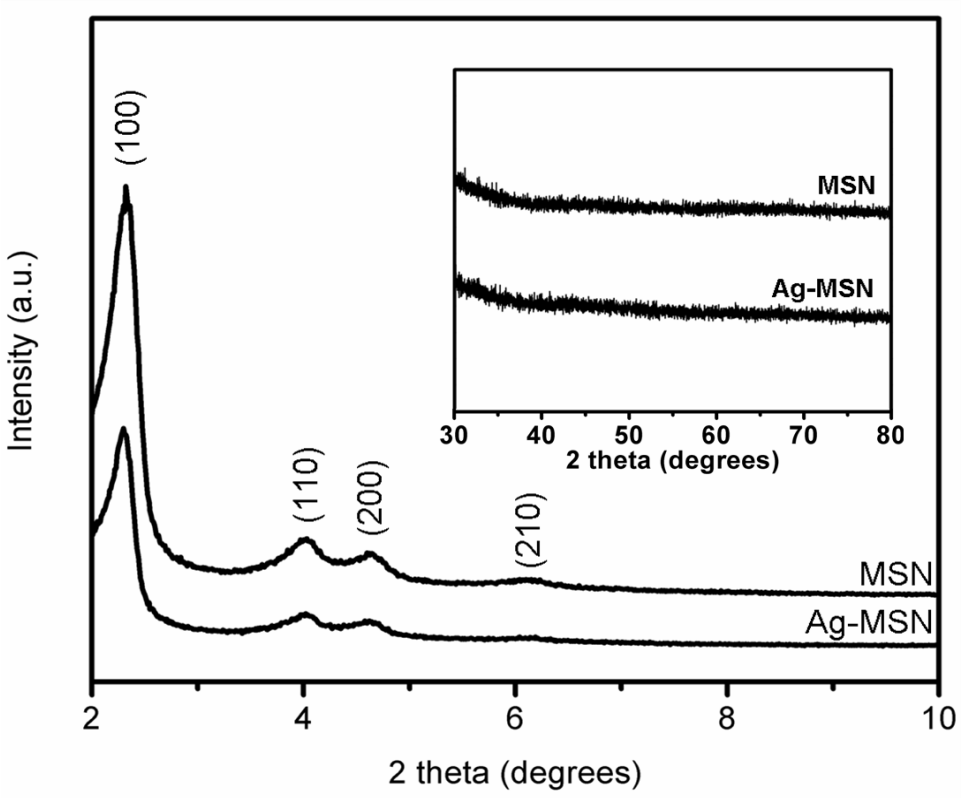

Figure 4.4 PXRD of MSN and Ag-MSN which is loaded with 20 wt.% Ag. Inset: lacks higher angle peaks, indicating silver is well dispersed.

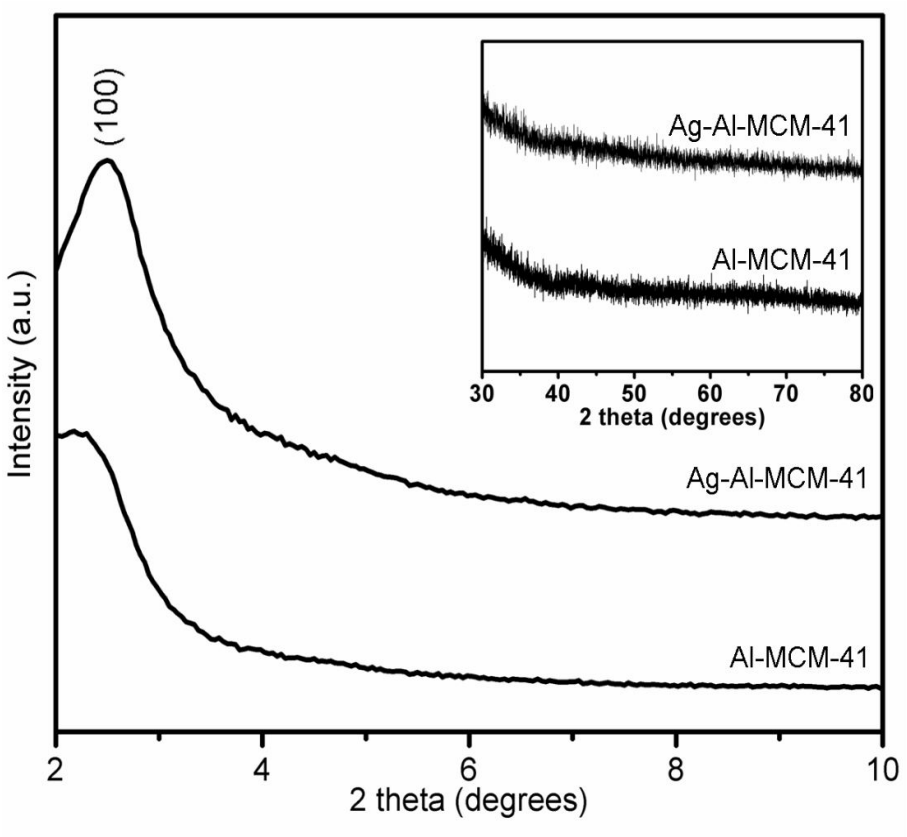

Figure 4.5 PXRD of bulk powder Al-MCM-41 and Ag-Al-MCM-41 which is loaded with 18 wt.% Ag. Inset: lacks higher angle peaks, indicating silver is well dispersed.

The PXRDs for all three MCM materials (Figures 4.3, 4.4, and 4.5) indicate that when wet impregnated with silver, there is no effect to the overall structure. Also, an examination of the higher angle regions show no peaks associated with silver nitrate or silver oxide, indicating that the silver is well dispersed within the structure.[28]

The UV-visible diffuse reflectance spectra (Figures 4.6, 4.7, 4.8) show a high intensity above 200 nm for all three silver loaded materials, indicative of the presence of Ag^{+}, which is commonly seen in literature appearing around

250 nm.[29, 30] A band at 290 nm indicates the presence of $Ag^{\delta+}$. There is a much more pronounced shoulder for Ag-MCM-41 compared to Ag-Al-MCM-41 in this region (Figure 4.7). This indicates a higher silver oxide content in Ag-MCM-41, which is expected because of its neutral framework.[29, 30] Al-MCM-41 has a negatively charged framework, which is expected to better stabilize the positive charge of the silver ions.

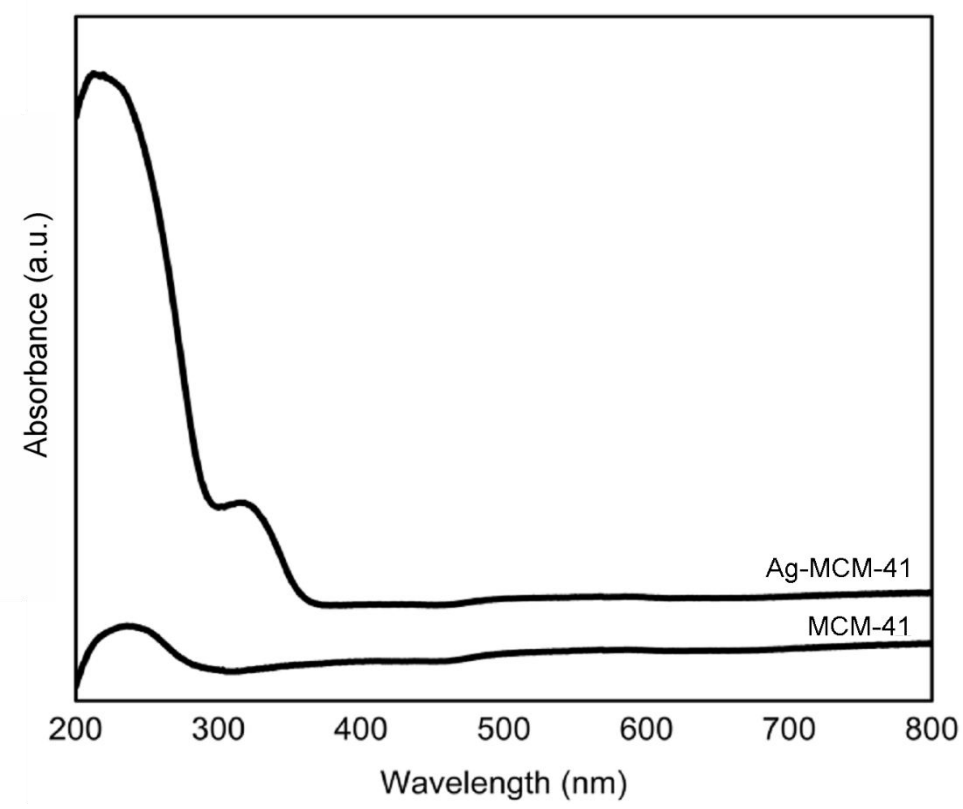

Figure 4.6 UV-Visible diffuse reflectance spectra of MCM-41 and Ag-MCM-41 loaded with 18 wt.% Ag.

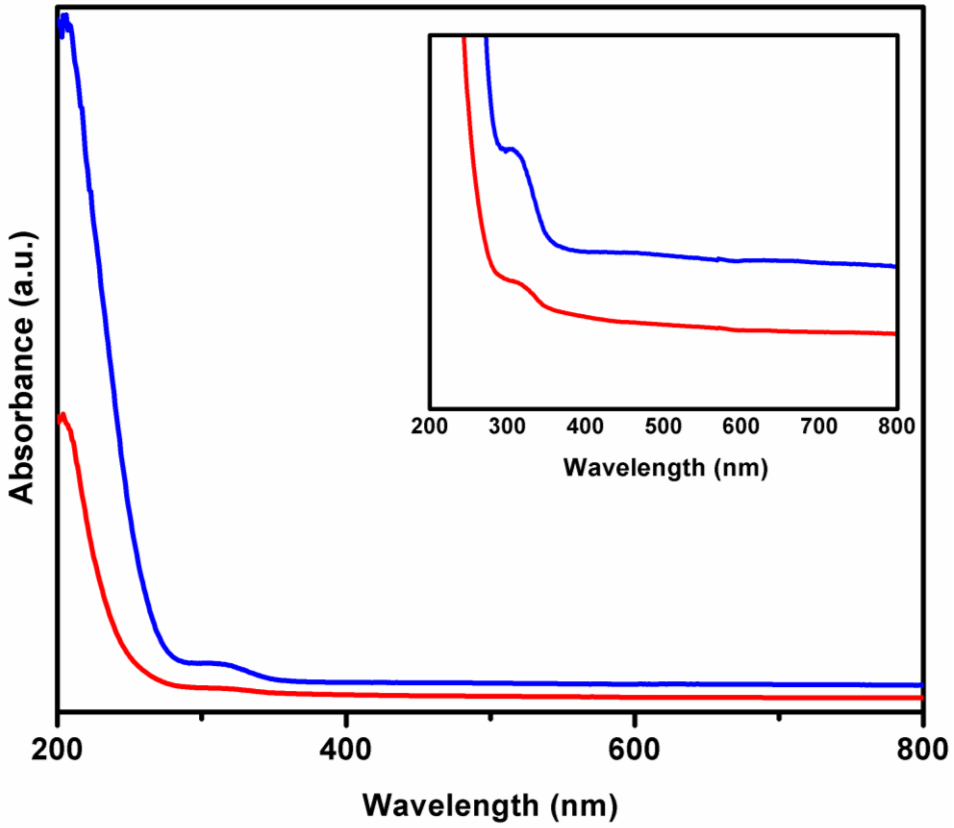

Figure 4.7 UV-Visible diffuse reflectance spectra of Ag-MCM-41 (blue) and Ag-Al-MCM-41 (red), both loaded with 18 wt.% Ag.

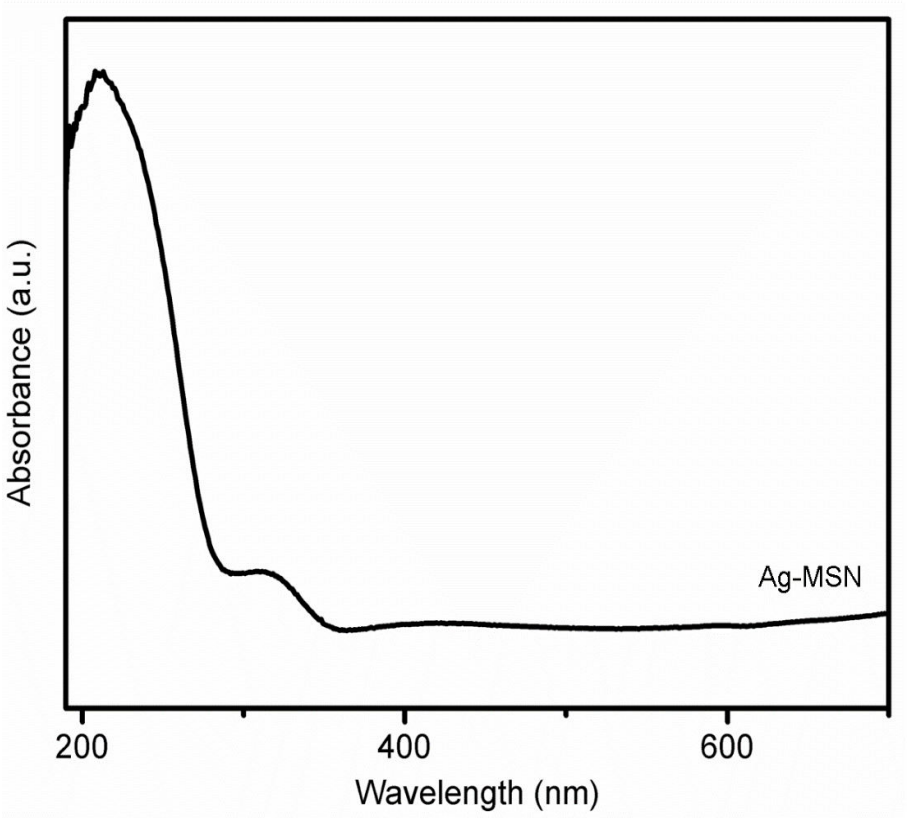

Figure 4.8 UV-Visible diffuse reflectance spectra of Ag-MSN loaded with 20 wt.% Ag.

The surface area of all three materials was determined through BET analysis. The majority of surface area for each framework was retained after being loaded with their optimized (described below) amount of silver *via* wet impregnation using silver nitrate (Table 4.1). MSN has the highest surface area, which is expected due to its small particle size in addition to having the same pore structure as MCM-41 and Al-MCM-41.[28]

Table 4.1 BET surface area analysis; MCM-41 and Al-MCM-41 are loaded with 18 wt.% and MSN is loaded with 20 wt.% silver

Sorbent	Surface Area Before Ag Loading (m^2/g)	Surface Area After Ag Loading (m^2/g)
MCM-41	883.6	528.4
Al-MCM-41	978.0	765.3
MSN	1068	703

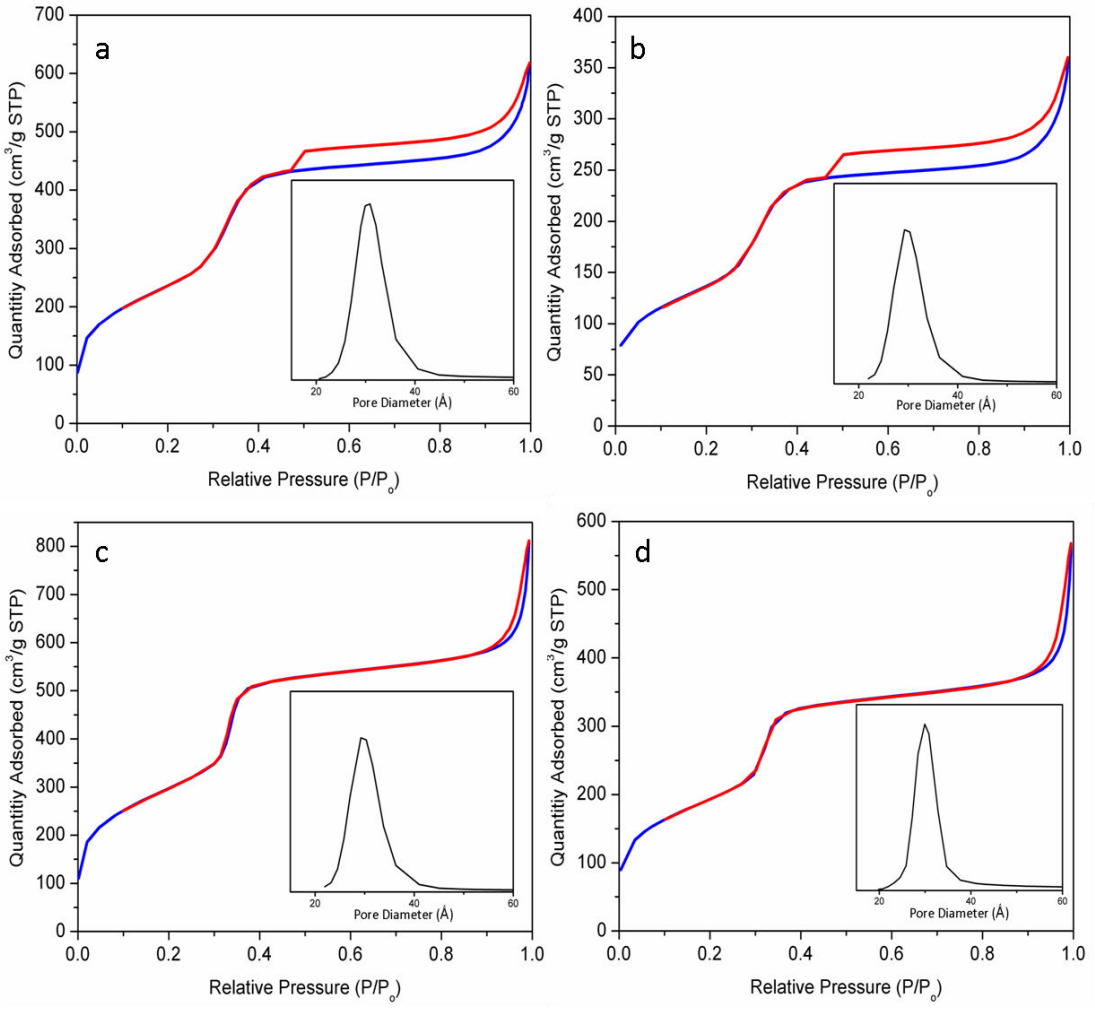

Figure 4.9 N_2 adsorption (blue) and desorption (red) isotherms for MCM-41 (a), Ag-MCM-41 (b), MSN (c), and Ag-MSN (d). Insets show pore size distribution.

Further analysis of the N_2 adsorption and desorption isotherms were performed on the native and silver loaded forms of MCM-41 and MSN. The pore volume and diameter was found to be larger for the MSN compared to MCM-41, as shown in Table 4.2. The pore volume decreased by ~ 30% with silver loading for MSN, and ~ 40% for MCM-41. The pore diameter remained relatively constant before and after silver loading, with only a slight decrease observed.[28]

Table 4.2 Physical characteristics obtained from N_2 isotherms

Sorbent	BJH Pore Volume (cm^3/g)[a]	BJH Pore Diameter (nm)[b]
MCM-41	1.05	3.12
Ag-MCM-41	0.61	3.06
MSN	1.35	3.17
Ag-MSN	0.93	3.16

[a]BJH adsorption pore volume; [b]BJH adsorption average pore diameter

STEM and SEM analyses were used to discern the different morphologies between the MSN and MCM-41. MCM-41, which is a bulk powder, contains a variety of particle shapes, mostly in the micron range, as shown in Figure 4.10. MSN, in contrast, consists of spherical nanoparticles with an average diameter of ~ 80 nm, as shown in Figure 4.11.[28]

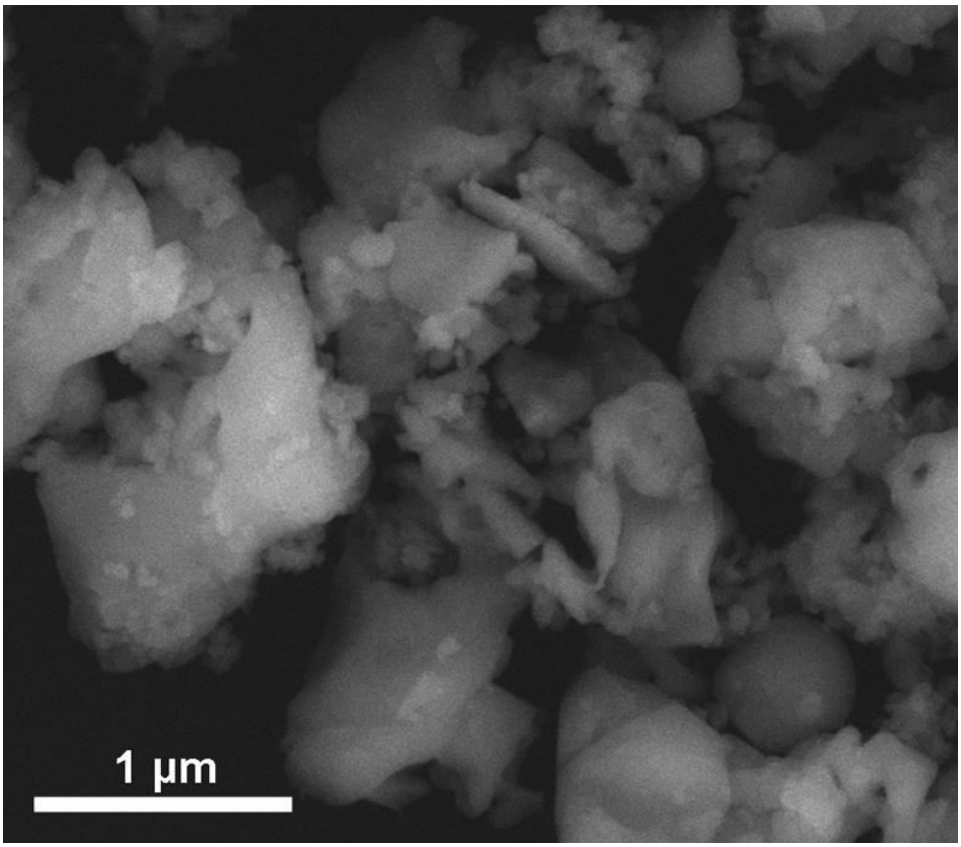

Figure 4.10 SEM micrograph of bulk powder MCM-41.

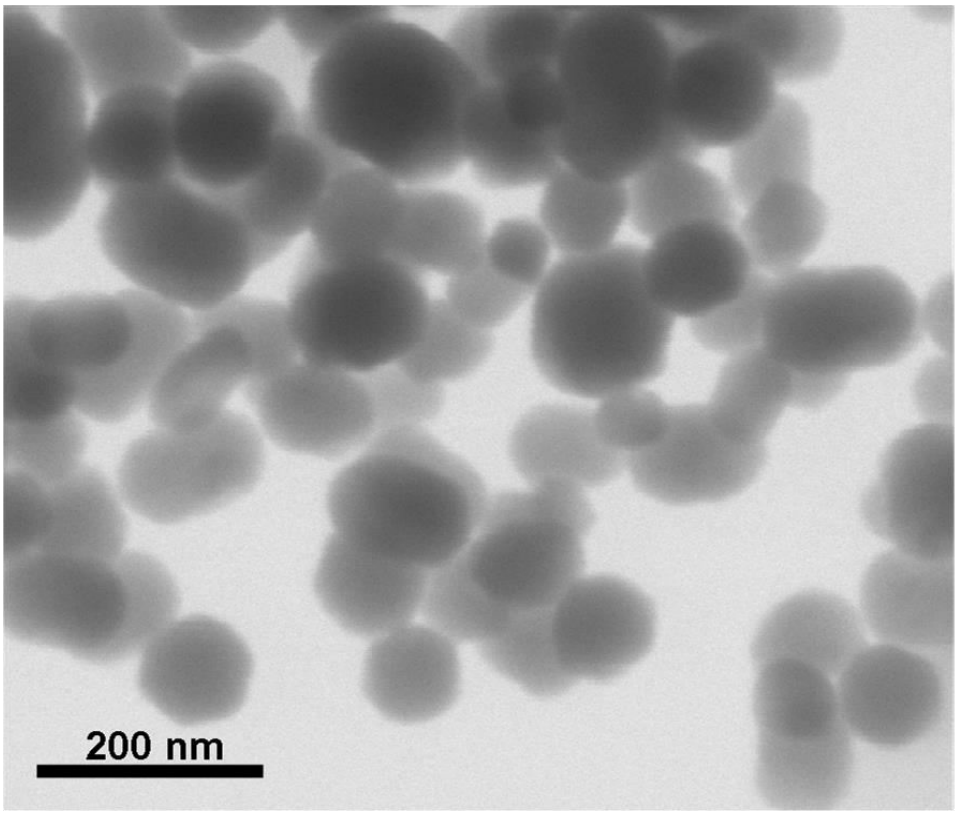

Figure 4.11 SEM micrograph of MSN.

Further analysis was done on MSN and Ag-MSN using TEM to elucidate the fine structure and silver distribution. TEM of MSN (Figure 4.12) reveals the 1D pores that run across the entire nanoparticle. Figure 4.13 shows that the silver is uniformly dispersed throughout the nanoparticle. Small silver clusters, likely composed of silver nitrate based on the UV-Vis DRS results, are present throughout the nanoparticle. The largest clusters are approximately 5 nm across while the majority of the visible clusters are less than 2 nm.[28]

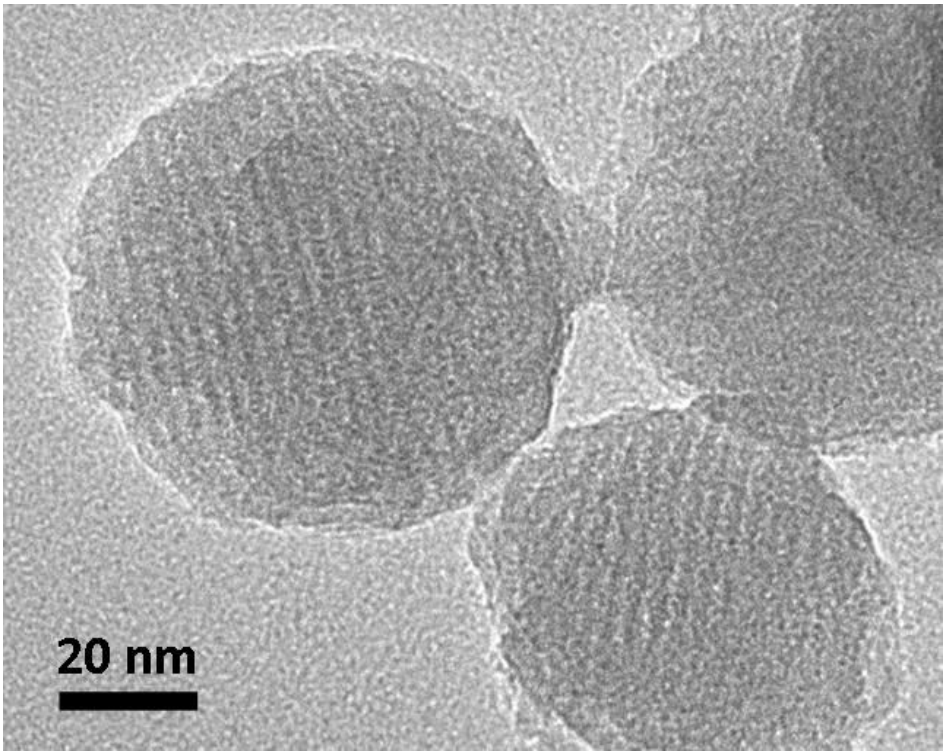

Figure 4.12 TEM micrograph of MSN.

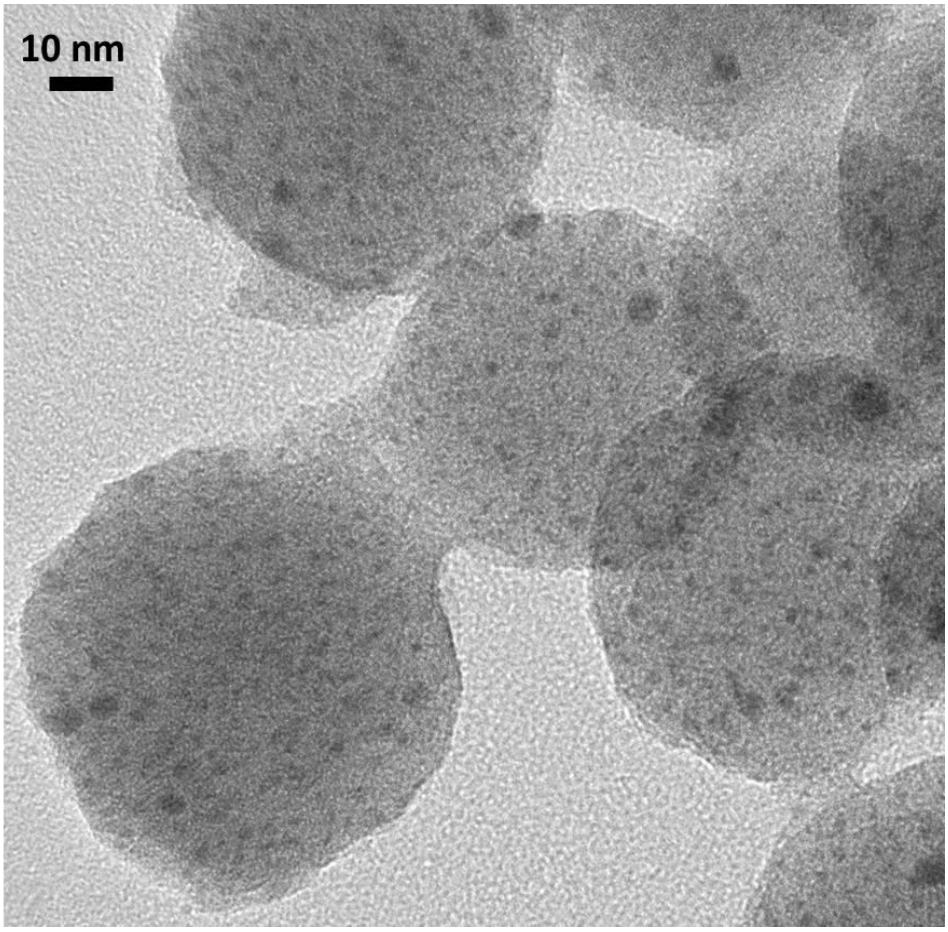

Figure 4.13 TEM micrograph of Ag-MSN.

4.3.2 Model Fuel Tests

To determine the ideal amount of silver nitrate to load into the MCM frameworks, 1-hour model fuel tests were performed using a variety of loading amounts. Al-MCM-41 and MCM-41 displayed a similar trend. The model adsorption capacities for MCM-41 are shown in Figure 4.14. The adsorption capacity reached a peak at 18 wt.% Ag, and then decreased at 21 wt.%. For Ag-MSN, as shown in Figure 4.15, the capacity reached a peak at 20 wt.%, where it absorbed 12.7 mgS/g. After 20 wt.%, a decrease was observed to only 9.4 mgS/g at 25 wt.%.[28] The

adsorption capacity increases with increased silver loading up until a point where the silver, which provides binding sites for the organosulfur compounds, is still highly dispersed. However, after a point the silver likely starts to aggregate. Only the surface of these aggregates is available to bind organosulfur, and as the aggregates get larger they can block the pores. This effect has been seen with silver loaded TiO_2, where increased silver loading leads to decreased surface area and pore volume. The authors attribute this to the formation of silver agglomerates.[31] For all remaining model fuel and JP-8 testing, 18 wt.% loading was used for MCM-41 and Al-MCM-41, and 20 wt.% was used for MSN.

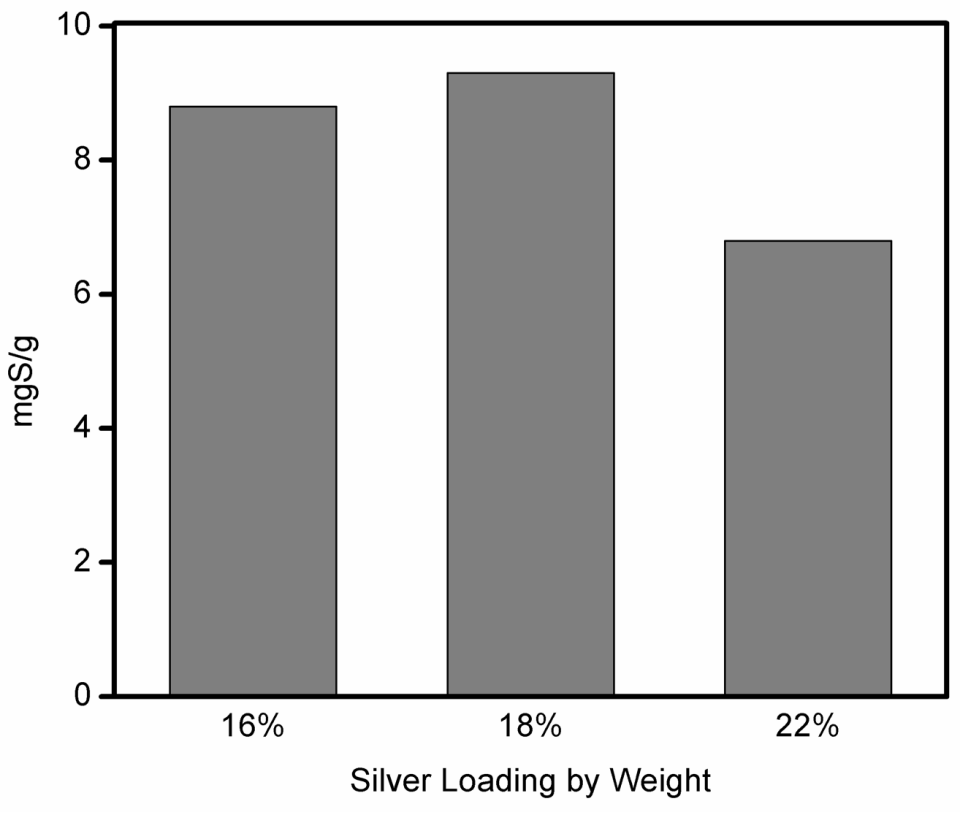

Figure 4.14 Optimization of silver loading for bulk powder MCM-41 using 500 ppm_wS model fuel and 1-hour fuel test.

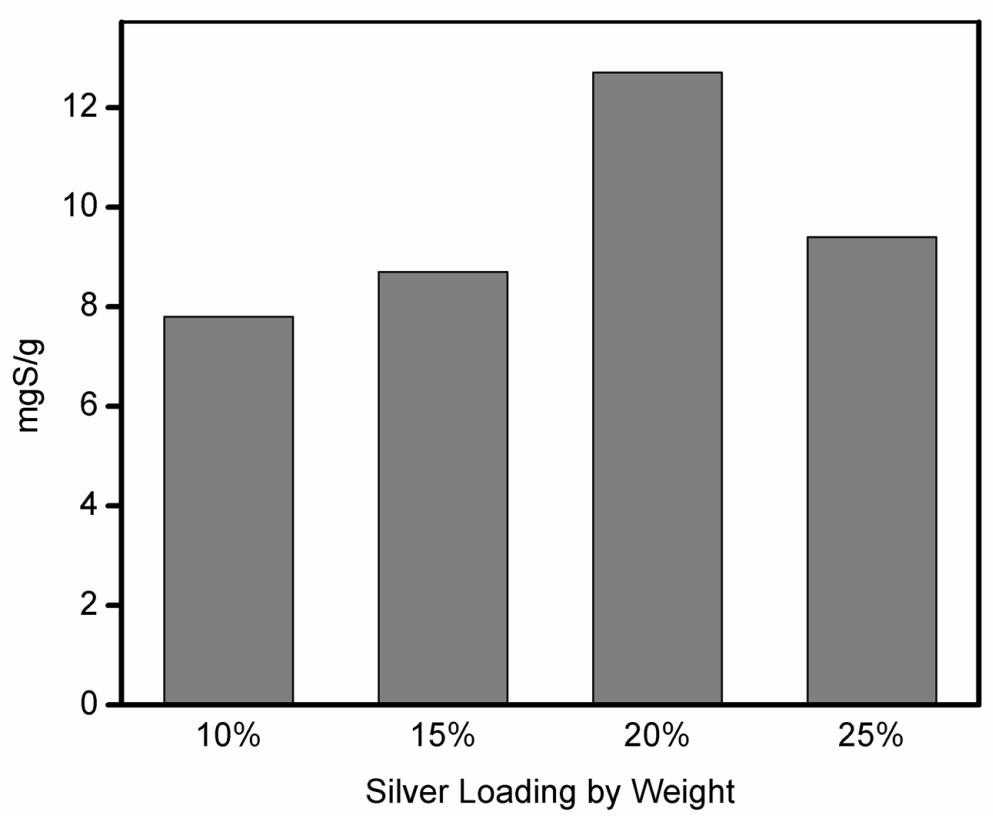

Figure 4.15 Optimization of silver loading for MSN using 500 ppm_wS model fuel and 1-hour fuel test.

4.3.3 JP-8 Fuel Tests

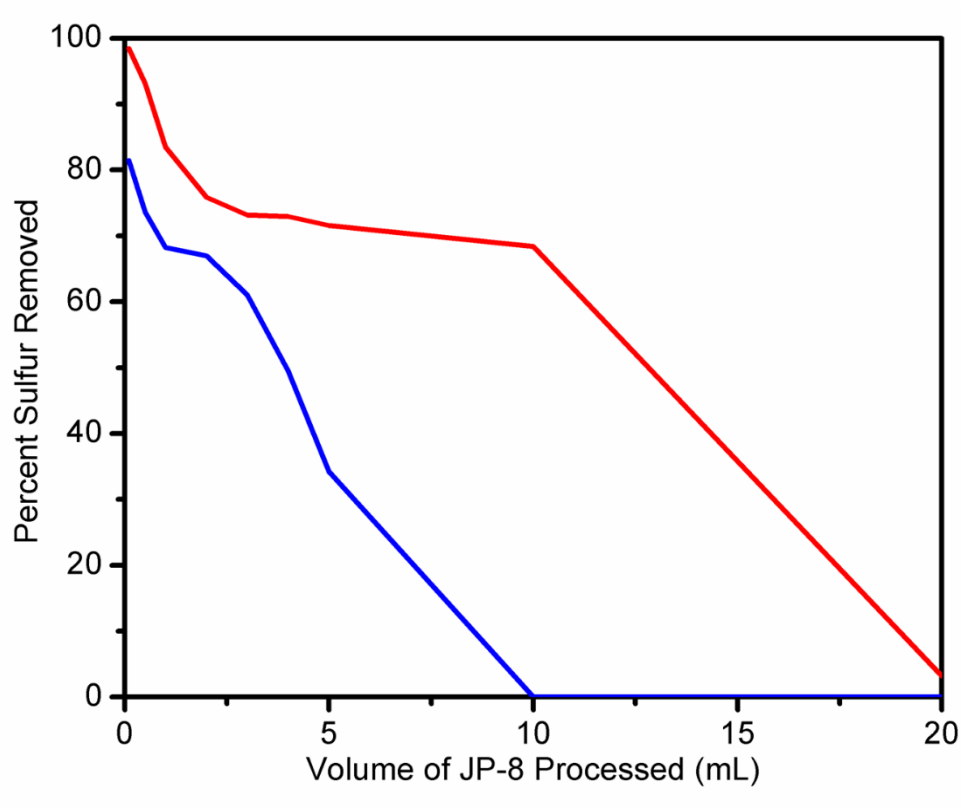

Figure 4.16 Column study of Al-MCM-41 loaded with 18 wt.% Ag (red) and column study after regeneration with isooctane (blue).

Figure 4.16 shows Ag-Al-MCM-41 regenerated using isooctane, which has been reported as a viable solvent for regeneration of desulfurization sorbents.[32] However, on the first cycle the initial outlet concentration of the fuel was 7.5 ppm_wS whereas after regeneration it was initially 88.9 ppm_wS. This demonstrates that isooctane is unable to produce a sorbent capable of reaching deep desulfurization levels. It is possible that some of the binding between the silver and organosulfur contaminants is too strong to be broken by an isooctane rinse. Figure 4.17 shows the same material regenerated with

diethyl ether, another solvent which has been demonstrated as effective for regenerating desulfurization sorbents.[33, 34] With this technique, the initial outlet concentration was only 2 ppm_wS higher in the second cycle, compared to the first, which is within the instrument error. Diethyl ether is the preferred solvent for solvent regeneration and was used for all remaining regeneration experiments.

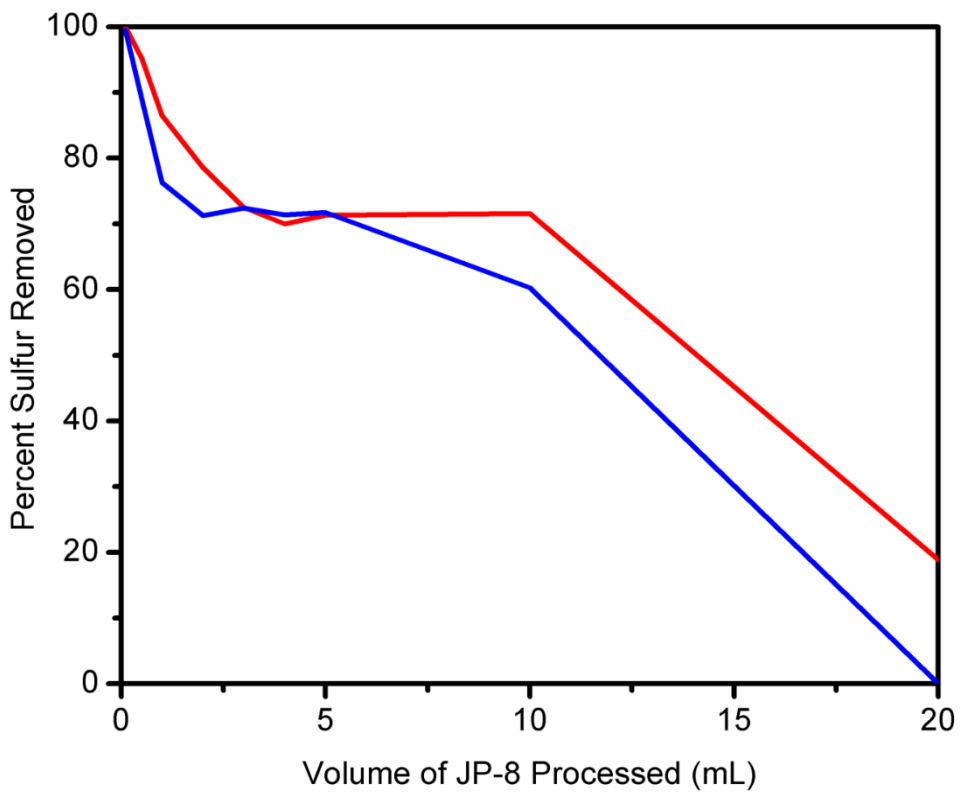

Figure 4.17 Column study of Al-MCM-41 loaded with 18 wt.% Ag (red) and column study after regeneration with diethyl ether (blue).

Ag-Al-MCM-41 retained 83% of its original capacity, shown in Figure 4.17, which is far superior to the reported 50% retained capacity with silver

loaded MCM-41 regenerated with heat.[18] Figure 4.18 shows the first two cycles of another batch of Ag-Al-MCM-41, following the same synthetic procedures as those used for the material shown in Figure 4.17. They also have nearly identical PXRD patterns and very similar first cycle results (minor differences result in different column packing in each trial). However, Figure 4.18 shows Ag-Al-MCM-41 retaining only 56% of its initial capacity. Overall, there were large discrepancies between batches for this sorbent, resulting in an average second cycle capacity of 63±14%. High aluminum content in MCM-41 has been linked to poor stability and can cause some framework collapse, which is likely the cause of poor reproducibility between batches.[35, 36] Ag-MCM-41, shown in Figure 4.19, resulted in consistent regenerability with an average second capacity of 71±1%. Due to its unreliable properties, Al-MCM-41 was not further considered as a viable sorbent for this application.

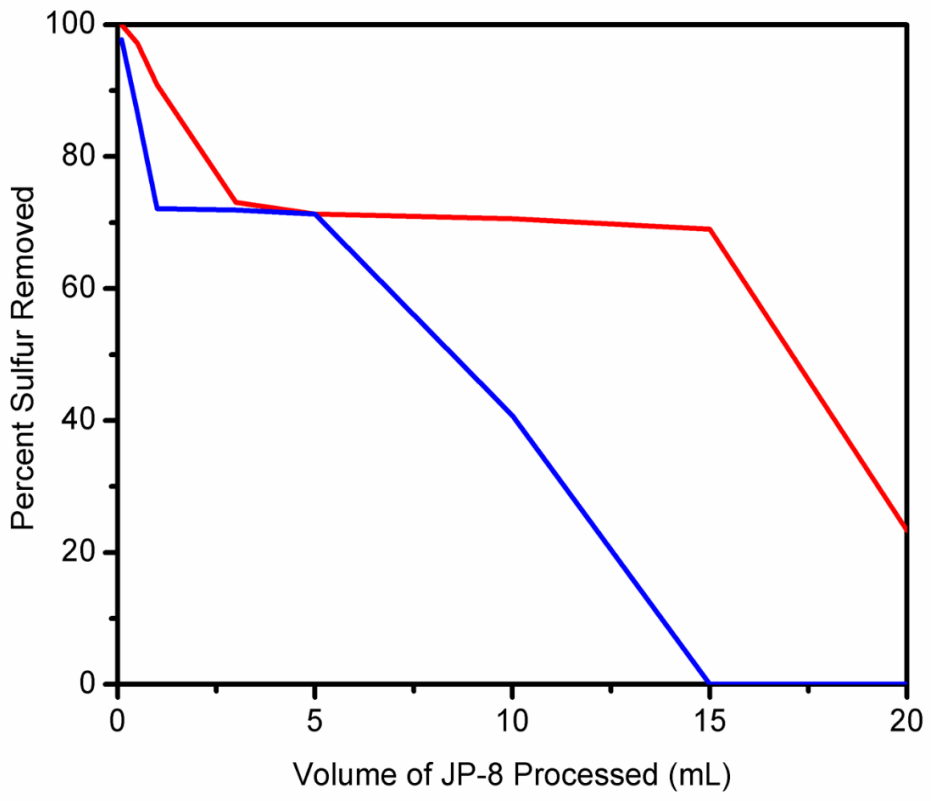

Figure 4.18 Column study of Ag-Al-MCM-41 (same synthetic procedure, but different batch from that shown in Figure 4.17) loaded with 18 wt.% Ag (red) and column study after regeneration with diethyl ether (blue).

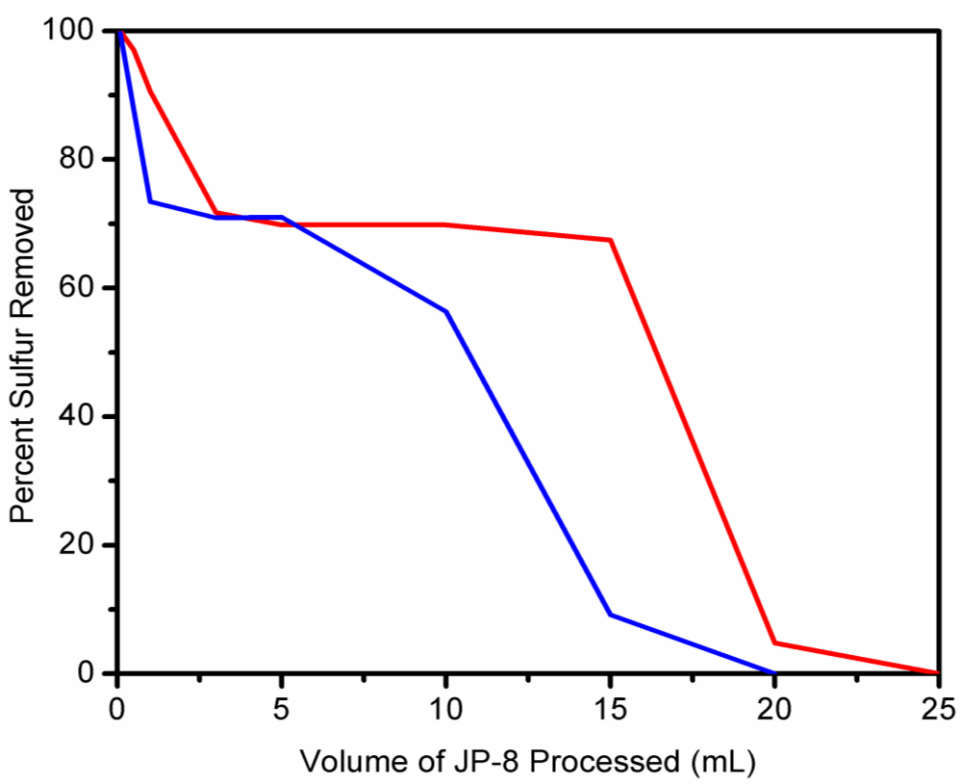

Figure 4.19 Column study of MCM-41 loaded with 18 wt.% Ag (red) and column study after regeneration with diethyl ether (blue).

In an effort to improve the adsorption capacity of Ag-MCM-41, we synthesized a nanoparticle form of MCM-41 in order to increase the overall surface area. Materials with increased surface consistently showed increased desulfurization adsorption capacities.[37] Figure 4.20 shows the first and second cycle for Ag-MSN. The first cycle processed significantly more fuel before being completely saturated. At 40 mL, the material was still capable of removing a small amount of sulfur, whereas Ag-MCM-41 was completely spent after 25 mL. In addition, the second cycle performed similarly to the first cycle of Ag-MCM-41.

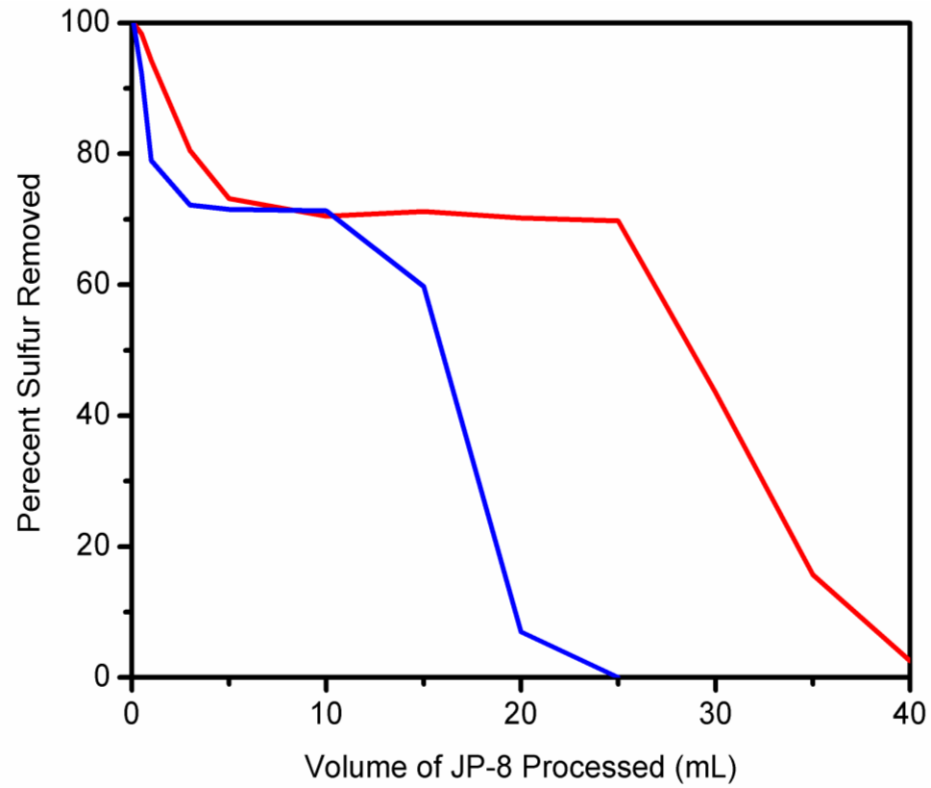

Figure 4.20 Column study of MSN loaded with 20 wt.% Ag (red) and column study after regeneration with diethyl ether (blue).

By converting the data in Figures 4.19 and 4.20 to adsorption capacities, we can compare the performance of the first and second cycles of Ag-MCM-41 and Ag-MSN. Ag-MCM-41 has a first cycle column capacity of 23.0 mgS/g, whereas Ag-MSN has a first cycle capacity of 41.9 mgS/g. After regeneration, Ag-MSN has a capacity of 21.0 mgS/g, nearly that of Ag-MCM-41's first cycle. Batch model fuel testing showed a first cycle capacity of 12.7 mgS/g for Ag-MSN and a drop to 9.2 mgS/g, corresponding to ~ 70% regeneration *via* this method. This 30% decrease is likely due to a loss in silver. ICP analysis confirms that ~ 30% of the silver content

was lost after regeneration. The column study shows a lower regenerability, likely due to the column conditions causing a greater silver loss.

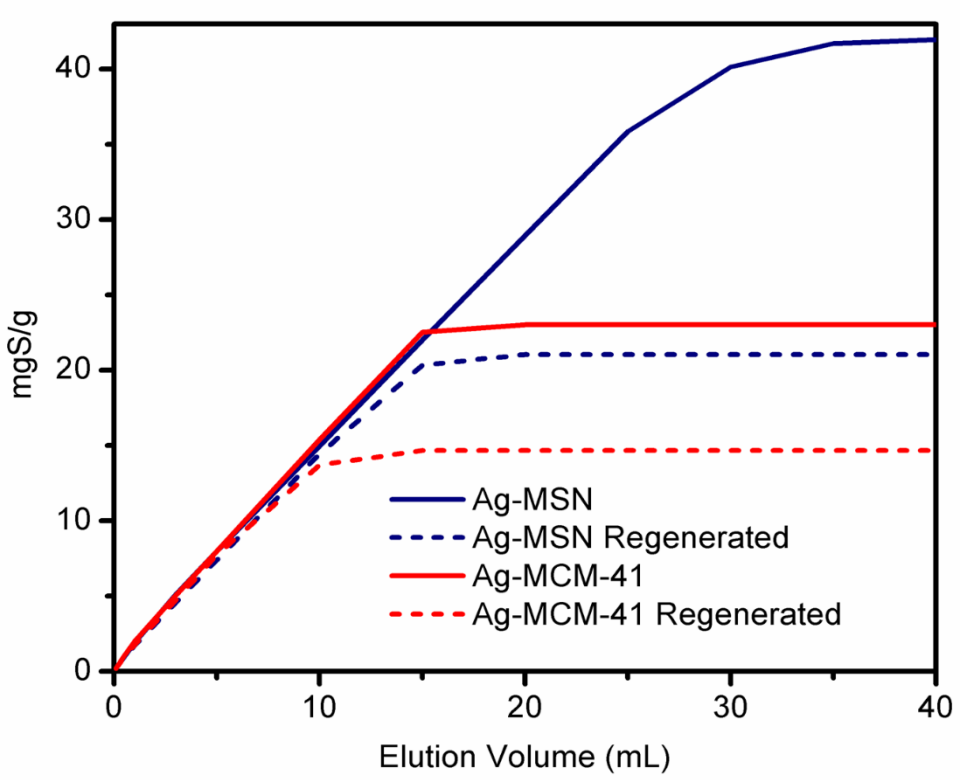

Figure 4.21 Column study of Ag-MCM-41 and Ag-MSN showing initial run and after one regeneration with diethyl ether, shown in terms of adsorption capacity.

A second regeneration cycle was performed on Ag-MSN, as shown in Figure 4.21. The second regeneration again shows approximately 50% decrease in capacity. All three cycles do initially start with 100% sulfur removal, demonstrating that over two cycles the ability of Ag-MSN to reach deep desulfurization levels of less than 1 ppm_wS is not diminished. But, the overall adsorption capacity is affected; the material reaches a point of saturation after processing far less fuel than in the original cycle.

This loss of function is attributed to a loss of silver occurring either during the desulfurization or regeneration process, which was confirmed by ICP.[28]

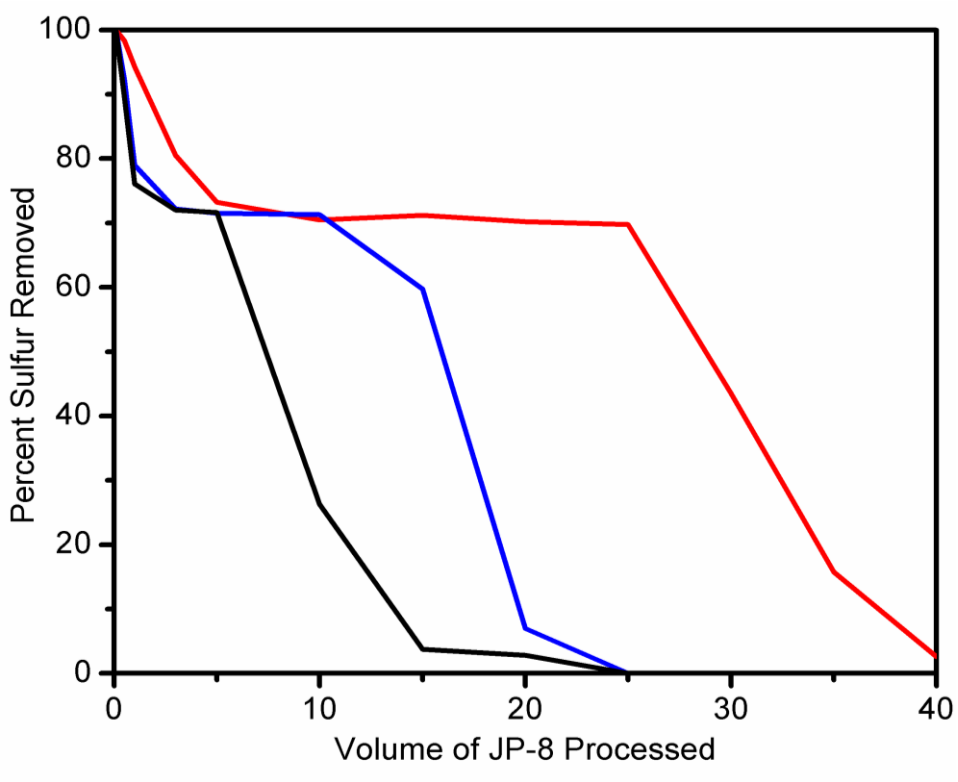

Figure 4.22 Column study of MSN loaded with 20 wt.% Ag (red) and column study after regeneration with diethyl ether (blue) and a second regeneration with diethyl ether (black).

Breakthrough capacities – the adsorption capacity of a material before the outlet concentration is above a designated threshold – were calculated for all three silver loaded frameworks. As shown in Table 4.3, Ag-MSN had the largest breakthrough capacity at 10 ppm_wS, and was significantly higher than the highest value that has been reported in literature.[28]

Table 4.3 Breakthrough capacities from column studies with JP-8 compared to the highest reported literature value tested with JP-8 (initial concentration 630 ppm_wS)

Sorbent	Breakthrough Capacity at 10 ppm_wS (mgS/g)
Ag-MCM-41	0.21
Ag-Al-MCM-41	0.39
Ag-MSN	0.98
Ag- TiO_x-Al_2O_3[38]	0.38

24-hour batch tests with JP-8 are shown in Table 4.4. The unloaded frameworks had very low capacities, but MSN had a significantly higher capacity than MCM-41, likely due to its surface area. Both Ag-MCM-41 and Ag-MSN have significantly higher capacities than those presented in literature. The silver efficiency of these materials is also of note: the more efficiently a material uses the metal with which it is loaded, the lower cost the sorbent will be (as silver is the most expensive part of these sorbents). Both the Ag-MCM-41 and Ag-MSN adsorbed more sulfur per mole of silver than the Ag-TiO_x-Al_2O_3 sorbent reported by Tatarchuk and coworkers.[38] The silver impregnated Ag-MCM-41 tested by Chen et al. with JP-5 was loaded with 0.60 g of $AgNO_3$ per gram of MCM-41, corresponded to 38 wt.% Ag.[18] Based on their reported data, this would correspond to silver efficiency of 0.28 mol S/mol Ag, substantially lower than our reported values, despite their framework being tested with JP-5, which is inherently easier to desulfurize. This demonstrates

that our 18 wt.% Ag loading of MCM-41 was far more optimized than their reported material.

Table 4.4 24-hour adsorption capacities using JP-8 for MCM-41 and MSN pre- and post-loading with optimized amount of silver compared to the highest previously published value (taken with 630 ppm_wS JP-8)[38]

Sorbent	Optimized Adsorption Capacity (mgS/g)	Silver Efficiency (mol S/mol Ag)
MCM-41	0.8	-
Ag-MCM-41	25.4	0.48
MSN	4.6	-
Ag-MSN	32.6	0.55
$Ag\text{-}TiO_x\text{-}Al_2O_3$[38]	8.01	0.27

4.3.4 Selectivity and Mechanism Studies

Comparison studies using a variety of single contaminant model fuels (see Figure 4.23) can reveal insight into the binding mechanism between framework and contaminant.[39-41] By exposing Ag-MSN to different model fuels in isomolar concentration, we were able to observe whether S-M binding, π-complexation, or both are occurring. Ag-MSN was placed in model fuels equivalent to 500 ppm_wS (for those containing sulfur), and the 1-hour adsorption capacities are shown in Figure 4.24. Dibenzothiophene and DMDBT have higher electron density on their sulfur atom than BT, as

calculated using density functional theory.[39] If S-M binding is occurring, the adsorption capacities should be larger for DBT and DMDBT than for BT. This trend was indeed observed, as shown in Figure 4.24. Furthermore, the sterically hindered sulfur on DMDBT had a lower adsorption capacity, pointing to direct S-M binding as a likely adsorption mechanism. Hindrance around the sulfur atom inhibits binding, whereas if binding was only occurring through π-complexation, steric hindrance around the sulfur atom should not have an affect. The sulfur-free naphthalene was still adsorbed by Ag-MSN in a lower capacity than the sulfur containing molecules, demonstrating that π-complexation must also be occurring.

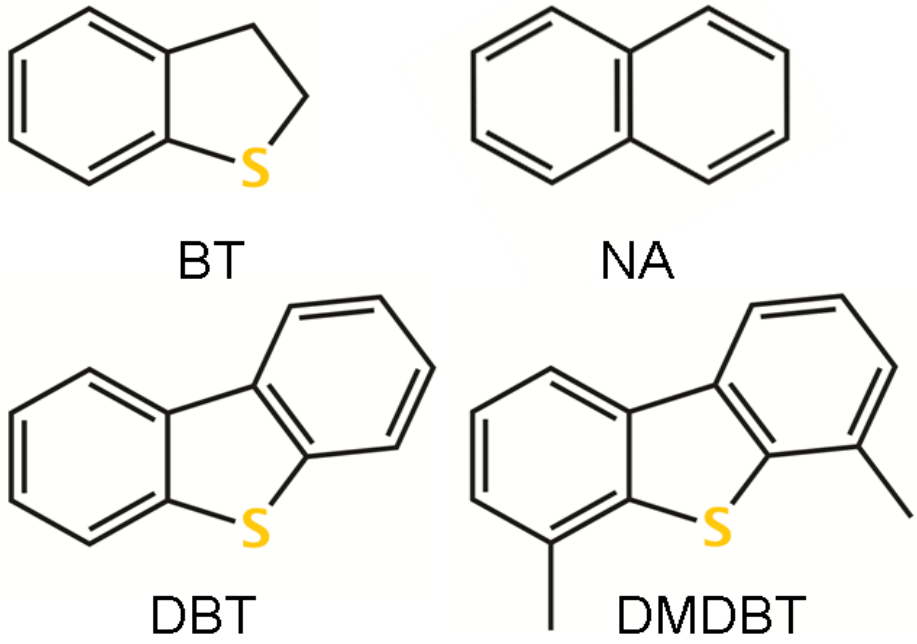

Figure 4.23 Structure of the four different model contaminants tested: benzothiophene (BT), naphthalene (NA), dibenzothiophene (DBT) and 4,6-dimethyldibenzothiophene (DMDBT).

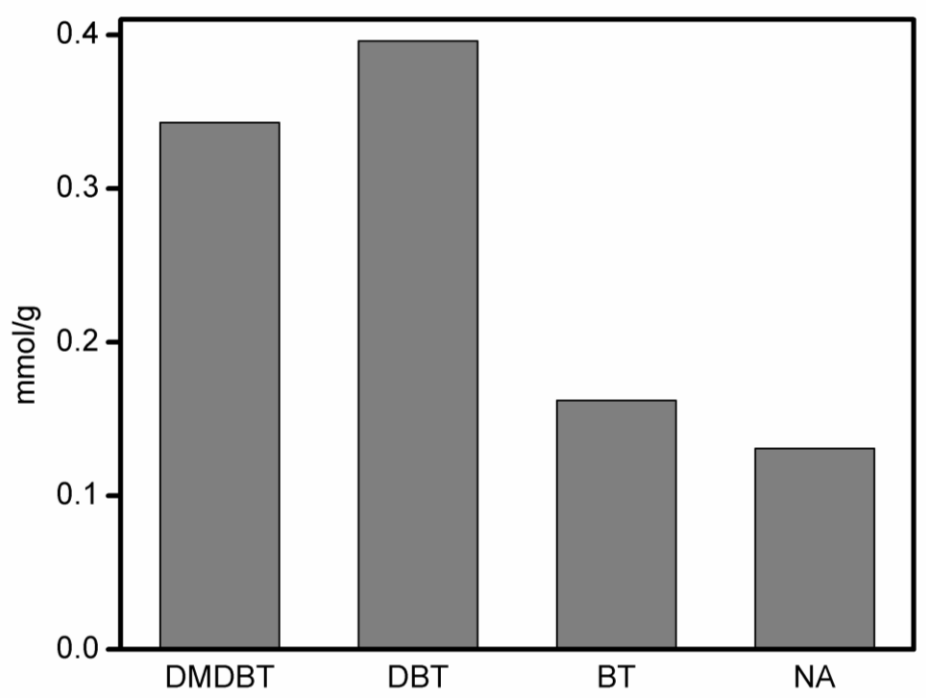

Figure 4.24 1-hour adsorption capacities for Ag-MSN in single contaminant model fuels. 4,6-dibenzothiophene (DMDBT), dibenzothiophene (DBT), and benzothiophene (BT) are all 500 ppm_wS and naphthalene (NA) is isomolar to them.

GC analysis was used to observe the selectivity of the sorbent towards sulfur aromatics over hydrocarbon aromatics. We studied a model fuel containing equimolar amounts of naphthalene and dibenzothiophene in decane, as has been reported previously for selectivity studies.[42] Table 4.5 summarizes the amounts of naphthalene and dibenzothiophene removed from a model fuel consisting of an equimolar solution in decane. Figure 4.25 pictorially represents the selectivity; while both dibenzothiophene and naphthalene are present, the material selectively removes the dibenzothiophene. While some of the naphthalene was removed, both materials adsorbed three times more dibenzothiophene.

Table 4.5 1-hour fuel tests results using two-contaminant model fuel of isomolar DBT and NA in decane

Sorbent	mmol/g NA	mmol/g DBT
Ag-MCM-41	0.04 (1)	0.14 (3)
Ag-Al-MCM-41	0.06 (1)	0.18 (4)

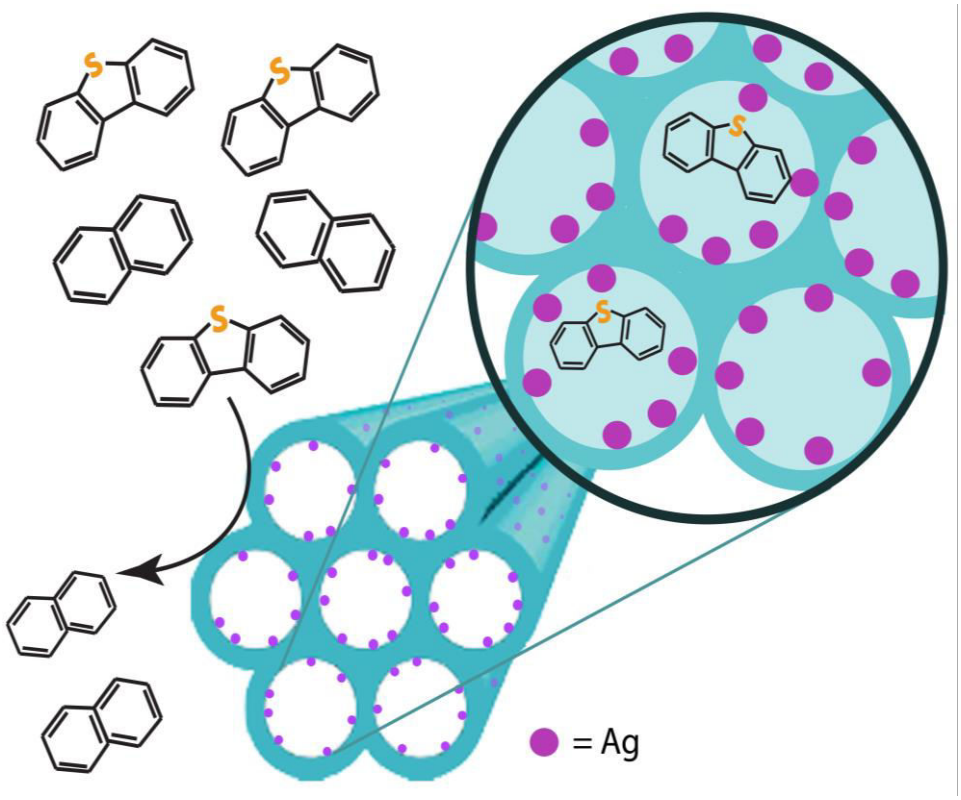

Figure 4.25 Selectivity of MCM-41 towards dibenzothiophene over NA.

FT-IR was used to examine the adsorption mechanism and regenerability of the materials using diethyl ether. When dibenzothiophene binds in a perpendicular

fashion with respect to the adsorbent surface, an increase in its peak at 731 cm^{-1} is observed, while parallel binding shifts this peak down, as shown in Figure 4.26.[43] A perpendicular orientation of the dibenzothiophene molecule would support a S-M binding mechanism, whereas parallel supports π-complexation. As seen in Figure 4.27, the peak is located at 743 cm^{-1}, indicating a perpendicular binding fashion, and thus supporting S-M binding. A similar shift was also observed with Ag-MCM-41. The figure shows the complete removal of the DBT peak after a rinse with diethyl ether. In Chapter 3, it was observed that Ag-Al-SBA-15 could be regenerated more efficiently with diethyl ether rather than isooctane. With the addition of the data in Figure 4.27, we see that diethyl ether is capable of removing essentially all of the adsorbed DBT.

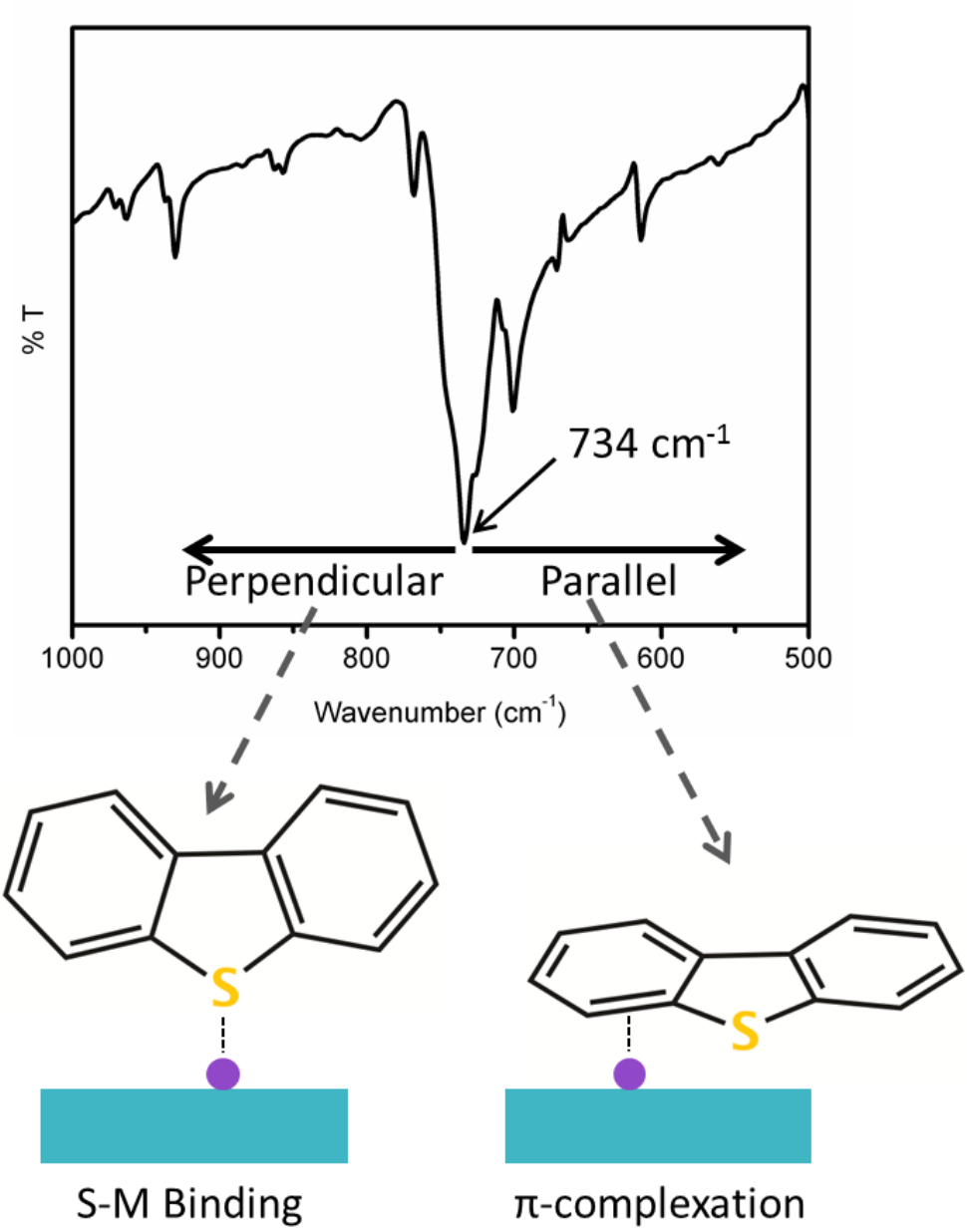

Figure 4.27 FT-IR of free DBT showing a band at 734 cm^{-1} that will shift depending on whether DBT is perpendicular or parallel to the sorbent surface. Bottom of figure shows the two possible binding modes: perpendicular implies direct S-M binding with the silver (purple), whereas parallel implies π-complexation.

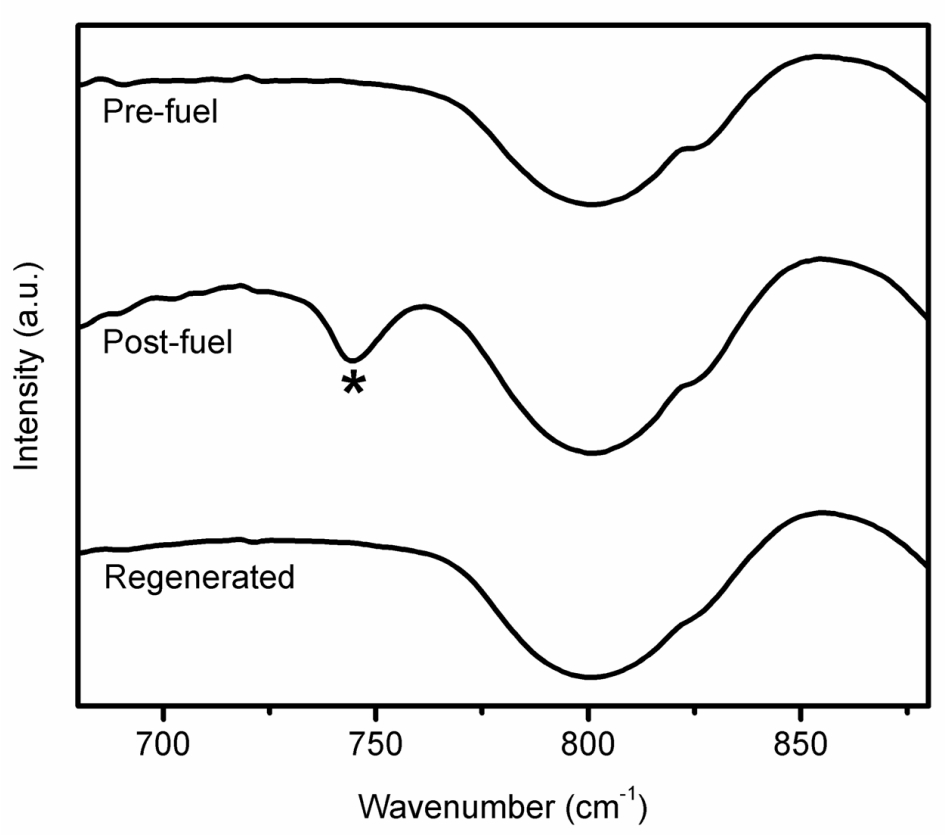

Figure 4.26 FT-IR of Ag-MSN prior to fuel exposure (top), after 1-hour in 500 ppm_wS model fuel of dibenzothiophene in decane (middle), and after solvent regeneration using diethyl ether (bottom). The stretch from DBT is denoted with an asterisk.

4.4 Conclusions

In summary, Ag-MSN is the most effective form of MCM-41 for the desulfurization of JP-8. Ag-MSN displays a 24-hour adsorption capacity of 32.6 mgS/g, which is significantly greater than previously published materials. Ag-MCM-41 displays a 24-hour capacity of 25.4 mgS/g. Ag-MSN has a record breakthrough capacity at 10 ppm_wS of 0.98 mgS/g for JP-8, while Ag-Al-MCM-41 and Ag-MCM-41 display 0.39 mgS/g and 0.21 mgS/g respectively. The regenerability of Ag-Al-MCM-41 was found to be highly inconsistent between batches compared to MCM-41. The model fuel regenerability of Ag-MSN is ~ 70%, which is much higher than other reports of Ag-MCM-41. Mechanism studies support an S-M binding as the major mode of adsorption, while π-complexation likely also occurs. Overall, the higher surface area of MSN compared to MCM-41 is responsible for its superior performance as a desulfurization sorbent. MCM-41 and its derivatives show promise as sorbents for adsorptive desulfurization. However, improvements in increasing their reusability are necessary for them to become viable options for solid oxide fuel cell applications.

4.5 References

1. Kresge, C. T.; Leonowicz, M. E.; Roth, W. J.; Vartuli, J. C.; Beck, J. S., Ordered mesoporous molecular sieves synthesized by a liquid-crystal template mechanism. *Nature* **1992,** 359, (6397), 710-712.

2. Algarra, M.; Jiminez, M. V.; Rodriguez-Castellin, E.; Jimenez-Lopez, A.; Jimenez-Jimenez, J., Heavy metals removal from electroplating wastewater by aminopropyl-Si MCM-41. *Chemosphere* **2005,** 59, (6), 779-786.

3. Kaftan, O.; Acikel, M.; Erogu, A. E.; Shahwan, T.; Artok, L.; Ni, C., Synthesis, characterization and application of a novel sorbent, glucamine-modified MCM-41, for the removal/preconcentration of boron from waters. *Analytica Chimica Acta* **2005,** 547, (1), 31-41.

4. Rivera-Jiménez, S. M.; Hernández-Maldonado, A. J., Nickel (II) grafted MCM-41: A novel sorbent for the removal of Naproxen from water. *Microporous and Mesoporous Materials* **2008,** 116, (1), 246-252.

5. Yoshitake, H.; Yokoi, T.; Tatsumi, T., Adsorption of chromate and arsenate by amino-functionalized MCM-41 and SBA-1. *Chemistry of Materials* **2002,** 14, (11), 4603-4610.

6. Ravikovitch, P. I.; Wei, D.; Chueh, W. T.; Haller, G. L.; Neimark, A. V., Evaluation of pore structure parameters of MCM-41 catalyst supports and catalysts by means of nitrogen and argon adsorption. *The Journal of Physical Chemistry B* **1997,** 101, (19), 3671-3679.

7. Corma, A.; Martinez, A.; Martinez-Soria, V., Hydrogenation of aromatics in diesel fuels on Pt/MCM-41 catalysts. *Journal of Catalysis* **1997,** 169, (2), 480-489.

8. Ahmed, S.; Rahman, F.; Al-Amer, A. M. J.; Al-Mutairi, E. M.; Baduruthamal, U.; Alam, K., Oxidative dehydrogenation of lower alkanes over metal incorporated MCM-41 catalysts. *Reaction Kinetics, Mechanisms and Catalysis* **2012,** 105, (2), 483-493.

9. Slowing, I. I.; Trewyn, B. G.; Lin, V. S. Y., Mesoporous silica nanoparticles for intracellular delivery of membrane-impermeable proteins. *Journal of the American Chemical Society* **2007,** 129, (28), 8845-8849.

10. Heilman, B. J.; St. John, J.; Oliver, S. R. J.; Mascharak, P. K., Light-triggered eradication of acinetobacter baumannii by means of NO delivery from a porous material with an entrapped metal nitrosyl. *Journal of the American Chemical Society* **2012,** 134, (28), 11573-11582.

11. Wang, A.; Wang, Y.; Kabe, T.; Chen, Y.; Ishihara, A.; Qian, W., Hydrodesulfurization of dibenzothiophene over siliceous MCM-41-supported catalysts: I. Sulfided Co-Mo catalysts. *Journal of Catalysis* **2001,** 199, (1), 19-29.

12. Song, C.; Madhusudan Reddy, K., Mesoporous molecular sieve MCM-41 supported Co-Mo catalyst for hydrodesulfurization of dibenzothiophene in distillate fuels. *Applied Catalysis A: General* **1999,** 176, (1), 1-10.

13. Chica, A.; Corma, A.; Domine, M. E., Catalytic oxidative desulfurization (ODS) of diesel fuel on a continuous fixed-bed reactor. *Journal of Catalysis* **2006,** 242, (2), 299-308.

14. Wang, Y.; Yang, R. T.; Heinzel, J. M., Desulfurization of jet fuel by π-complexation adsorption with metal halides supported on MCM-41 and SBA-15 mesoporous materials. *Chemical Engineering Science* **2008,** 63, (2), 356-365.

15. Wang, Y.; Yang, R. T.; Heinzel, J. M., Desulfurization of Jet Fuel JP-5 Light Fraction by MCM-41 and SBA-15 Supported Cuprous Oxide for Fuel Cell Applications. *Industrial & Engineering Chemistry Research* **2009,** 48, (1), 142-147.

16. Samadi-Maybodi, A.; Teymouri, M.; Vahid, A.; Miranbeigi, A., In situ incorporation of nickel nanoparticles into the mesopores of MCM-41 by manipulation of solvent-solute interaction and its activity toward adsorptive desulfurization of gas oil. *Journal of Hazardous Materials* **2011,** 192, (3), 1667-1674.

17. Subhan, F.; Liu, B. S.; Zhang, Y.; Li, X. G., High desulfurization characteristic of lanthanum loaded mesoporous MCM-41 sorbents for diesel fuel. *Fuel Processing Technology* **2012,** 97, (0), 71-78.

18. Chen, H.; Wang, Y.; Yang, F. H.; Yang, R. T., Desulfurization of high-sulfur jet fuel by mesoporous π-complexation adsorbents. *Chemical Engineering Science* **2009,** 64, (24), 5240-5246.

19. Meng, X.; Qiu, G.; Wang, G.; Cai, Q.; Wang, Y., Durable and regenerable mesoporous adsorbent for deep desulfurization of model jet fuel. *Fuel Processing Technology* **2013,** 111, (0), 78-85.

20. Slowing, I. I.; Vivero-Escoto, J. L.; Wu, C.-W.; Lin, V. S. Y., Mesoporous silica nanoparticles as controlled release drug delivery and gene transfection carriers. *Advanced Drug Delivery Reviews* **2008,** 60, (11), 1278-1288.

21. Slowing, I. I.; Trewyn, B. G.; Giri, S.; Lin, V. S. Y., Mesoporous Silica Nanoparticles for Drug Delivery and Biosensing Applications. *Advanced Functional Materials* **2007,** 17, (8), 1225-1236.

22. Lee, C.-H.; Cheng, S.-H.; Wang, Y.-J.; Chen, Y.-C.; Chen, N.-T.; Souris, J.; Chen, C.-T.; Mou, C.-Y.; Yang, C.-S.; Lo, L.-W., Near-Infrared Mesoporous Silica Nanoparticles for Optical Imaging: Characterization and In Vivo Biodistribution. *Advanced Functional Materials* **2009,** 19, (2), 215-222.

23. Tan, P.; Qin, J.-X.; Liu, X.-Q.; Yin, X.-Q.; Sun, L.-B., Fabrication of magnetically responsive core-shell adsorbents for thiophene capture: AgNO3-functionalized Fe3O4@mesoporous SiO2 microspheres. *Journal of Materials Chemistry A* **2014,** 2, (13), 4698-4705.

24. Matsumoto, A.; Chen, H.; Tsutsumi, K.; Grun, M.; Unger, K., Novel route in the synthesis of MCM-41 containing framework aluminum and its characterization. *Microporous and Mesoporous Materials* **1999,** 32, (1), 55-62.

25. Gonzales, M. A.; Han, H.; Moyes, A.; Radinos, A.; Hobbs, A. J.; Coombs, N.; Oliver, S. R. J.; Mascharak, P. K., Light-triggered carbon monoxide delivery with Al-MCM-41-based nanoparticles bearing a designed manganese carbonyl complex. *Journal of Materials Chemistry B* **2014,** 2, (15), 2107-2113.

26. Lindlar, B.; Kogelbauer, A.; Prins, R., Chemical, structural, and catalytic characteristics of Al-MCM-41 prepared by pH-controlled synthesis. *Microporous and Mesoporous Materials* **2000,** 38, (2-3), 167-176.

27. Chen, X.; Huang, L.; Ding, G.; Li, Q., Characterization and catalytic performance of mesoporous molecular sieves Al-MCM-41 materials. *Catalysis Letters* **1997,** 44, (1-2), 123-128.

28. Palomino, J. M.; Tran, D. T.; Hauser, J. L.; Dong, H.; Oliver, S., Mesoporous Silica Nanoparticles for High Capacity Adsorptive Desulfurization. *Journal of Materials Chemistry A* **2014**, Accepted Manuscript.

29. Sohrabnezhad, S.; Pourahmad, A., As-synthesis of nanostructure AgCl/Ag/MCM-41 composite. *Spectrochimica Acta Part A: Molecular and Biomolecular Spectroscopy* **2012,** 86, (0), 271-275.

30. Yin, A.; Wen, C.; Dai, W.-L.; Fan, K., Ag/MCM-41 as a highly efficient mesostructured catalyst for the chemoselective synthesis of methyl glycolate and ethylene glycol. *Applied Catalysis B: Environmental* **2011,** 108-109, 90-99.

31. Nair, S.; Tatarchuk, B. J., Supported silver adsorbents for selective removal of sulfur species from hydrocarbon fuels. *Fuel* **2010,** 89, (11), 3218-3225.

32. Tran, D. T.; Dunbar, Z. W.; Chu, D., Regenerable sulfur adsorbent for liquid phase JP-8 fuel using gold/silica based materials. *International Journal of Hydrogen Energy* **2012,** 37, (13), 10430-10434.

33. McKinley, S. G.; Angelici, R. J., Deep desulfurization by selective adsorption of dibenzothiophenes on Ag^{+}/SBA-15 and Ag^{+}/SiO_2. *Chemical Communications* **2003**, (20), 2620-2621.

34. Shah, A. T.; Li, B.; Abdalla, Z. E. A., Direct synthesis of Cu-SBA-16 by internal pH-modification method and its performance for adsorption of dibenzothiophene. *Microporous and Mesoporous Materials* **2010,** 130, (1), 248-254.

35. Chen, L. Y.; Ping, Z.; Chuah, G. K.; Jaenicke, S.; Simon, G., A comparison of post-synthesis alumination and sol-gel synthesis of MCM-41 with high framework aluminum content. *Microporous and Mesoporous Materials* **1999,** 27, (2-3), 231-242.

36. Janicke, M. T.; Landry, C. C.; Christiansen, S. C.; Birtalan, S.; Stucky, G. D.; Chmelka, B. F., Low Silica MCM-41 Composites and Mesoporous Solids. *Chemistry of Materials* **1999,** 11, (5), 1342-1351.

37. Shahadat Hussain, A. H. M.; Tatarchuk, B. J., Adsorptive desulfurization of jet and diesel fuels using $Ag/TiO_x–Al_2O_3$ and $Ag/TiO_x–SiO_2$ adsorbents. *Fuel* **2013,** 107, 465-473.

38. Hussain, A. H. M. S.; Yang, H.; Tatarchuk, B. J., Investigation of Organosulfur Adsorption Pathways from Liquid Fuels onto Ag/TiO_x-Al_2O_3 Adsorbents at Ambient Conditions. *Energy & Fuels* **2013,** 27, (8), 4353-4362.

39. Ke, T.; Xin, H., Deep Desulfurization of Model Gasoline by Adsorption on Mesoporous CeMCM-41. *Petroleum Science and Technology* **2010,** 28, (6), 573-581.

40. Lu, H.; Deng, C.; Ren, W.; Yang, X., Oxidative desulfurization of model diesel using [(C4H9)4N]6Mo7O24 as a catalyst in ionic liquids. *Fuel Processing Technology* **2014,** 119, 87-91.

41. Bu, J.; Loh, G.; Gwie, C. G.; Dewiyanti, S.; Tasrif, M.; Borgna, A., Desulfurization of diesel fuels by selective adsorption on activated carbons: Competitive adsorption of polycyclic aromatic sulfur heterocycles and polycyclic aromatic hydrocarbons. *Chemical Engineering Journal* **2011,** 166, (1), 207-217.

42. Haji, S.; Erkey, C., Removal of Dibenzothiophene from Model Diesel by Adsorption on Carbon Aerogels for Fuel Cell Applications. *Industrial & Engineering Chemistry Research* **2003,** 42, (26), 6933-6937.

43. Shang, H.; Liu, C.; Wei, F., FT-IR Study of Carbon Nanotube Supported Co-Mo Catalysts. *Journal of Natural Gas Chemistry* **2004,** 13, 95-100.

Chapter 5

Mesoporous Silica-Zirconia Frameworks as Desulfurization Adsorbents

Abstract

A series of silica-zirconia sorbent materials templated by variable length long-chain primary alkylamines is explored for the desulfurization of JP-8 jet fuel. Octylamine, dodecylamine, and hexadecylamine were explored as templating agents, resulting in three different pore sizes and surface area. Pure silica frameworks and those with an Si:Zr synthesis molar ratio ranging from 44:1 to 11:1 were investigated. Optimization tests were performed with model jet fuel and the results are confirmed with real JP-8. Those templated by hexadecylamine and octylamine had lower capacities than those templated with dodecylamine. The optimum sorbent was identified as dodecylamine-templated silica-zirconia synthesized from a gel Si:Zr molar ratio of 15:1. With optimized silver loading of 12 wt.%, a saturation adsorption capacity of 39.4 mgS/g and a silver efficiency of 1.21 molS/molAg was observed for JP-8. Mechanism studies show that this material is capable of both S-M binding and π-complexation, but S-M binding is the dominant desulfurization mechanism. Model fuel regeneration studies show an improvement over those reported with Ag-MSN in Chapter 4.

5.1 Introduction

Highly effective desulfurization adsorbents are needed for the desulfurization of JP-8 to make the use of this fuel for solid oxide fuel cells in the military a reality. In an effort to meet this demand, a myriad of common high surface area frameworks have been explored, including zeolites, MCM-41, and SBA-15. While some of these frameworks show promise, a more unique framework may offer a solution. Research has been done on more exotic frameworks, such as metal-organic frameworks. However, these are impractical to produce in the amounts required because they often use complex procedures that are difficult to scale up or the use of organic linkers that are much more expensive than the components of inorganic metal oxide frameworks.[1, 2] There is a need for new frameworks that are both affordable and robust.

5.1.1 Primary Alkylamines as Templating Agents

The use of tertiary amines, such as cetyltrimethylammonium bromide (CTAB) to produce MCM-41, is very common for producing mesoporous materials. However, primary amines, including octylamine (OA), dodecylamine (DDA), and hexadecylamine (HDA), shown in Figure 5.1, have also been used effectively as templating agents. The size of the headgroup in proportion to the chain length is very important in the production of micelles, the formation of cylindrical or rod-like micelles (which would be an ideal template pores) favors smaller headgroups than those necessary for spherical micelles.[3, 4] Primary alkylamines do have smaller

headgroups than CTAB, which is capable of forming both spherical and cylindrical micelles.[5] This decrease in headgroup size can be compensated for by also decreasing the chain length.[3] However, despite their small headgroup, primary alkylamines have been observed to form cylindrical micelles.[6-8] of Prado and coworkers were able to produce mesoporous silicas using OA as the template with pore sizes ranging from 2.15 to 2.51 nm and surface areas as high as 983 m^2/g.[9] DDA has been used to create titania with a surface area above 500 m^2/g (titania with high surface area is much more difficult to synthesize than high surface area silicas) and mesoporous silica with a surface area above 1000 m^2/g.[10, 11] Hexadecylamine has successfully been used as a substitute for CTAB in the synthesis of MCM-41 like materials[12, 13] and high surface area mixed metal oxides exceeding 1300m^2/g.[14, 15]

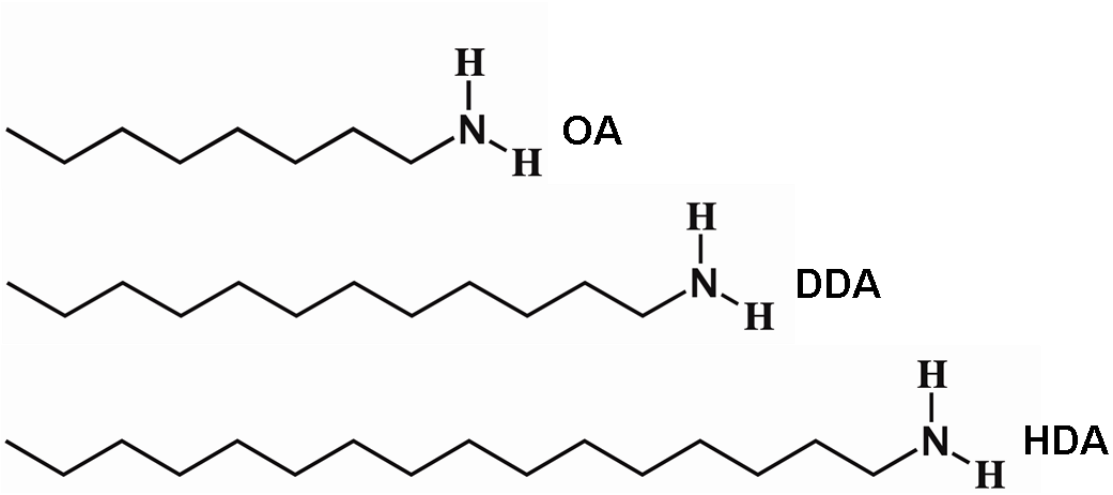

Figure 5.1 Structures of three primary alkylamines that can be used as templating agents for mesoporous materials: octylamine (OA), dodecylamine (DDA), and hexadecylamine (HDA).

5.1.2 Zirconia for Desulfurization

Zirconia-containing mesoporous frameworks have been explored for both catalytic and adsorptive desulfurization.[16-20] Kwon and coworkers showed 20% greater sulfur adsorption for a mesoporous silica/zirconia material compared to the pure silica version, even though the latter had a higher surface area. The Si/Zr material was successfully solvent-regenerated to 78.6% with methyl isobutyl ketone.[16] Kumar and coworkers examined zirconia-based materials prepared by precipitation and reflux followed various procedures for doping with sulfate with a range of surface areas (16.84-322.0 m^2/g).[17] The sulfated and pure zirconia samples were capable of adsorbing between 40 and 50% of the dibenzothiophene present in a model fuel and the adsorption was found to be exothermic in nature.[17] Copper supported on zirconia has been shown to be effective in the adsorption of thiophene from n-octane.[18] In this study, porous zirconia was obtained by calcination of commercial zirconium hydroxide, which was then wet impregnated with 1-6 wt.% copper nitrate and reduced under hydrogen at 300^{o}C.[18] Ultimately, zirconia loaded with 3 wt.% copper was able to remove 15.7 mgS/g thiophene from a model fuel, which is impressive considering the low amount of copper loaded onto the framework.[18] In an effort to better understand the adsorption mechanism of zirconia, Larrubia and coworkers used FT-IR studies to probe the interactions between benzothiophene (BT), DBT, and dimethyldibenzothiophene (DMDBT) and the surface of zirconia. They found that these organosulfur compounds were adsorbed

onto zirconia through Lewis-type acid-base interactions occurring between the sulfur and the sorbent's surface.[20]

Herein, we describe a series of silver loaded mesoporous silica-zirconia based materials synthesized with three different surfactant chain lengths and varying zirconia content. Both model fuel and actual JP-8 were studied to ascertain an optimal sorbent for the desulfurization of JP-8 fuel.

5.2 Experimental

5.2.1 Materials

All chemicals were used as received without further purification. Tetraethylorthosilicate (TEOS), dodecylamine (DDA), hexadecylamine (HDA), octylamine (OA) benzothiophene (BT), and dibenzothiophene (DBT) were all obtained from Acros Organics. Naphthalene (NA) was obtained from Fisher Scientific. 70% zirconium n-propoxide in isopropanol was obtained from Alfa Aesar. 200 proof ethanol was obtained from Decon Laboratories, Inc. Silver nitrate was obtained through MP Biomedicals, decane from TCI, and 4,6-dimethyldibenzothiophene (DMDBT) from Frontier Scientific.

5.2.2 Synthesis of HDA based frameworks

The synthesis of HDA based frameworks is a modified version published by Tuel and coworkers.[21] In a typical synthesis, 1.445 grams of HDA was dissolved in 6.013 grams of ethanol with magnetic stirring; then 11.133 grams of water was added to the solution and stirring continued for at least 5 minutes. A second solution of 4.16 grams TEOS and the desired amount of zirconium n-propoxide in 70% isopropanol was mixed and added in a quick dropwise fashion to the first solution, over about 30 seconds. Stirring was continued for 30 minutes followed by static room temperature aging overnight. The solid underwent the same filtration, reflux, and calcination procedures as the DDA materials.

5.2.3 Synthesis of DDA based frameworks

In a typical synthesis, 1.355 grams of DDA was dissolved in 7.139 grams of ethanol with magnetic stirring; then 11.135 grams of water was added to the solution and stirring continued for at least 5 minutes. A second solution of 4.16 grams TEOS and the desired amount of zirconium n-propoxide in 70% isopropanol was mixed and added in a quick dropwise fashion to the first solution, over about 30 seconds. Stirring was continued for 1 hour followed by static room temperature aging overnight. The solid was filtered and rinsed with doubly deionized water and ethanol, then refluxed for 1 hour in approximately 100 grams of 200 proof ethanol, followed by filtration and ethanol rinsing. The solid was then calcined at 450 ^{o}C for 7 hours with a 1 ^{o}C/min. ramp rate.

5.2.4 Synthesis of OA based frameworks

In a typical synthesis, 1.15 grams of OA, 5.99 grams of ethanol, and 11.769 grams of doubly deionized water was magnetically stirred for at least 5 minutes. A second solution of 4.16 grams TEOS and the desired amount of zirconium n-propoxide in 70% isoproponal was mixed and added in a quick dropwise fashion to the first solution, over about 30 seconds. Stirring was continued for 1 hour followed by static room temperature aging overnight. The solid was filtered, dried, and then calcined at 450 ^{o}C for 7 hours with a 1 ^{o}C/min. ramp rate.

5.2.5 Silver loading

The desired amount of silver was loaded onto the frameworks *via* wet impregnation: silver nitrate was dissolved in a water/ethanol solution and then added dropwise to the framework until moist. The framework was then dried at 110 ^{o}C under vacuum. This process was repeated until all the silver solution was loaded onto the framework.

5.2.6 Characterization

Powder X-ray Diffraction (PXRD) was performed on a Rigaku MiniFlex+ X-ray diffractometer with Cu-Kα radiation. Samples were analyzed from 1.5º to 10º (2θ) with a step size of 0.01º, unless noted otherwise, and a scan rate of 1^{o} per minute. BET surface area of the samples was measured by physical adsorption of N_2 at 77 K using a Micromeritics physisorption analyzer (TriStar II 3020 v1.03). Adsorption/desorption isotherm measurements were collected in the relative pressure range (P/P_o) from 0.01 to 1.00. Scanning electron microscopy (SEM) and scanning transmission electron microscopy (STEM) data were collected with a FEI Quanta 3D Dualbeam microscope. Inductively Coupled Plasma (ICP) was collected on a Perkin-Elmer Optima 7000 DV. UV–Vis diffuse reflectance spectra (UV–Vis DRS) were obtained by using a Varian Cary 5000 UV–Vis–NIR spectrophotometer (Harrick Praying Mantis diffuse reflectance cell attachment, Teflon standard). Transmission electron microscopy (TEM) data were collected using a JEOL 2100F microscope

operated at 200 kV. Samples were prepared for TEM by sonication in acetone for 3 minutes prior to dispersal on a TEM grid covered in holey carbon film.

5.2.7 Model Fuel and JP-8 Testing

All model fuel tests were performed with a 50:1 fuel to sorbent weight ratio. Model fuels were made with n-decane and BT, DBT, DMDBT, or NA as the contaminant. All sulfur containing model fuels were 500ppm$_w$S (11.38 mM) and the NA model fuel was also 11.38 mM. Model fuel batch tests were performed over 1 hour unless otherwise noted. JP-8 batch tests were performed over 24 hours with approximately 40 mg of sorbent in 5 g of JP-8. The JP-8 used for all experiments had an average initial sulfur concentration of 750 ppm$_w$S. Both column and 24-hour batch (beaker) test experiments were analyzed for total sulfur concentration using a UV total sulfur analyzer (multi EA 3100, Analytikjena) with a detection limit of 45 ppb. Model fuel test concentrations were determined by UV-Vis on a Hewlett-Packard Model 8452A spectrophotometer. FT-IR data was collected after exposing sorbents to 500 ppm$_w$S model fuel of DBT in n-decane for 1 hour, rinsing with decane to remove any physisorbed DBT, followed by drying at 110 °C under vacuum before forming KBr pellets. Infrared spectra were recorded using a Perkin-Elmer Spectrum-One FT-IR.

5.3 Results and Discussion

5.3.1 Characterization

Materials using each of three templating agents were synthesized. The amounts of zirconia were varied for the materials made with HDA and DDA. DDA-X denotes material made with DDA templating agent where X is the gel mole ratio of Si:Zr. HDA-X represents a material made with HDA as the templating agent. OA-15 was prepared with octylamine and has a Si:Zr ratio of 15:1.

Initial characterization was performed using powder X-ray diffraction (PXRD). Figure 5.2 compares the PXRDs of the materials made from each of the templating agents. HDA, the longest surfactant consisting of a 16-carbon chain, has the lowest angle (100) peak. DDA, with a 12-carbon chain, produces a (100) peak between that of HDA and OA. And OA, with just 8 carbons, has the highest angle (100) peak. The trend in d-spacing is expected, with the shortest surfactant resulting in the smallest d-spacing and the longest surfactant producing the largest d-spacing. Table 5.1 quantifies the PXRD data shown in Figure 5.2. The difference in d-spacing between HDA-15 and DDA-15 results in a decrease of ~ 7 Å, and again a ~ 7 Å decrease between DDA-15 and OA-15. Overall, the HDA-15 and DDA-15 solids appear to have more long-range order than that of OA-15.

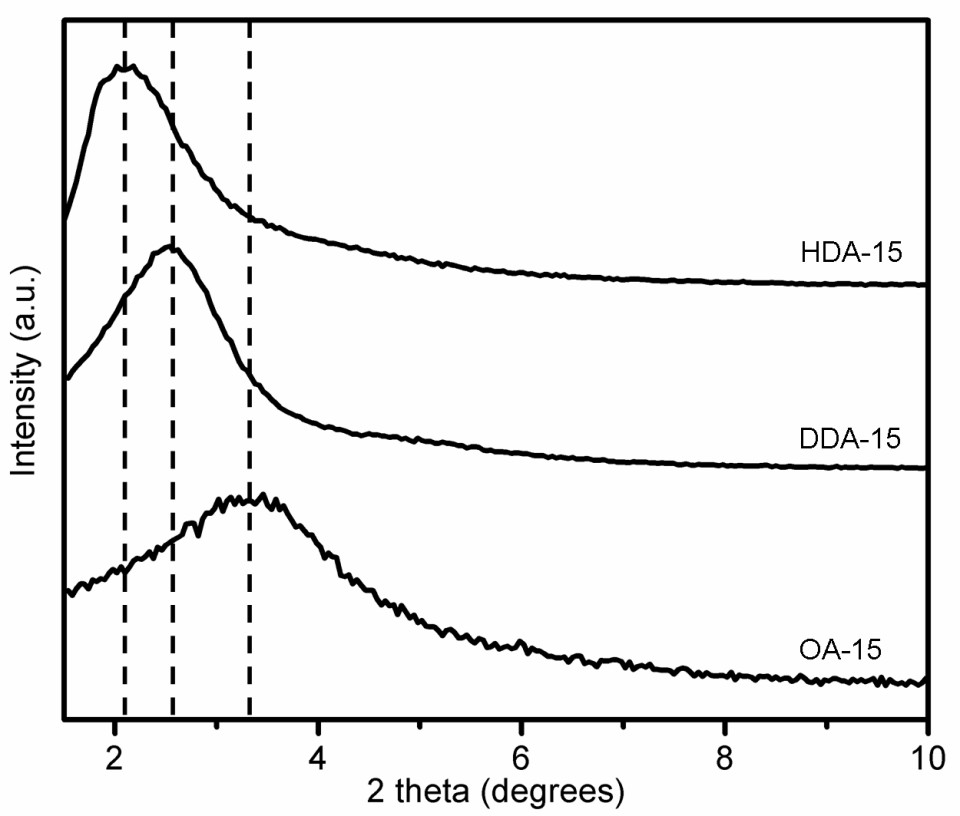

Figure 5.2 PXRD of unloaded, calcined HDA-15, DDA-15, and OA-15 with the difference in d_{100} spacing between the materials denoted with dashed lines.

Table 5.1 Summary of PXRD findings

Material	$d_{(100)}$ 2 theta (degrees)	$d_{(100)}$ spacing (Å)
OA-15	3.34	26.44
DDA-15	2.54	34.68
HDA-15	2.10	42.03

PXRDs of a range of Si:Zr ratios were taken for materials templated with DDA, shown in Figure 5.3. The (100) d-spacing remains constant for all materials. A slight decrease in long-range order was observed by a decrease in peak height for

DDA-11, which has the highest zirconia content. DDA-44, which had the lowest zirconia content, and DDA-SiO_2 which is pure silica, appeared to have the greatest long range order. However, the differences between the entire range of materials was subtle.

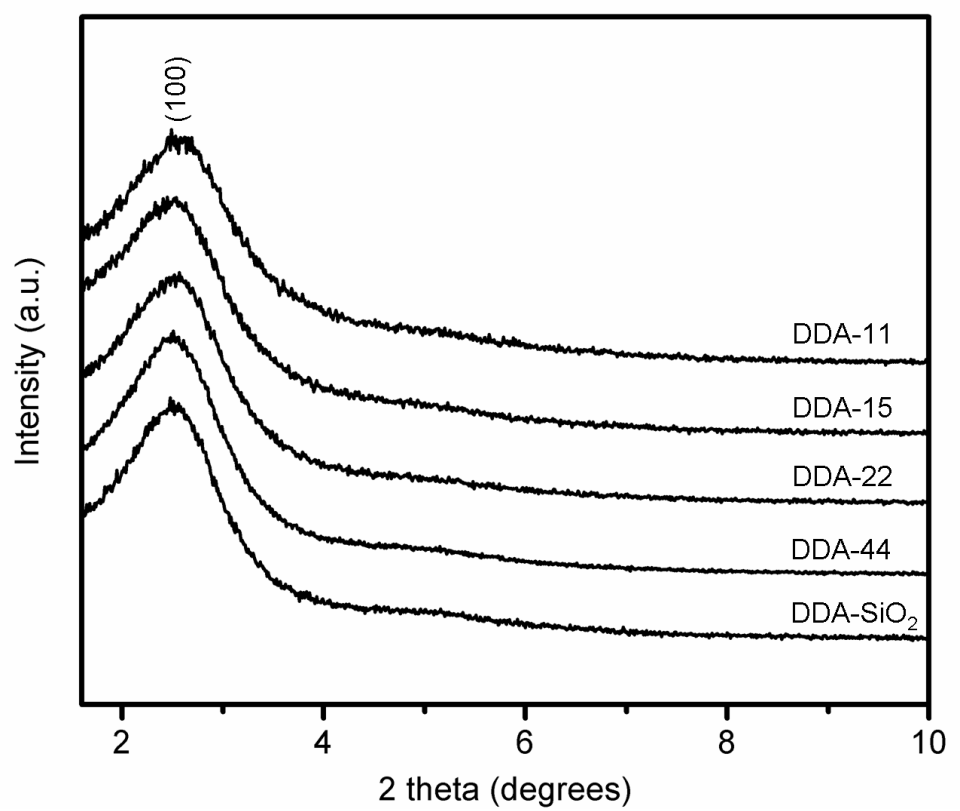

Figure 5.3 PXRD of the entire series of DDA based materials.

Table 5.2 summarizes the BET surface area results, with the surface area of DDA based sorbents higher than that of HDA, and the pure silica version having the highest of the DDA materials. The surface area trend agrees with that seen by Tuel and coworkers.[21] Their silica/zirconia frameworks with HDA as the surfactant

displayed a higher surface area for a gel ratio of 15:1 over 25:1.[21] DDA-15 impregnated with 11 wt.% Ag had a surface area of 843 m^2/g, demonstrating that the material retains its very high surface area after silver impregnation, and retains more of its surface area than DDA-SiO_2.

Table 5.2 Surface area (m^2/g) of DDA based sorbents after calcination as measured by BET, and surface area after two of the materials were loaded with 11 wt.% Ag

Material	Surface Area (m^2/g)	Silver loaded Surface Area (m^2/g)
DDA-SiO_2	1573	807
DDA-44	1513	
DDA-22	1434	
DDA-15	1471	843
DDA-11	1246	

BJH calculations from the N_2 isotherms (Figure 5.4 and 5.5) were used to calculate pore widths and pore volumes of DDA-15 and HDA-15, as shown in Table 5.3. The pore width of HDA-15 of 34 Å is 7 Å greater than DDA-15's pore width of 27 Å. This corresponds well to the PXRD data. The pore widths are also similar to those seen for other silica based materials templated with HDA and DDA.[11, 22, 23] A comparison of the pore size distributions (insets of Figure 5.4 and 5.5) show that HDA-15 has broader distribution compared to DDA-15.

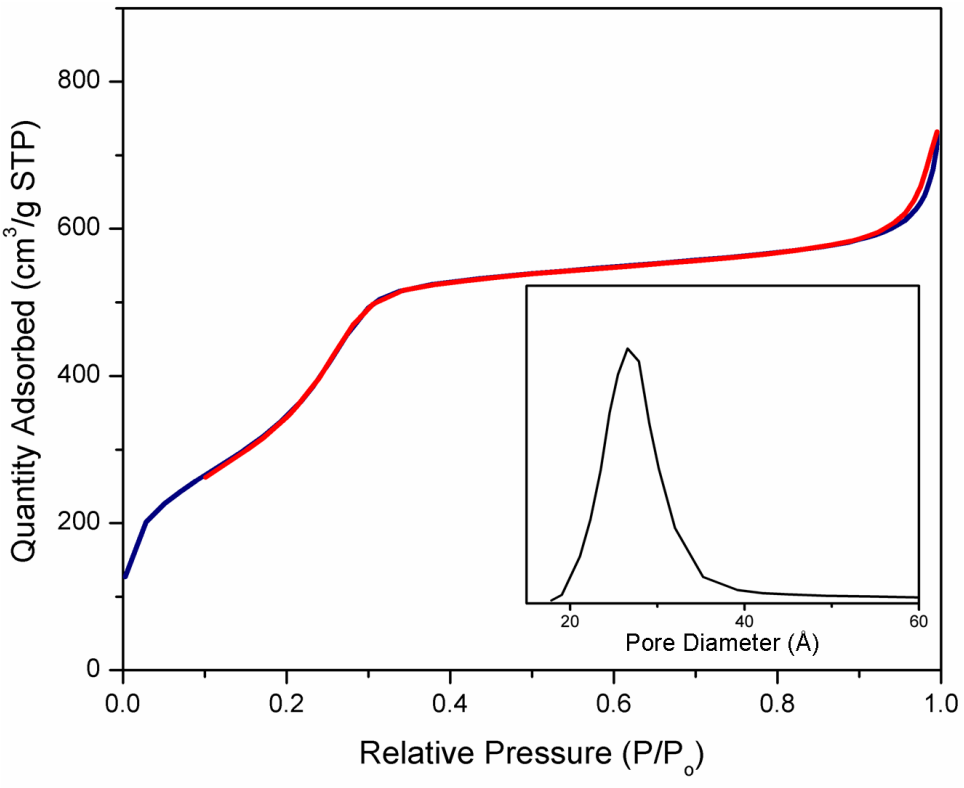

Figure 5.4 N_2 adsorption (blue) and desorption (red) isotherms for DDA-15. Inset shows the pore size distribution.

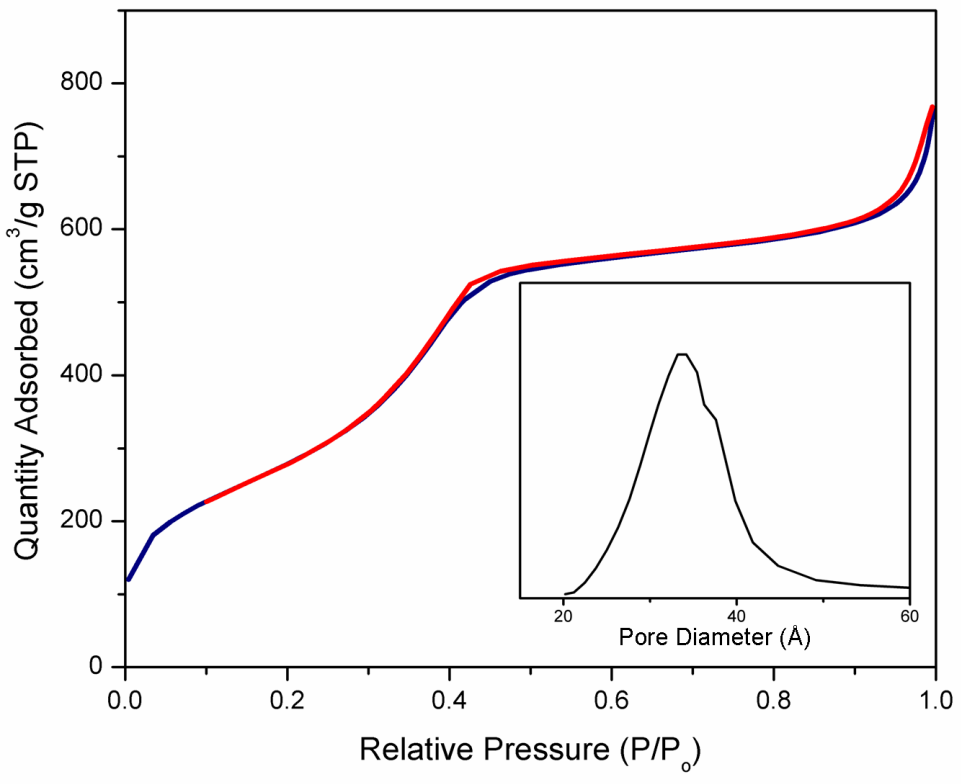

Figure 5.5 N_2 adsorption (blue) and desorption (red) isotherms for HDA-15. Inset shows the pore size distribution.

Table 5.3 Surface area and pore characteristics of sorbents after calcination as measured by BET

Material	BET Surface Area (m^2/g)	BJH Pore Width (Å)	BJH Pore Volume (cm^3/g)
DDA-15	1471	27	1.35
HDA-15	1055	34	1.32

The diffuse reflectance UV-Vis data for DDA-SiO_2 and DDA-15 indicates that silver species present are primarily as Ag^+, given the large band just above 200

nm (Figure 5.6). A small amount of $Ag^{\delta+}$ corresponds to the smaller band just above 300 nm.[24, 25] There was no appreciable difference in silver species based on the presence of zirconia, as the spectra were identical for both DDA-SiO_2 and DDA-15.

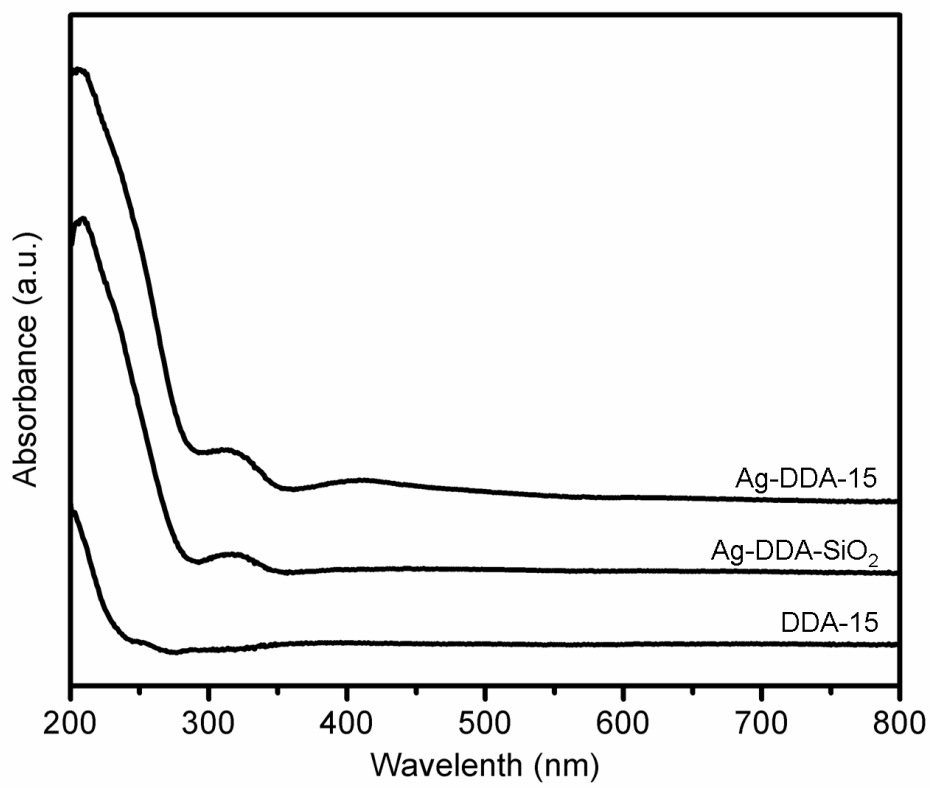

Figure 5.6 UV-Vis diffuse reflectance spectra of DDA-templated materials.

SEM images show that DDA-15 is bulk powder, but with a highly textured morphology (Figure 5.7). The powder contains fine particles ranging in diameter from hundreds of nanometers to several microns. Both templating agents, HDA and DDA, result in similar powder morphologies. Figure 5.8 provides a closer look at the

morphology of DDA-15 and demonstrates that there are no changes to the bulk characteristics after silver loading.

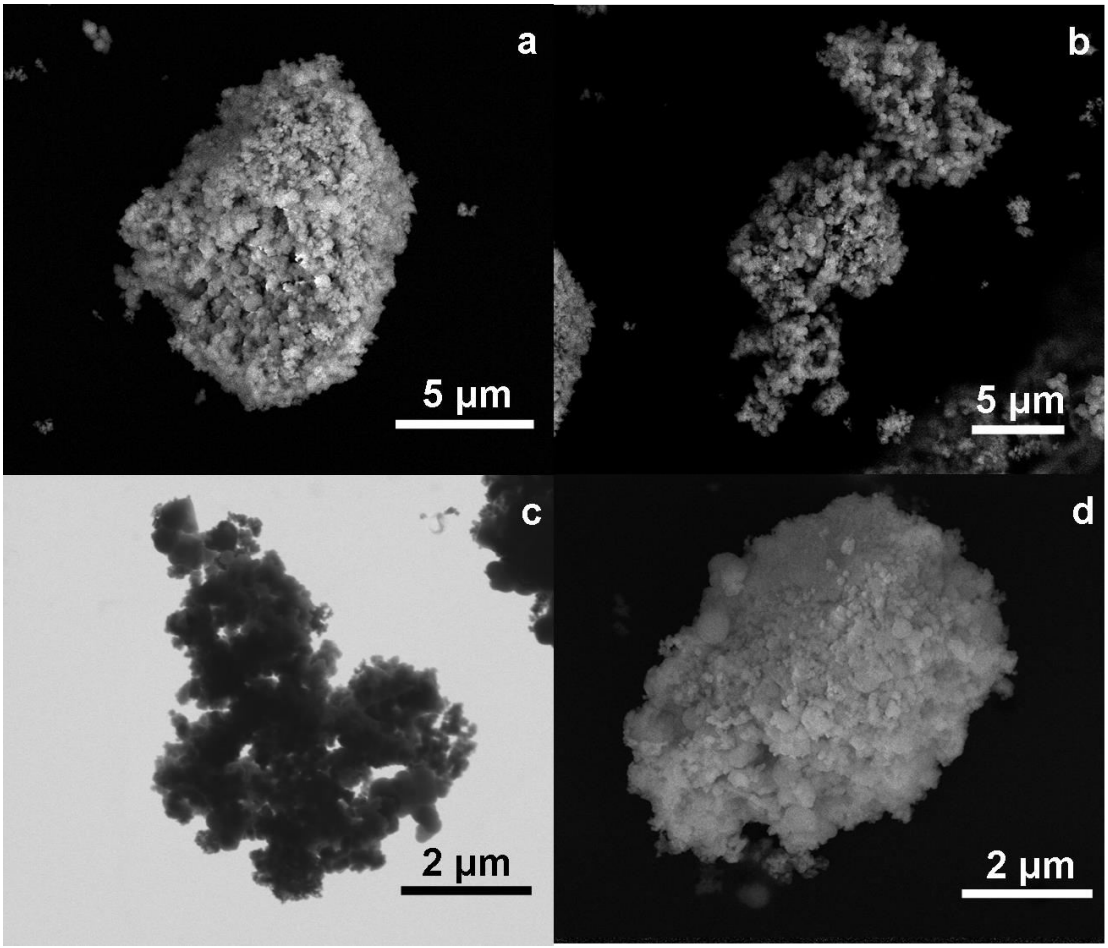

Figure 5.7 SEM micrographs of DDA-15 (a and b), STEM micrograph of DDA-15 (c), and SEM of HDA-15 (d).

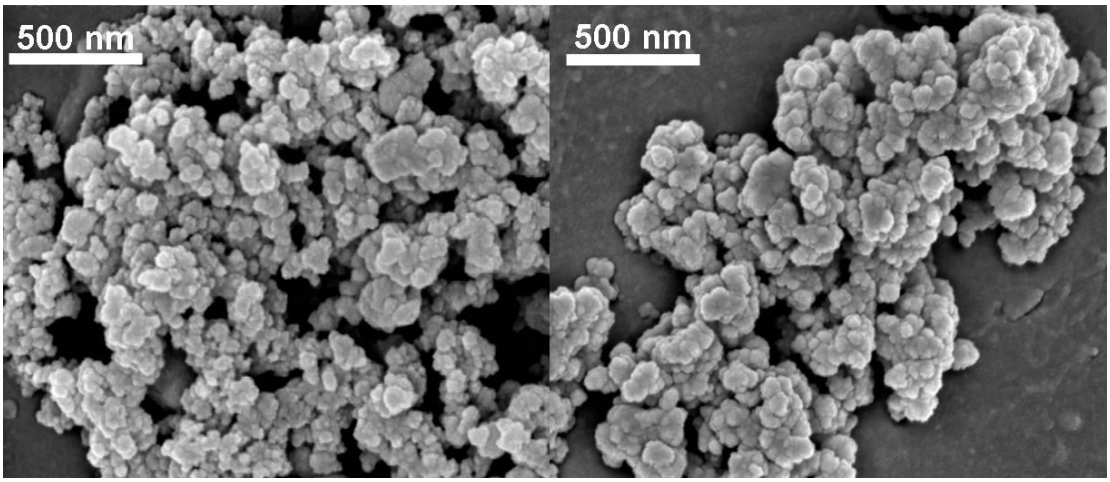

Figure 5.8 SEM micrograph of DDA-15 before silver loading (left) and after loading with 11 wt.% silver (right).

TEM of DDA-15, Figure 5.9, does not reveal any ordered array to the packing of the pores like those seen in MCM-41. This coincides with the PXRD, which would have shown (110) and (200) peaks if the pores were in an ordered hexagonal array. Figure 5.10 shows DDA-15 after being loaded with 11 wt.% Ag. The silver looks relatively well dispersed, with about 10 nm across areas covered with silver equally spaced throughout.

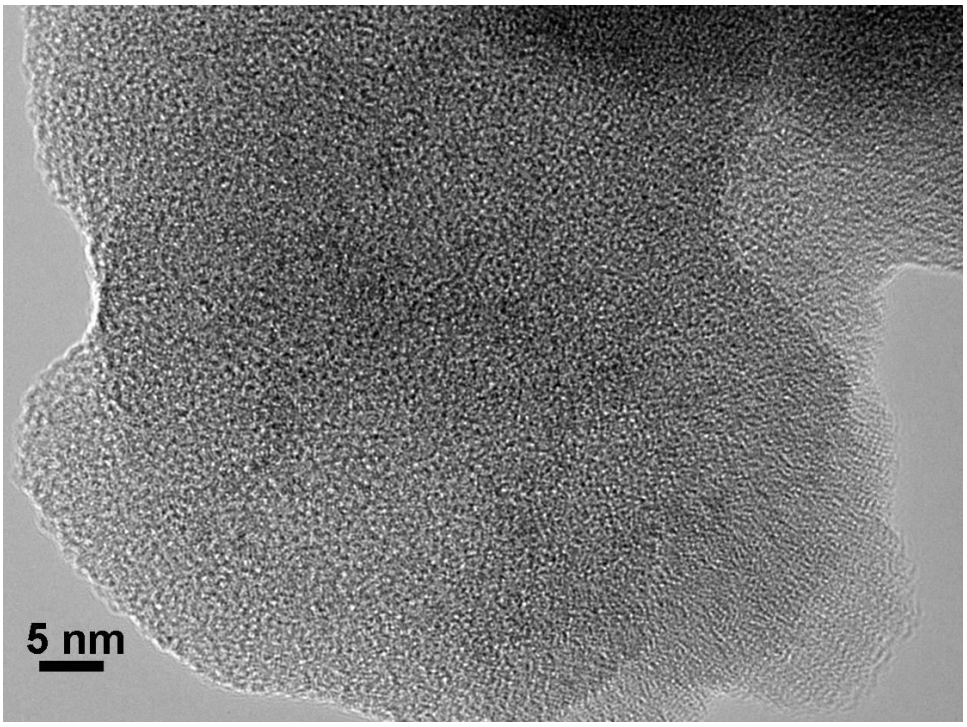

Figure 5.9 TEM micrograph of DDA-15.

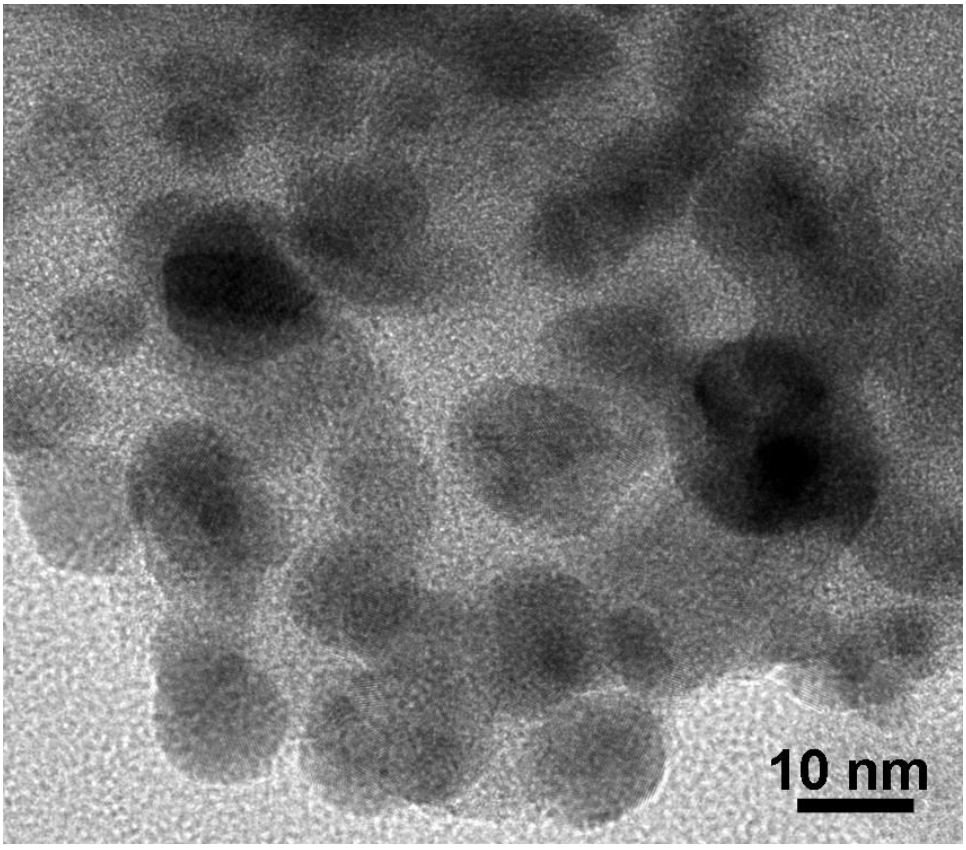

Figure 5.10 TEM micrograph of Ag-DDA-15.

5.3.2 Model Fuel Tests

The degree of silver loading was optimized using material DDA-15, as it had the qualities of both high surface area and high zirconia content. It was demonstrated that as the silver content increases, adsorption capacity increases up to a maximum and then a decrease is observed (Figure 5.11). This peak is attributed to an increase in silver adsorption sites with loading. Silver aggregates likely start to form at higher silver concentration, which can block the pores, resulting in a lower adsorption capacity. This phenomenon has been observed with other silver-loaded materials,

where Tatarchuk and coworkers found that as silver loading increased beyond 4 wt.%, the surface area, pore volume, and dispersion decreased.[26] As a result, they observed lower adsorption capacities with these materials loaded with more silver.[26] For DDA-15, the optimized silver loading was determined to be 11 wt.% and was subsequently used for all model and JP-8 fuel tests herein for the entire series of materials (with the exception of OA-15, for which 10 wt.% Ag was found to be the optimized loading).

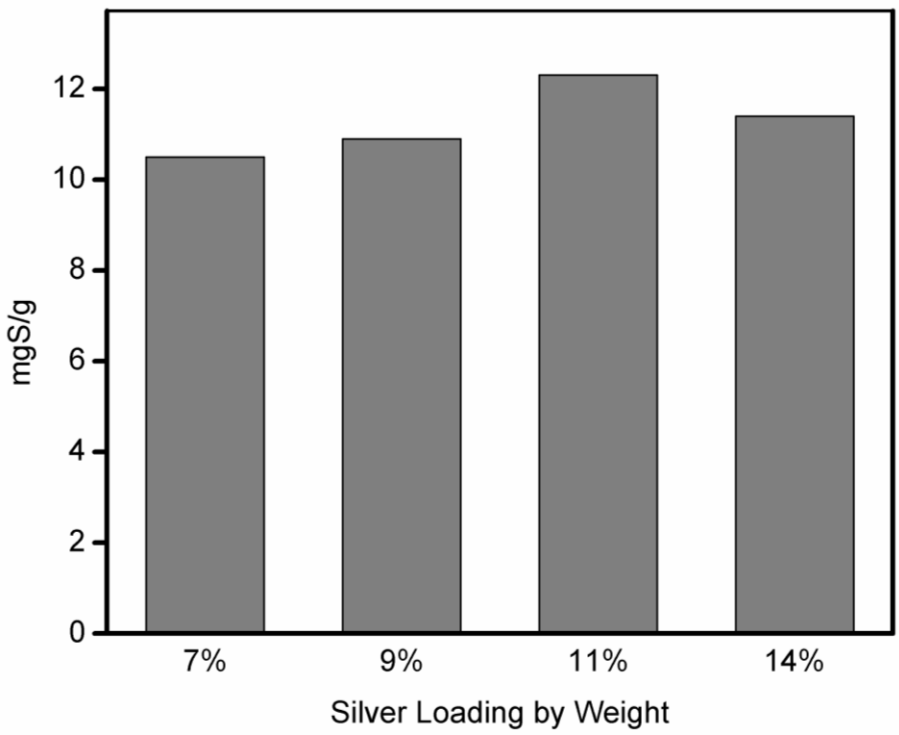

Figure 5.11 Optimization of silver loading level for DDA-15 using 1-hour fuel tests of 500 ppm_wS DBT in n-decane.

Table 5.4 displays the model fuel adsorption capacities for all DDA based frameworks loaded with 11 wt.% Ag. The adsorption capacity is correlated to both zirconia content and surface area. DDA-SiO_2 has the highest surface area, yet much lower adsorption capacity than the remaining zirconia containing frameworks. Of those containing zirconia, 15:1 is the optimum Si:Zr ratio. The capacity increases with increased zirconia but decreases at 11:1, likely due to the lower surface area of material DDA-11.

The increased adsorption capacity for zirconia containing materials is likely linked to the increased surface acidity. The same trend is seen with the HDA based materials: optimal adsorption capacity is observed with a Si:Zr ratio of 15:1 (Table 5.5). Surface acidity has been linked to desulfurization adsorption capacity for zirconia, as well as alumina and mixed metal oxides.[20, 27-30] The majority of organosulfur compounds in jet fuel are categorized as Lewis bases, which are known to bind to Lewis acidic sites.[29, 30] HDA-15 has the optimum silica to zirconia ratio. The larger pore sizes made by using HDA as the templating agent ultimately lower the surface area, which accounts for the decrease in adsorption capacity. The pores of both materials are of sufficient size to accommodate the organosulfur compounds commonly found in JP-8. This is not the case for smaller pore frameworks such as zeolites that cannot accommodate dibenzothiophene and its methylated derivatives.[31]

Table 5.4 1-hour adsorption capacities of DDA based frameworks loaded with 11 wt.% Ag using 500 ppm_wS model fuel of DBT in n-decane

Material	Adsorption Capacity (mgS/g)
DDA-SiO_2	7.4
DDA-44	9.2
DDA-22	9.8
DDA-15	12.3
DDA-11	10.5

Table 5.5 1-hour adsorption capacities of HDA based frameworks loaded with 11 wt.% Ag using 500 ppm_wS model fuel of DBT in n-decane

Material[a]	Adsorption Capacity (mgS/g)
HDA-44	7.9
HDA-22	8.7
HDA-15	9.9
HDA-11	9.3

To further confirm zirconia's role in increasing adsorption capacity, DDA-15 and DDA-SiO_2 were tested unloaded with model fuel. Even though DDA-SiO_2 has about 7% more surface area than DDA-15, DDA-15 absorbed more than twice the

amount of sulfur (Table 5.6). This clearly demonstrates that the silica-zirconia surface is more active than pure silica as well as the key role of the silver loading.

Table 5.6 1-hour adsorption capacities of unloaded DDA based frameworks using 500 ppm_wS model fuel of DBT in n-decane

Material	Adsorption Capacity (mgS/g)
DDA-15	1.4
DDA-SiO_2	0.6

Frameworks made by all three surfactants with the optimal Si:Zr ratio were compared in model fuel. OA-15 was tested with just 10 wt.% silver because higher silver content resulted in a decrease in adsorption capacity. DDA-15 is by far the most optimum of the three frameworks, having both the highest capacity and the highest silver efficiency, shown in Table 5.7. While OA-15 absorbed less than HDA-15, it did show a slightly higher silver efficiency than HDA-15.

Table 5.7 1-hour adsorption capacities using 500 ppm_wS model fuel of DBT in n-decane

Material[a]	Silver Loading (wt.%)	Adsorption Capacity (mgS/g)	Silver Efficiency (molS/molAg)
OA-15	10	9.4	0.33
DDA-15	11	12.3	0.38
HDA-15	11	9.9	0.30

It is important for a sorbent to quickly adsorb contaminants, especially for applications where it could be used in a column for on-demand, on-site desulfurization. We therefore performed adsorption kinetics studies (Figure 5.12). DDA-15 reaches its equilibrium capacity in model fuel within 3 minutes, and is 70% saturated in only 22 seconds. These characteristics make it ideal for column use where fast adsorption is essential. Compared to other materials tested with model fuels under ambient conditions, this is a significant improvement. Previous kinetic studies of non-silver loaded frameworks, such as zirconia based adsorbents, reach equilibrium after 22 hours whereas even carbon nanoparticles take 20 minutes.[17, 32] Silver loaded mesoporous aluminosilicates take approximately 5 minutes to reach equilibrium with dibenzothiophene adsorption.[33]

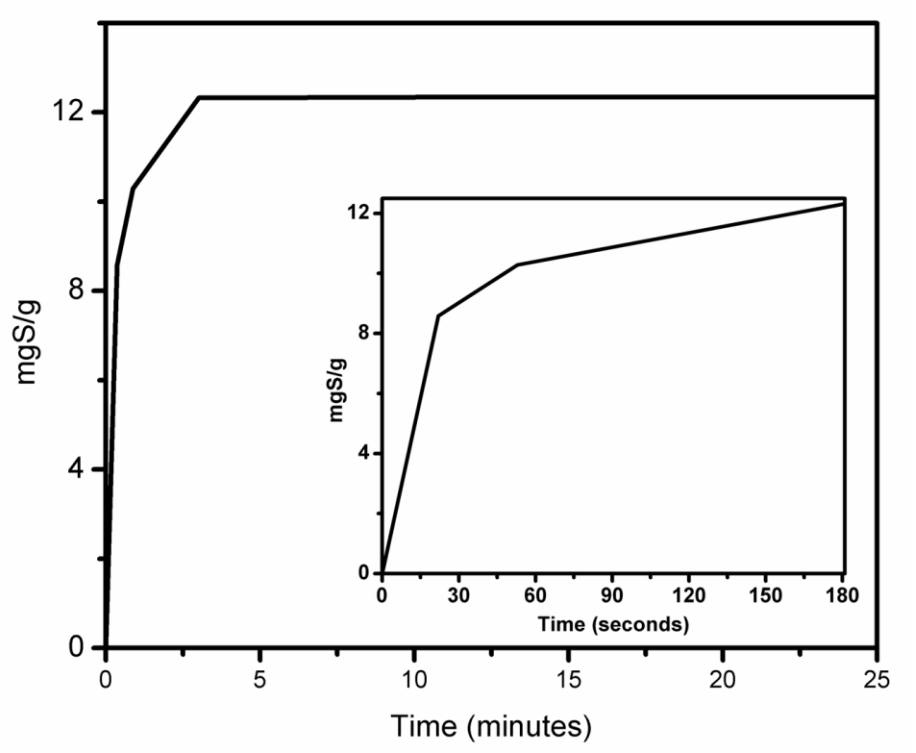

Figure 5.12 Adsorption capacity as a function of time for DDA-15 in 500 ppm_wS model fuel of DBT in n-decane as monitored by UV-Vis shows the rapid uptake. Inset: magnified data for the first 3 minutes, showing that 70% of the adsorption capacity is reached after 22 seconds and maximum adsorption capacity by 180 seconds.

Regeneration and reusability are important properties for desulfurization adsorbents. Figure 5.13 shows that there is an initial drop after the first regeneration, with 80% of adsorption capacity retained. The second regeneration cycle, however, displays a relatively low drop, retaining 93% of its capacity between cycles 2 and 3. We attribute this retention to an initial loss of silver during the first regeneration, with silver content stabilizing for future cycles.

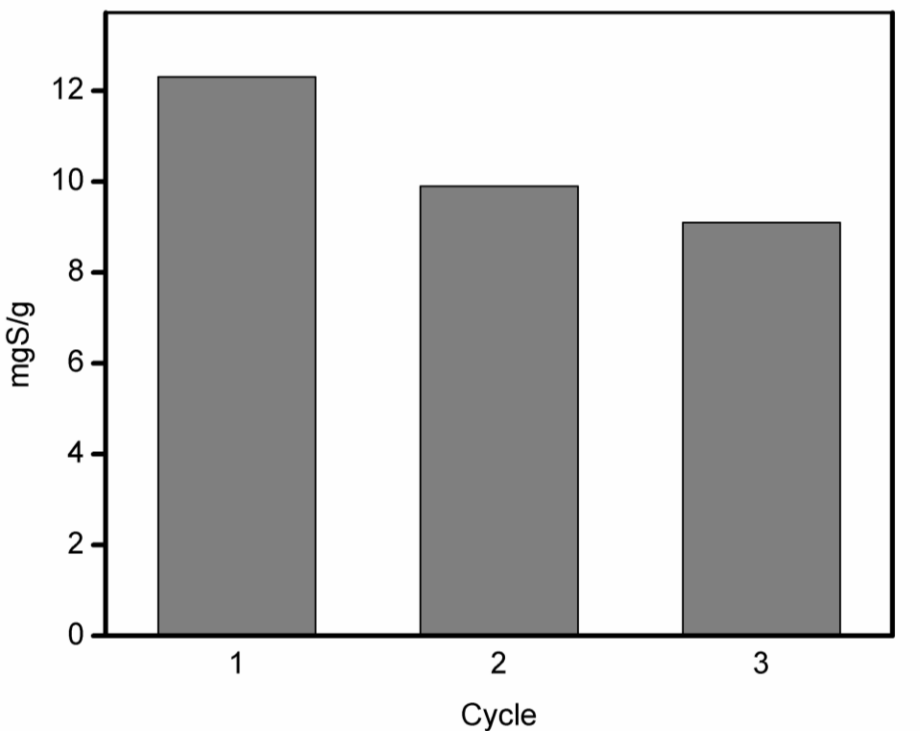

Figure 5.13 1-hour adsorption capacities for regeneration of DDA-15 in 500 ppm_wS DBT.

5.3.3 JP-8 Testing

Real jet fuel tests were performed using JP-8 under ambient conditions to assess the material's utility for military applications. 24-hour adsorption capacity studies were performed for the most optimized material: silver loaded DDA-15. These results are presented in Table 5.8 where they are compared to another material prepared by our lab, Ag-MSN, which is 80 nm MCM-41 nanoparticles loaded with 20 wt.% Ag.[34] The comparison of these two materials shows that while silver loaded DDA-15 only has 84% the adsorption capacity of Ag-MSN towards JP-8, it does so with far less silver loading. Silver is the most expensive component of both of these

materials. The more efficiently the silver is used, the more cost effective the sorbent. Ag-MSN is optimized to 20 wt.% Ag compared to 11 wt.% for DDA-15. Furthermore, as shown in Table 5.8 and highlighted in Figure 5.14, DDA-15 utilizes the silver sites more efficiently. Ag-MSN has a silver adsorption site efficiency of 0.79 molS/molAg, whereas DDA-15 has an efficiency of 1.2 molS/molAg. This increase is likely due to the framework itself adsorbing a high degree of sulfur compounds. As shown in Table 5.8, the unloaded framework adsorbs 4.6 mgS/g.

Table 5.8 24-hour fuel test data in JP-8

Material	Silver Content (wt%)	Adsorption Capacity (mgS/g)	Silver Efficiency (mol S/mol Ag)
DDA-15	0	4.6	-
DDA-15	11	39.4	1.21
Ag-MSN	20	47.1	0.79

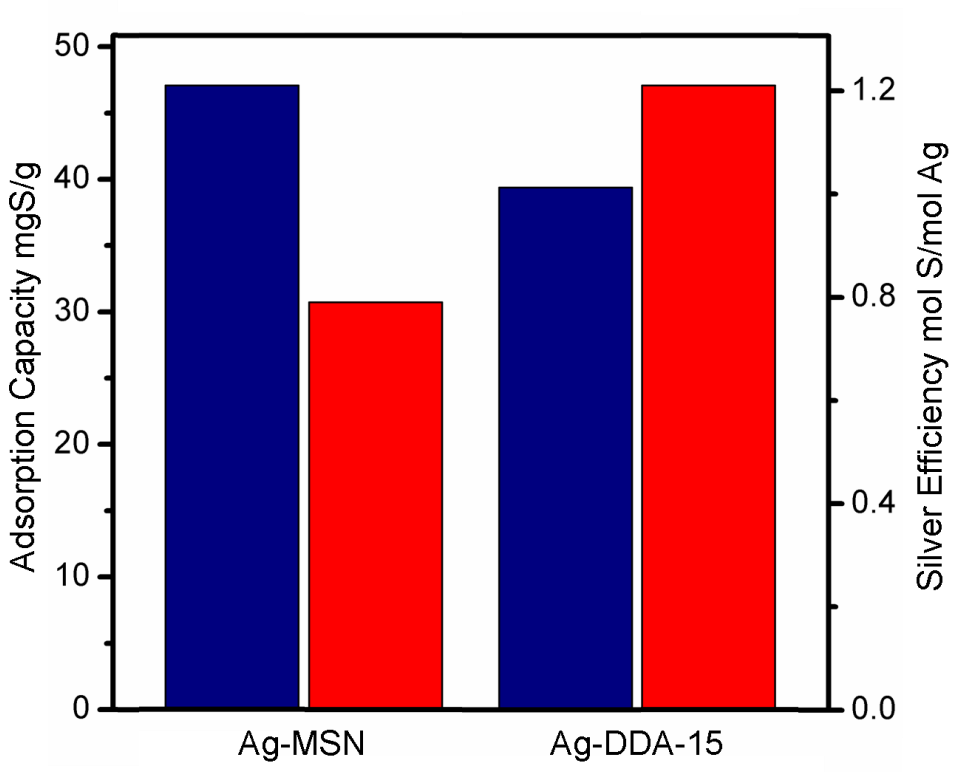

Figure 5.14 Comparison of DDA-15 and Ag-MSN 24-hour adsorption capacity (blue) in JP-8 compared with the silver efficiency (red).

5.3.4 Mechanism Studies

A variety of model fuels where studied to both show the ability of DDA-15 to adsorb DMDBT and to help elucidate the binding mechanism.[35-37] The larger adsorption capacities for DBT and DMDBT compared to BT (Figure 5.15) are similar to the trend seen with other reported sorbents and those tested in our lab, and are explained by the higher electron density of the sulfur on DBT and DMDBT.[34, 37] DMDBT has significant steric hindrance around the sulfur atom, which would explain its slightly lower capacity than the non-sterically hindered DBT. The effect of steric

hindrance and the decreased capacity for the lower electron density of BT all point to sulfur as the binding site. DDA-15 does have an appreciable adsorption capacity for NA, but it is far lower than that of the sulfur containing compounds. This is explained by the capacity of the material to form π-bonds. It is therefore likely that both S-M and π-bonding occur with this material, which would account for its adsorption of carbon-only aromatic compounds. It would also explain the observed larger capacities for organosulfur compounds, especially those with high electron densities around the sulfur atom.

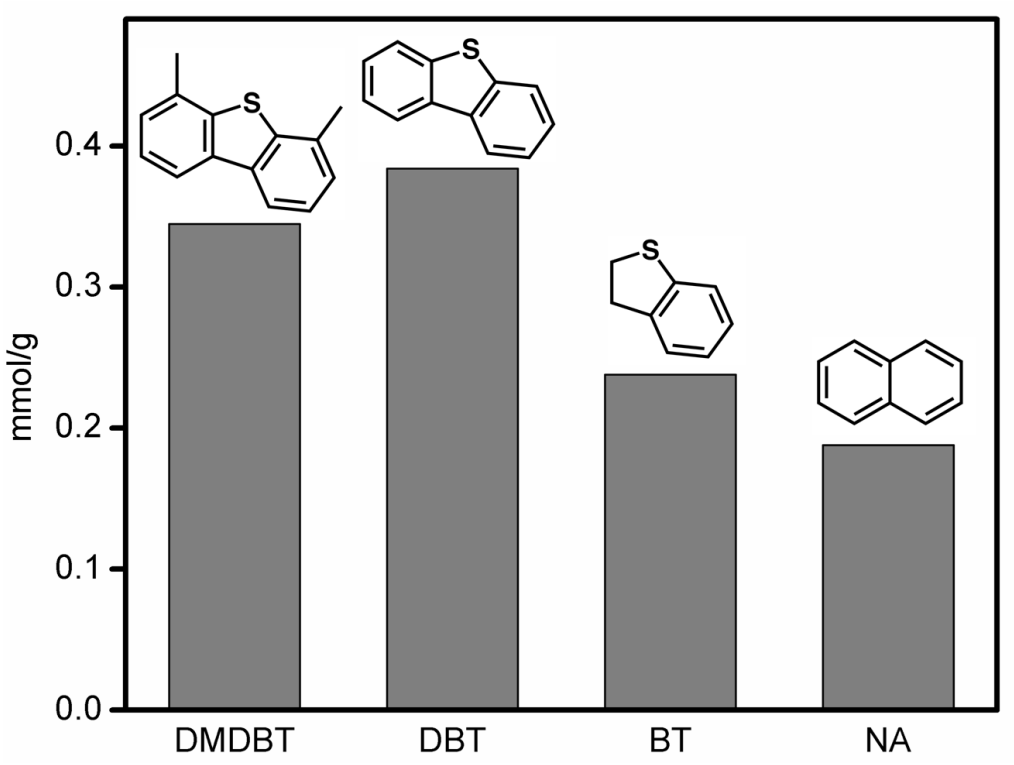

Figure 5.15 1-hour adsorption capacities for DDA-15 in single contaminant model fuels. 4,6-dibenzothiophene (DMDBT), dibenzothiophene (DBT) and benzothiophene (BT) are all 500 ppm_wS and naphthalene (NA) was used at isomolar level.

FT-IR also supports an S-M binding mechanism for DBT. A shift of unbound DBT from 734 cm^{-1} to 744 cm^{-1} for DBT bound to DDA-15 was observed after a 1-hour fuel test. This shift corresponds to a perpendicular orientation of DBT to the surface of DDA-15.[38] The combination of the model fuel studies and FT-IR show that material DDA-15 is capable of both S-M and π-bonding. In addition to helping reveal the binding mode, Figure 5.16 also demonstrates that diethyl ether is effective at regeneration, as no stretches from DBT are present after the framework has been rinsed with diethyl ether.

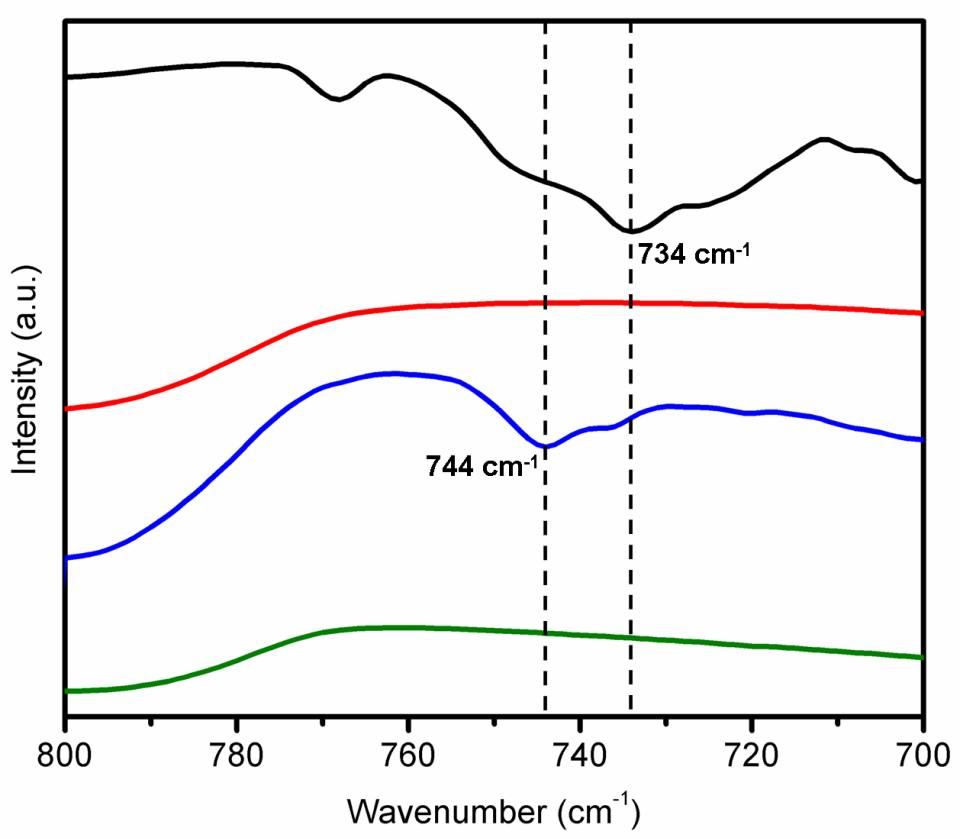

Figure 5.16 FT-IR of dibenzothiophene (black), Ag-DDA-15 prior to fuel exposure (red), after 1 hr in 500 ppm_wS model fuel of dibenzothiophene in decane (blue), and after solvent regeneration using diethyl ether (green). The stretch from unbound dibenzothiophene is marked with a dotted line at 734 cm^{-1} and bound dibenzothiophene at 744 cm^{-1}.

5.4 Conclusions

High surface area silica-zirconia frameworks are very promising materials for the desulfurization of JP-8. Their high capacity coupled with a record in silver efficiency makes them a more affordable option compared to Ag-MSN. Optimization of pore size and zirconia content revealed DDA-15 to be the ideal framework. After loading with 11 wt.% Ag, the material displays a 24-hour saturation adsorption capacity of 39.4 mgS/g and a silver efficiency of 1.21 molS/molAg in real JP-8 under ambient conditions. The material displays the ability to be solvent regenerated at room temperature, which is highly advantageous to thermal regeneration processes and in avoiding silver oxidation, which would lower the overall adsorption capacity. Further testing reveals the capability of the material for both S-M binding and π-complexation. This material is a significant advancement to the realization of onsite desulfurization of JP-8 with cost-effective adsorbents.

5.5 References

1. Dai, W.; Hu, J.; Zhou, L.; Li, S.; Hu, X.; Huang, H., Removal of Dibenzothiophene with Composite Adsorbent MOF-5/Cu(I). *Energy & Fuels* **2013,** 27, (2), 816-821.

2. Khan, N. A.; Jhung, S. H., Low-temperature loading of Cu+ species over porous metal-organic frameworks (MOFs) and adsorptive desulfurization with Cu+-loaded MOFs. *Journal of Hazardous Materials* **2012,** 237-238, 180-185.

3. Israelachvili, J. N., *Intermolecular and Surface Forces*. 3 ed.; Elsevier Science: 2011.

4. Goyal, P. S.; Dasannacharya, B. A.; Kelkar, V. K.; Manohar, C.; Srinivasa Rao, K.; Valaulikar, B. S., Shapes and sizes of micelles in CTAB solutions. *Physica B: Condensed Matter* **1991,** 174, (1-4), 196-199.

5. Lin, Z.; Cai, J. J.; Scriven, L. E.; Davis, H. T., Spherical-to-Wormlike Micelle Transition in CTAB Solutions. *The Journal of Physical Chemistry* **1994,** 98, (23), 5984-5993.

6. Carreon, M. A.; Guliants, V. V., Mesostructured vanadium-phosphorus-oxide phases. *Microporous and Mesoporous Materials* **2002,** 55, (3), 297-304.

7. Vinogradov, V. V.; Agafonov, A. V.; Vinogradov, A. V., Sol-gel synthesis of nanostructured materials based on aluminum oxide with preset texture properties. *Protection of Metals and Physical Chemistry of Surfaces* **2010,** 46, (5), 582-586.

8. Macquarrie, D. J.; Gilbert, B. C.; Gilbey, L. J.; Caragheorgheopol, A.; Savonea, F.; Jackson, D. B.; Onida, B.; Garrone, E.; Luque, R., Structured mesoporous organosilicas from an acetonitrile-water template system. *Journal of Materials Chemistry* **2005,** 15, (35-36), 3946-3951.

9. Prado, A. G. S.; Airoldi, C., Different neutral surfactant template extraction routes for synthetic hexagonal mesoporous silicas. *Journal of Materials Chemistry* **2002,** 12, (12), 3823-3826.

10. Yoshitake, H.; Sugihara, T.; Tatsumi, T., Preparation of Wormhole-like Mesoporous TiO2 with an Extremely Large Surface Area and Stabilization of Its Surface by Chemical Vapor Deposition. *Chemistry of Materials* **2002,** 14, (3), 1023-1029.

11. Wang, Y.; Caruso, F., Mesoporous Silica Spheres as Supports for Enzyme Immobilization and Encapsulation. *Chemistry of Materials* **2005,** 17, (5), 953-961.

12. Kumar, D.; Schumacher, K.; du Fresne von Hohenesche, C.; Grun, M.; Unger, K. K., MCM-41, MCM-48 and related mesoporous adsorbents: their synthesis and characterisation. *Colloids and Surfaces A: Physicochemical and Engineering Aspects* **2001,** 187-188, 109-116.

13. Tuel, A.; Gontier, S., Synthesis and Characterization of Trivalent Metal Containing Mesoporous Silicas Obtained by a Neutral Templating Route. *Chemistry of Materials* **1996,** 8, (1), 114-122.

14. J. Jones, D.; Jimenez-Jimenez, J.; Jimenez-Lopez, A.; Maireles-Torres, P.; Olivera-Pastor, P.; Rodriguez-Castellon, E.; Roziere, J., Surface characterisation of zirconium-doped mesoporous silica. *Chemical Communications* **1997**, (5), 431-432.

15. Gontier, S.; Tuel, A., Synthesis and characterization of Ti-containing mesoporous silicas. *Zeolites* **1995,** 15, (7), 601-610.

16. Kwon, J.-M.; Moon, J.-H.; Bae, Y.-S.; Lee, D.-G.; Sohn, H.-C.; Lee, C.-H., Adsorptive Desulfurization and Denitrogenation of Refinery Fuels Using Mesoporous Silica Adsorbents. *ChemSusChem* **2008,** 1, (4), 307-309.

17. Kumar, S.; Srivastava, V. C.; Badoni, R. P., Studies on adsorptive desulfurization by zirconia based adsorbents. *Fuel* **2011,** 90, (11), 3209-3216.

18. Baeza, P.; Aguila, G.; Gracia, F.; Araya, P., Desulfurization by adsorption with copper supported on zirconia. *Catalysis Communications* **2008,** 9, (5), 751-755.

19. Wang, B.; Zhu, J.; Ma, H., Desulfurization from thiophene by SO42/ZrO2 catalytic oxidation at room temperature and atmospheric pressure. *Journal of Hazardous Materials* **2009,** 164, (1), 256-264.

20. Larrubia, M. A.; Gutièrrez-Alejandreb, A. d.; Ramìrez, J.; Busca, G., A FT-IR study of the adsorption of indole, carbazole, benzothiophene, dibenzothiophene and 4,6-dibenzothiophene over solid adsorbents and catalysts. *Applied Catalysis A: General* **2002,** 224, (1-2), 167-178.

21. Tuel, A.; Gontier, S.; Teissier, R., Zirconium containing mesoporous silicas: new catalysts for oxidation reactions in the liquid phase. *Chemical Communications* **1996**, (5), 651-652.

22. Buchel, G.; Grun, M.; Unger, K. K.; Matsumoto, A.; Kazuo, T., Tailored syntheses of nanostructured silicas: Control of particle morphology, particle size and pore size. *Supramolecular Science* **1998,** 5, (3-4), 253-259.

23. Overbury, S. H.; Ortiz-Soto, L.; Zhu, H.; Lee, B.; Amiridis, M.; Dai, S., Comparison of Au Catalysts Supported on Mesoporous Titania and Silica:

Investigation of Au Particle Size Effects and Metal-Support Interactions. *Catalysis Letters* **2004,** 95, (3-4), 99-106.

24. Shimizu, K.-i.; Satsuma, A., Selective catalytic reduction of NO over supported silver catalysts-practical and mechanistic aspects. *Physical Chemistry Chemical Physics* **2006,** 8, (23), 2677-2695.

25. Yin, A.; Wen, C.; Dai, W.-L.; Fan, K., Ag/MCM-41 as a highly efficient mesostructured catalyst for the chemoselective synthesis of methyl glycolate and ethylene glycol. *Applied Catalysis B: Environmental* **2011,** 108-109, (0), 90-99.

26. Nair, S.; Tatarchuk, B. J., Supported silver adsorbents for selective removal of sulfur species from hydrocarbon fuels. *Fuel* **2010,** 89, (11), 3218-3225.

27. Shahadat Hussain, A. H. M.; Tatarchuk, B. J., Mechanism of hydrocarbon fuel desulfurization using Ag/TiO2-Al2O3 adsorbent. *Fuel Processing Technology* **2014,** 126, (0), 233-242.

28. Nair, S.; Shahadat Hussain, A. H. M.; Tatarchuk, B. J., The role of surface acidity in adsorption of aromatic sulfur heterocycles from fuels. *Fuel* **2013,** 105, 695-704.

29. Xu, X.; Zhang, S.; Li, P.; Shen, Y., Desulfurization of Jet-A fuel in a fixed-bed reactor at room temperature and ambient pressure using a novel selective adsorbent. *Fuel* **2014,** 117, Part A, 499-508.

30. Shen, Y.; Li, P.; Xu, X.; Liu, H., Selective adsorption for removing sulfur: a potential ultra-deep desulfurization approach of jet fuels. *RSC Advances* **2012,** 2, (5), 1700-1711.

31. Xiao, J.; Li, Z.; Liu, B.; Xia, Q.; Yu, M., Adsorption of Benzothiophene and Dibenzothiophene on Ion-Impregnated Activated Carbons and Ion-Exchanged Y Zeolites. *Energy & Fuels* **2008,** 22, (6), 3858-3863.

32. Fallah, R. N.; Azizian, S., Rapid and facile desulphurization of liquid fuel by carbon nanoparticles dispersed in aqueous phase. *Fuel* **2012,** 95, 93-96.

33. Tang, H.; Li, W.; Zhang, T.; Li, Q.; Xing, J.; Liu, H., Improvement in diesel desulfurization capacity by equilibrium isotherms analysis. *Separation and Purification Technology* **2011,** 78, (3), 352-356.

34. Palomino, J. M.; Tran, D. T.; Hauser, J. L.; Dong, H.; Oliver, S., Mesoporous Silica Nanoparticles for High Capacity Adsorptive Desulfurization. *Journal of Materials Chemistry A* **2014**, Accepted Manuscript.

35. Ke, T.; Xin, H., Deep Desulfurization of Model Gasoline by Adsorption on Mesoporous CeMCM-41. *Petroleum Science and Technology* **2010,** 28, (6), 573-581.

36. Lu, H.; Deng, C.; Ren, W.; Yang, X., Oxidative desulfurization of model diesel using [(C4H9)4N]6Mo7O24 as a catalyst in ionic liquids. *Fuel Processing Technology* **2014,** 119, 87-91.

37. Bu, J.; Loh, G.; Gwie, C. G.; Dewiyanti, S.; Tasrif, M.; Borgna, A., Desulfurization of diesel fuels by selective adsorption on activated carbons: Competitive adsorption of polycyclic aromatic sulfur heterocycles and polycyclic aromatic hydrocarbons. *Chemical Engineering Journal* **2011,** 166, (1), 207-217.

38. Shang, H.; Liu, C.; Wei, F., FT-IR Study of Carbon Nanotube Supported Co-Mo Catalysts. *Journal of Natural Gas Chemistry* **2004,** 13, 95-100.

1Chapter 6

Conclusions and Future Work

6.1 Conclusions

The work described in this thesis represents a significant advance in the field of adsorptive desulfurization and the synthesis of mesoporous materials. These novel sorbents display a record performance for desulfurization of JP-8 and a regenerability higher than those of other reported materials.

We report the first synthesis of hierarchical mesoporous monoliths containing Zeolite Y and Al-SBA-15. While neither of these monoliths showed record performance, the creation of these monoliths was novel and an advance in and of itself. Overall, this work revealed that hierarchical monoliths do not pose an advantage over the bulk mesoporous material, resulting in the focus of this research to center on bulk powders.

Al-SBA-15, SBA-15, and ligand functionalized SBA-15 were all successfully synthesized. Extensive testing of different metals loading into with these frameworks revealed the following trend in adsorption capacity:

$$Ag^{+} > Ce^{3+} > Ni^{2+}$$

Silver consistently showed much better capacities than cerium and nickel, resulting in all further tests focusing on silver loading. These metal ions were loaded into the

frameworks under different procedures. A comparison of loading procedure of (Al)-SBA-15 was as follows:

Wet impregnation > Aminopropyl functionalization > Exchange

Silver exchanged Al-SBA-15 only removed 0.74 mgS/g after 30 minutes in model fuel, but performing the silver exchange at 70^{o}C increased this to 3.99 mgS/g. However, after the 70^{o}C exchange, if the material was treated at 550^{o}C for 8 hours in air (likely converting silver ions to silver oxide), the capacity decreased to 3.72 mgS/g. By decorating the surface of SBA-15 with aminopropyl groups, the 30-minute adsorption capacity was further increased to 4.70 mgS/g, following a 70^{o}C exchange with silver. However, wet impregnating Al-SBA-15 with 18 wt.% Ag nearly doubled the model fuel results of the ligand functionalized SBA-15.

These results allowed us to focus our further research on silver loaded materials and to exclusively use wet impregnation as our loading procedure. Overall, 18 wt.% Ag-Al-SBA-15 and Ag-SBA-15 were found to be highly promising as a desulfurization sorbent for JP-8, with 24-hour adsorption capacities of 31.47 mgS/g and 36.31 mgS/g, respectively. Ag-Al-SBA-15 is capable of reaching 20 ppm_wS levels and with a high silver efficiency of 0.57 molS/molAg. This material outperformed existing published sorbents in terms of overall adsorption capacity. However, it was not capable of achieving a sub 1 ppm_wS level. While SBA-15 and Al-SBA-15 are promising materials for the desulfurization of jet fuel, their pore size is larger than that required to accommodate the contaminants of JP-8. As such, MCM-41 with its smaller pore size and higher surface area was investigated.

Three forms of MCM-41 were explored: pure silica MCM-41, aluminated MCM-41 (Al-MCM-41), and MCM-41 nanoparticles (MSN). Al-MCM-41 and MSN were synthesized by our lab, while commercial MCM-41 was used. Ag-MSN was found to be the most effective form of MCM-41 for the desulfurization of JP-8. Ag-MSN displays a 24-hour adsorption capacity of 32.6 mgS/g, which is a 3-fold increase over previously published materials. Ag-MCM-41 displays a 24-hour capacity of 25.4 mgS/g, a 2-fold increase over previously published materials. Ag-MSN also has a record breakthrough capacity at 10 ppm_wS of 0.98 mgS/g for JP-8, while Ag-Al-MCM-41 and Ag-MCM-41 display 0.39 mgS/g and 0.21 mgS/g, respectively. However, Ag-Al-MCM-41 was found to be highly inconsistent between batches, displaying low reproducibility of regeneration experiments compared to MCM-41. The model fuel regenerability of Ag-MSN is ~ 70%, which is much higher than other reports of Ag-MCM-41. Mechanism studies using FT-IR and model fuel tests support an S-M binding as the mode of adsorption, while π-complexation likely also occurs.

In an effort to explore more novel frameworks and those with a more active surface chemistry, a series of mesoporous silica-zirconia frameworks were synthesized. Three different chain lengths of primary alkylamines were explored as templating agents to vary the pore size. The Si:Zr ratio was also explored, looking at ratios ranging from ∞ to 11:1. This optimization of pore size and zirconia content revealed DDA-15, synthesized with a gel Si:Zr molar ratio of 15:1 and using

dodecylamine as the templating agent, to be the ideal framework. The high capacity of DDA-15 coupled with a record in silver efficiency makes it a more affordable option compared to Ag-MSN. After loading with 11 wt.% Ag, the material displays a 24-hour saturation adsorption capacity of 39.4 mgS/g and a silver efficiency of 1.21 molS/molAg in real JP-8 under ambient conditions. Ag-MSN tested with the same batch of JP-8 removed 47.1 mgS/g, but it uses nearly twice the amount of sulfur. DDA-15 displays the ability to be solvent regenerated at room temperature using model fuel studies. Furthermore, FT-IR testing reveals the capability of the material for both S-M binding and π-complexation. This material is a significant advance to the realization of onsite desulfurization of JP-8 with low-cost effective adsorbents.

6.2 Future Work

While the adsorption capacity of both the MCM-41 derivatives and the silica-zirconia materials is impressive, the regenerability of these materials needs improvement. Ideally, no loss in capacity should be observed over numerous cycles. With these current materials, the interactions between the framework and the silver are too weak to prevent silver loss. An ideal way to prevent this would be to better anchor the silver sites to the framework.

Anchoring was briefly investigated in Chapter 3, where SBA-15 was decorated with aminopropyl groups prior to metal loading. Further testing with various ligands should be explored. In addition to amino terminated ligands, thiol terminated ligands may be even more advantageous in holding the silver

in place. Post-synthetic addition of ligands could easily be performed on the high surface area materials reported in this thesis, including MSN and DDA-SiO_2.

Aside from ligand functionalization, the MSN framework could be further modified. As reported, it is currently a pure silica framework. An aluminosilicate version and other mixed metal oxide versions could be explored. Additionally, before ligand functionalization of MSN, it may be beneficial to synthesize with a slightly larger templating agent, as decorating with ligands will lower the overall pore diameter.

Materials that utilize metal oxides instead of metal ions have also shown favorable regeneration. While these materials do show lower overall adsorption capacities, it may be worth exploring silver oxide and other d- and f-block metal oxides as coatings for the high surface area materials presented in this thesis.

Appendix

Solvothermal Synthesis

Table A1: Sovothermal synthesis conditions and ratios

sample	compound	ratio(n)	F.W.(g/mol)	wt. Used(g)	T ©C	time(hrs)
JSJ3	PbF_2	1.00	245.2	0.57	100	72
	10-Camphorsulfonic acid	2.00	232.3	1.1		
	Perchloric acid	2.50	100.46	0.86		
6/25/2010	H2O	200.00	18.016	8.58		
sample	compound	ratio(n)	F.W.(g/mol)	wt. Used(g)	T ©C	time(hrs)
JSJ5	PbF_2	1.00	245.2	0.5769	125	72
	10-Camphorsulfonic acid	2.00	232.3	1.0931		
	Perchloric acid	2.50	100.46	0.8441		
6/25/2010	H2O	200.00	18.016	8.478		
sample	compound	ratio(n)	F.W.(g/mol)	wt. Used(g)	T ©C	time(hrs)
JSJ7	PbF_2	1.00	245.2	0.58	150	72
	10-Camphorsulfonic acid	2.00	232.3	1.1		
	Perchloric acid	2.50	100.46	0.9		
6/25/2010	H2O	200.00	18.016	8.55		
sample	compound	ratio(n)	F.W.(g/mol)	wt. Used(g)	T ©C	time(hrs)
JSJ9	PbF_2	1.00	245.2	0.78	175	72
	10-Camphorsulfonic acid	2.00	232.3	1.44		
	Perchloric acid	2.50	100.46	0.95		
6/25/2010	H2O	200.00	18.016	8.4		
sample	compound	ratio(n)	F.W.(g/mol)	wt. Used(g)	T ©C	time(hrs)
JSJ11	PbF_2	1.00	245.2	0.51	100	72
	10-Camphorsulfonic acid	4.00	232.3	2.08		
	Perchloric acid	2.50	100.46	0.86		
6/29/2010	H2O	200.00	18.016	7.76		
sample	compound	ratio(n)	F.W.(g/mol)	wt. Used(g)	T ©C	time(hrs)
JSJ13	PbF_2	1.00	245.2	0.6	100	72
	10-Camphorsulfonic acid	2.00	232.3	1.24		
	Perchloric acid	2.50	100.46	0.86		
6/29/2010	H2O	200.00	18.016	8.3		

sample	compound	ratio(n)	F.W.(g/mol)	wt. Used(g)	T ©C	time(hrs)
JSJ15	PbF_2	1.00	245.2	0.66	150	48
	10-Camphorsulfonic acid	2.00	232.3	1.3		
6/29/2010	H2O	200.00	18.016	8.94		

sample	compound	ratio(n)	F.W.(g/mol)	wt. Used(g)	T ©C	time(hrs)
JSJ17	PbF_2	1.00	245.2	0.63	100	48
	10-Camphorsulfonic acid	2.00	232.3	1.16		
7/6/2010	H2O	200.00	18.016	9.07		

sample	compound	ratio(n)	F.W.(g/mol)	wt. Used(g)	T ©C	time(hrs)
JSJ19	PbF_2	1.00	245.2	0.61	125	72
	10-Camphorsulfonic acid	2.00	232.3	1.17		
7/6/2010	H2O	200.00	18.016	9.03		

sample	compound	ratio(n)	F.W.(g/mol)	wt. Used(g)	T ©C	time(hrs)
JSJ21	PbF_2	1.00	245.2	0.3	100	72
	10-Camphorsulfonic acid	4.00	232.3	1.14		
7/6/2010	H2O	400.00	18.016	8.96		

sample	compound	ratio(n)	F.W.(g/mol)	wt. Used(g)	T ©C	time(hrs)
JSJ23	PbF_2	1.00	245.2	0.31	125	72
	10-Camphorsulfonic acid	4.00	232.3	1.16		
7/6/2010	H2O	400.00	18.016	9.19		

sample	compound	ratio(n)	F.W.(g/mol)	wt. Used(g)	T ©C	time(hrs)
JSJ25	$AgNO_3$	1.00	169.87	0.24	100	96
	10-Camphorsulfonic acid	2.00	232.3	0.58		
	4-4'-bipy	1.00	156.19	0.27		
7/9/2010	H2O	400.00	18.016	9.33		

sample	compound	ratio(n)	F.W.(g/mol)	wt. Used(g)	T ©C	time(hrs)
JSJ27	$AgNO_3$	1.00	169.87	0.22	125	168
	10-Camphorsulfonic acid	2.00	232.3	0.56		
	4-4'-bipy	1.00	156.19	0.26		
7/6/2010	H2O	400.00	18.016	8.97		

sample	compound	ratio(n)	F.W.(g/mol)	wt. Used(g)	T ©C	time(hrs)
JSJ29	PbF_2	1.00	245.2	0.63	100	120
	10-Camphorsulfonic acid	2.00	232.3	1.17		
7/6/2010	H2O	200.00	18.016	8.9		
sample	compound	ratio(n)	F.W.(g/mol)	wt. Used(g)	T ©C	time(hrs)
JSJ31	PbF_2	1.00	245.2	0.37	100	96
	10-Camphorsulfonic acid	2.00	232.3	0.59		
7/13/2010	H2O	400.00	18.016	9.22		
sample	compound	ratio(n)	F.W.(g/mol)	wt. Used(g)	T ©C	time(hrs)
JSJ33	PbF_2	1.00	245.2	0.15	100	72
	10-Camphorsulfonic acid	2.00	232.3	0.29		
7/13/2010	H2O	800.00	18.016	9.2		
sample	compound	ratio(n)	F.W.(g/mol)	wt. Used(g)	T ©C	time(hrs)
JSJ35	$AgNO_3$	1.00	169.87	0.26	100	72
	10-Camphorsulfonic acid	2.00	232.3	0.56		
	4-4'-bipy	0.50	156.19	0.14		
7/16/2010	H2O	400.00	18.016	9.32		
sample	compound	ratio(n)	F.W.(g/mol)	wt. Used(g)	T ©C	time(hrs)
JSJ37	$AgNO_3$	1.00	169.87	0.21	100	72
	10-Camphorsulfonic acid	2.50	232.3	0.77		
	4-4'-bipy	0.50	156.19	0.014		
7/16/2010	H2O	400.00	18.016	9.7		
sample	compound	ratio(n)	F.W.(g/mol)	wt. Used(g)	T ©C	time(hrs)
JSJ39	PbF_2	1.00	245.2	0.18	100	72
	10-Camphorsulfonic acid	4.00	232.3	0.58		
7/6/2010	H2O	800.00	18.016	9.28		
sample	compound	ratio(n)	F.W.(g/mol)	wt. Used(g)	T ©C	time(hrs)
JSJ41	PbF_2	1.00	245.2	0.51	100	96
	10-Camphorsulfonic acid	2.00	232.3	0.93		
7/6/2010	H2O	250.00	18.016	9		

sample	compound	ratio(n)	F.W.(g/mol)	wt. Used(g)	T ©C	time(hrs)
JSJ43	PbF_2	1.00	245.2	0.41	100	96
	10-Camphorsulfonic acid	2.00	232.3	0.76		
7/6/2010	H2O	300.00	18.016	8.97		
sample	compound	ratio(n)	F.W.(g/mol)	wt. Used(g)	T ©C	time(hrs)
JSJ45	PbF_2	1.00	245.2	0.35	100	96
	10-Camphorsulfonic acid	3.00	232.3	0.98		
7/6/2010	H2O	400.00	18.016	9.37		
sample	compound	ratio(n)	F.W.(g/mol)	wt. Used(g)	T ©C	time(hrs)
JSJ47	$AgNO_3$	1.50	169.87	0.36	100	72
	10-Camphorsulfonic acid	3.00	232.3	1.04		
	4-4'-bipy	1.00	156.19	0.25		
7/16/2010	H2O	400.00	18.016	9.87		
sample	compound	ratio(n)	F.W.(g/mol)	wt. Used(g)	T ©C	time(hrs)
JSJ49	PbF_2	1.00	245.2	0.4	100	72
	10-Camphorsulfonic acid	2.50	232.3	1.01		
7/6/2010	H2O	300.00	18.016	9.11		
sample	compound	ratio(n)	F.W.(g/mol)	wt. Used(g)	T ©C	time(hrs)
JSJ51	PbF_2	1.00	245.2	0.24	100	96
	10-Camphorsulfonic acid	3.00	232.3	0.71		
7/6/2010	H2O	500.00	18.016	9.05		
sample	compound	ratio(n)	F.W.(g/mol)	wt. Used(g)	T ©C	time(hrs)
JSJ 129	CuBF4	1.52	345.25	0.3618	115	96
	4-4'-bipy	1.34	156.19	0.2094		
8/12/2011	H2O	800.00	18.016	9.96		
sample	compound	ratio(n)	F.W.(g/mol)	wt. Used(g)	T ©C	time(hrs)
JSJ 129i	CuBF4	2.00	345.25	0.472	115	96
	4-4'-bipy	1.34	156.19	0.2025		
8/12/2011	H2O	800.00	18.016	9.998		
sample	compound	ratio(n)	F.W.(g/mol)	wt. Used(g)	T ©C	time(hrs)
JSJ 129ii	CuBF4	1.52	345.25	0.5	100	72
	4-4'-bipy	1.34	156.19	0.25		
8/12/2011	H2O	800.00	18.016	10.5		

sample	compound	ratio(n)	F.W.(g/mol)	wt. Used(g)	T ©C	time(hrs)
JSJ 129iii	CuBF4	1.00	345.25	0.4	100	72
	AgNO3	1.00	169.87	0.25		
	4-4'-bipy	1.00	156.19	0.3		
8/12/2011	H2O	400.00	18.016	10		
sample	compound	ratio(n)	F.W.(g/mol)	wt. Used(g)	T ©C	time(hrs)
JSJ139	$CuNO_3$	1.00	187.56	0.2412	RT	slow evap
	HMT	1.00	140.186	0.188		
	EDSA	1.00	190.2	0.3637		
9/22/2011	H2O	400.00	18.016	25		
sample	compound	ratio(n)	F.W.(g/mol)	wt. Used(g)	T ©C	time(hrs)
JSJ139i	$CuNO_3$	1.00	187.56	0.243	RT	slow evap
	HMT	1.00	140.186	0.1751		
	EDSA salt	1.00	246	0.3309		
9/22/2011	H2O	400.00	18.016	25		
sample	compound	ratio(n)	F.W.(g/mol)	wt. Used(g)	T ©C	time(hrs)
TP3	Copper Acetate	1.00	199.65	0.3743	150	96
6/28/2011	Hexamethylenetetramine	2.00	140.186	0.6892		
	Sodium Nitrate	2.00	84.9947	0.6892		
	H2O	400.00	18.016	8.88814		
sample	compound	ratio(n)	F.W.(g/mol)	wt. Used(g)	T ©C	time(hrs)
TP3i	Copper Acetate	1.00	199.65	0.3743	175	96
6/28/2011	Hexamethylenetetramine	2.00	140.186	0.6892		
	Sodium Nitrate	1.00	84.9947			
	H2O	400.00	18.016	8.88814		
sample	compound	ratio(n)	F.W.(g/mol)	wt. Used(g)	T ©C	time(hrs)
TP5	YbCl6	1.00	387.49	0.1951	150	72
6/29/2011	Hexamethylenetetramine	5.00	140.186	0.3492		
	H2O	1000.00	18.016	9.0628		
sample	compound	ratio(n)	F.W.(g/mol)	wt. Used(g)	T ©C	time(hrs)
TP5i	YbCl6	1.00	387.49	0.1947	150	144
6/29/2011	Hexamethylenetetramine	5.00	140.186	0.3508		
	H2O	1000.00	18.016	9.0188		

sample	compound	ratio(n)	F.W.(g/mol)	wt. Used(g)	T ©C	time(hrs)
TP7	YbCl6	1.00	387.49	0.3876	150	144
6/29/2011	Hexamethylenetetramine	3.00	140.186	0.4191		
	H2O	500.00	18.016	9.0764		
sample	**compound**	**ratio(n)**	**F.W.(g/mol)**	**wt. Used(g)**	**T ©C**	**time(hrs)**
TP9	Copper Acetate	1.00	199.65	0.2793	RT	slow evap
6/29/2011	Hexamethylenetetramine	2.00	140.186	0.3882		
	Sodium Nitrate	2.00	84.9947	0.2354		
	H2O	400.00	18.016	10.0375		
sample	**compound**	**ratio(n)**	**F.W.(g/mol)**	**wt. Used(g)**	**T ©C**	**time(hrs)**
TP9i	Copper Acetate	1.00	199.65	0.2784	RT	slow evap
6/29/2011	Hexamethylenetetramine	2.00	140.186	0.4016		
	EDSA Salt	2.00	234.16	0.6554		
	H2O	400.00	18.016	9.848		
sample	**compound**	**ratio(n)**	**F.W.(g/mol)**	**wt. Used(g)**	**T ©C**	**time(hrs)**
TP11	YbCl6	1.00	387.49	0.3901	RT	slow evap
6/30/2011	Hexamethylenetetramine	5.00	140.186	0.7012		
	H2O	500.00	18.016	8.9921		
sample	**compound**	**ratio(n)**	**F.W.(g/mol)**	**wt. Used(g)**	**T ©C**	**time(hrs)**
TP15	YbCl6	1.00	387.49	0.1142	150	120
6/30/2011	Hexamethylenetetramine	2.00	140.186	0.1563		
	EDSA Salt	2.00	234.16	0.2593		
	H2O	1000.00	18.016	10.0527		
sample	**compound**	**ratio(n)**	**F.W.(g/mol)**	**wt. Used(g)**	**T ©C**	**time(hrs)**
TP15i	YbCl6	1.00	387.49	0.1165	RT	slow evap
6/30/2011	Hexamethylenetetramine	2.00	140.186	0.2591		
	EDSA Salt	2.00	234.16	0.2657		
	H2O	1000.00	18.016	9.9962		
sample	**compound**	**ratio(n)**	**F.W.(g/mol)**	**wt. Used(g)**	**T ©C**	**time(hrs)**
TP21	Copper Acetate	1.00	199.65	0.2748	125	120
7/6/2011	Hexamethylenetetramine	2.00	140.186	0.392		
	Sodium Nitrate	2.00	84.9947	0.2393		
	H2O	400.00	18.016	9.9906		

sample	compound	ratio(n)	F.W.(g/mol)	wt. Used(g)	T ©C	time(hrs)
TP21i	Copper Acetate	1.00	199.65	0.2758	125	120
7/6/2011	Hexamethylenetetramine	2.00	140.186	0.3891		
	EDSA Salt	2.00	234.16	0.6487		
	H2O	400.00	18.016	10.023		
sample	**compound**	**ratio(n)**	**F.W.(g/mol)**	**wt. Used(g)**	**T ©C**	**time(hrs)**
TP23	YbCl6	1.00	387.49	0.1268	150	96
7/7/2011	Hexamethylenetetramine	5.00	140.186	0.2331		
	H2O	1500.00	18.016	9.0289		
sample	**compound**	**ratio(n)**	**F.W.(g/mol)**	**wt. Used(g)**	**T ©C**	**time(hrs)**
TP23i	YbCl6	1.00	387.49	0.1301	150	96
7/7/2011	Hexamethylenetetramine	4.00	140.186	0.1847		
	H2O	1500.00	18.016	8.9883		
sample	**compound**	**ratio(n)**	**F.W.(g/mol)**	**wt. Used(g)**	**T ©C**	**time(hrs)**
TP25	YbCl6	1.00	387.49	0.0559	150	96
7/7/2011	Hexamethylenetetramine	2.00	140.186	0.0786		
	EDSA Salt	2.00	234.16	0.1309		
	H2O	2000.00	18.016	10.0122		
sample	**compound**	**ratio(n)**	**F.W.(g/mol)**	**wt. Used(g)**	**T ©C**	**time(hrs)**
TP27	Silver Nitrate	0.00029	169.87	0.0579	RT	slow evap
7/13/2011	Hexamethylenetetramine	0.00029	140.186	0.0415		
	Dichloromethane (Ch2Cl2)	0.04698	84.93	3.99		
	Ethanol	0.08563	46.07	3.99		
sample	**compound**	**ratio(n)**	**F.W.(g/mol)**	**wt. Used(g)**	**T ©C**	**time(hrs)**
TP29	ErNO3	1.00	353.27	0.25	125	96
7/14/2011	Urea	17.00	60.06	0.5716		
	H2O	800.00	18.016	8.013		
sample	**compound**	**ratio(n)**	**F.W.(g/mol)**	**wt. Used(g)**	**T ©C**	**time(hrs)**
TP29i	ErNO3	1.00	353.27	0.5748	125	96
7/14/2011	Urea	17.00	60.06	0.2574		
	H2O	800.00	18.016	8.046		

sample	compound	ratio(n)	F.W.(g/mol)	wt. Used(g)	T ©C	time(hrs)
TP31	ErNO3	1.00	353.27	0.2522	150	96
7/14/2011	Urea	17.00	60.06	0.5798		
	H2O	800.00	18.016	8.0276		
sample	**compound**	**ratio(n)**	**F.W.(g/mol)**	**wt. Used(g)**	**T ©C**	**time(hrs)**
TP31i	ErNO3	1.00	353.27	0.2498	150	96
7/14/2011	Urea	17.00	60.06	0.5698		
	H2O	800.00	18.016	8.0694		
sample	**compound**	**ratio(n)**	**F.W.(g/mol)**	**wt. Used(g)**	**T ©C**	**time(hrs)**
TP33	Copper Acetate	0.00029	199.65	0.061	RT	slow evap
7/15/2011	Hexamethylenetetramine	0.00029	140.186	0.0571		
	Ethanol	0.08563	46.07	3.9603		
	Dichloromethane (Ch2Cl2)	0.04698	84.93	4.0277		
sample	**compound**	**ratio(n)**	**F.W.(g/mol)**	**wt. Used(g)**	**T ©C**	**time(hrs)**
TP33i	Copper Acetate	0.00029	199.65	0.0577	RT	slow evap
7/15/2011	Hexamethylenetetramine	0.00029	140.186	0.0430		
	Sodium Sulfite	0.00029	126.043	0.0404		
	Ethanol	0.08563	46.07	3.9428		
	Dichloromethane (Ch2Cl2)	0.04698	84.93	4.0420		
sample	**compound**	**ratio(n)**	**F.W.(g/mol)**	**wt. Used(g)**	**T ©C**	**time(hrs)**
TP35	Copper Nitrate	0.00029	232.59	0.0708	RT	slow evap
7/15/2011	Hexamethylenetetramine	0.00029	140.186	0.0410		
	Ethanol	0.08563	46.07	3.9615		
	Dichloromethane (Ch2Cl2)	0.04698	84.93	4.0239		
sample	**compound**	**ratio(n)**	**F.W.(g/mol)**	**wt. Used(g)**	**T ©C**	**time(hrs)**
TP37	ErCl3	2.50	273.64	0.1422	175	168
7/20/2011	EDSA	1.00	190.20	0.418		
	TEA	1.55	101.19			
	H2O	2570.00	18.016	10.0547		

sample	compound	ratio(n)	F.W.(g/mol)	wt. Used(g)	T ©C	time(hrs)
TP37i	ErCl3	2.50	273.64	0.1418	175	168
7/20/2011	EDSA	1.00	190.2	0.0465		
	TEA	1.55	101.19			
	H2O	2570.00	18.016	10.0752		
sample	**compound**	**ratio(n)**	**F.W.(g/mol)**	**wt. Used(g)**	**T ©C**	**time(hrs)**
TP39	ErCl3	2.50	273.64	0.1444	200	144
7/20/2011	EDSA	1.00	190.2	0.041		
	TEA	1.55	101.19			
	H2O	2570.00	18.016	10.0525		
sample	**compound**	**ratio(n)**	**F.W.(g/mol)**	**wt. Used(g)**	**T ©C**	**time(hrs)**
TP41	Gadolinium(III) Nitrate	2.50	451.36	0.2448	175	168
7/22/2011	EDSA	1.00	190.2	0.0458		
	TEA	1.55	101.19			
	H2O	2570.00	18.016	10.1944		
sample	**compound**	**ratio(n)**	**F.W.(g/mol)**	**wt. Used(g)**	**T ©C**	**time(hrs)**
TP43	Lanthanum(III) Nitrate	2.50	433.01	0.2479	175	168
7/22/2011	EDSA	1.00	190.2	0.0421		
	TEA	1.55	101.19			
	H2O	2570.00	18.016	9.9990		
sample	**compound**	**ratio(n)**	**F.W.(g/mol)**	**wt. Used(g)**	**T ©C**	**time(hrs)**
TP45	Neodymium(III) Nitrate	2.50	438.35	0.2479	175	168
7/22/2011	EDSA	1.00	190.2	0.0430		
	TEA	1.55	101.19			
	H2O	2570.00	18.016	10.0042		
sample	**compound**	**ratio(n)**	**F.W.(g/mol)**	**wt. Used(g)**	**T ©C**	**time(hrs)**
TP47	Gadolinium Flouride	2.50	214.25	0.1169	175	168
7/22/2011	EDSA	1.00	190.2	0.0419		
	TEA	1.55	101.19			
	H2O	2570.00	18.016	9.9976		
sample	**compound**	**ratio(n)**	**F.W.(g/mol)**	**wt. Used(g)**	**T ©C**	**time(hrs)**
TP49	Copper tetrafluoroborate	0.00029	345.25	0.1000	RT	slow evap
7/25/2011	Hexamethylenetetramine	0.00029	140.186	0.0406		
	Ethanol	0.08563	46.07	3.9500		
	Dichloromethane (Ch2Cl2)	0.04698	84.93	3.9900		

sample	compound	ratio(n)	F.W.(g/mol)	wt. Used(g)	T ©C	time(hrs)
TP51	Copper tetrafluoroborate	1.35	345.25	0.48	175	96
7/27/2011	4,4'-bipyridine	1.34	156.19	0.2154		
	H2O	550.00	18.016	10.22		
sample	**compound**	**ratio(n)**	**F.W.(g/mol)**	**wt. Used(g)**	**T ©C**	**time(hrs)**
TP53	Copper Acetate	1.35	199.65	0.271	100	72
7/29/2011	Hexamethylenetetramine	1.34	140.186	0.1892		
	EDSA Hydrate	1.52	208.21	0.3356		
	H2O	550.00	18.016	10.0432		
sample	**compound**	**ratio(n)**	**F.W.(g/mol)**	**wt. Used(g)**	**T ©C**	**time(hrs)**
TP53i	Copper Acetate	1.35	199.65	0.271	RT	slow evap
7/29/2011	Hexamethylenetetramine	1.34	140.186	0.1898		
	EDSA Hydrate	1.52	208.21	0.3233		
	H2O	550.00	18.016	9.999		
sample	**compound**	**ratio(n)**	**F.W.(g/mol)**	**wt. Used(g)**	**T ©C**	**time(hrs)**
TP55	Copper Acetate	1.35	199.65	0.2715	100	72
7/29/2011	Hexamethylenetetramine	0.67	140.186	0.0946		
	EDSA Hydrate	1.52	208.21	0.3253		
	H2O	550.00	18.016	9.9952		
sample	**compound**	**ratio(n)**	**F.W.(g/mol)**	**wt. Used(g)**	**T ©C**	**time(hrs)**
TP55i	Copper Acetate	1.35	199.65	0.2708	RT	slow evap
7/29/2011	Hexamethylenetetramine	0.67	140.186	0.0952		
	EDSA Hydrate	1.52	208.21	0.3206		
	H2O	550.00	18.016	10.0768		

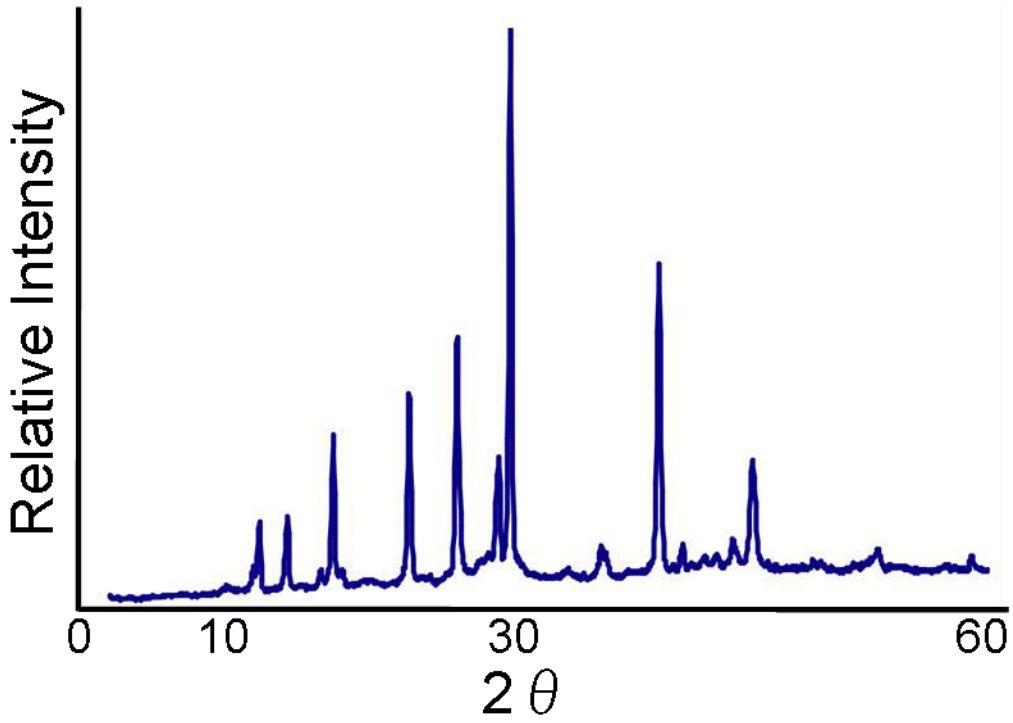

Figure A1. JSJ129 PXRD showed a new pattern but too small of crystals for structure solution.

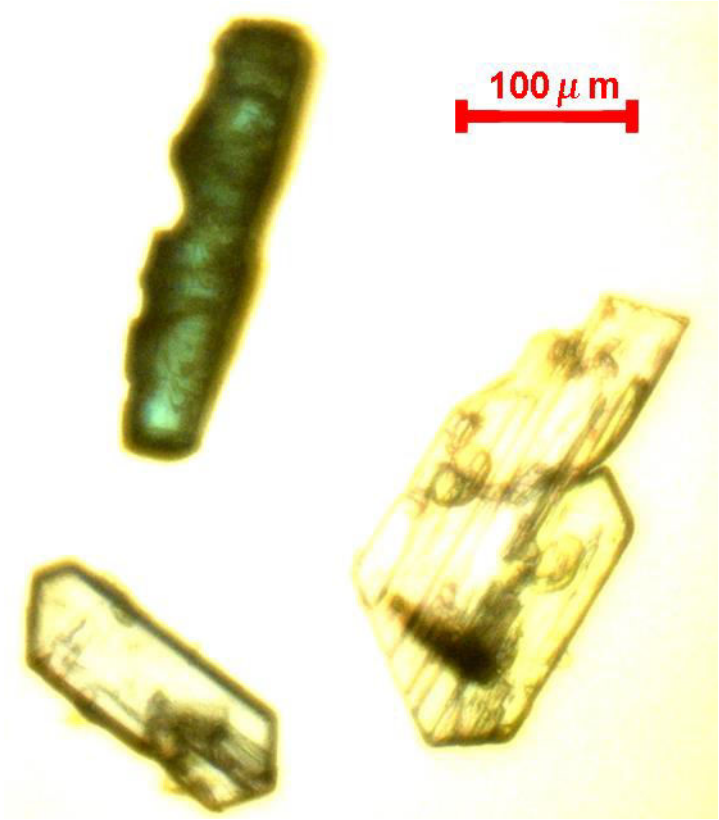

Figure A2. JSJ129 optical micrograph showing pale yellow/colorless crystals and dark blue/green crystal.

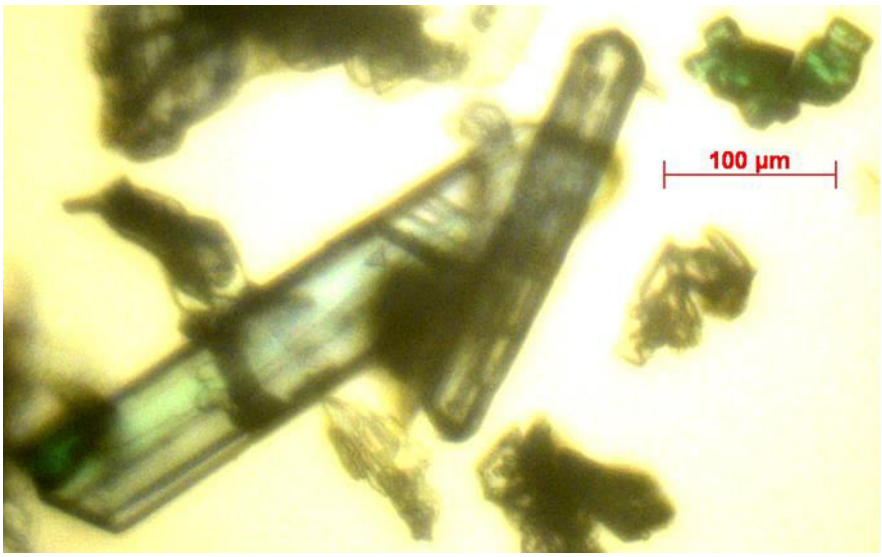

Figure A3. JSJ129 optical micrograph, second view to show light blue crystals.

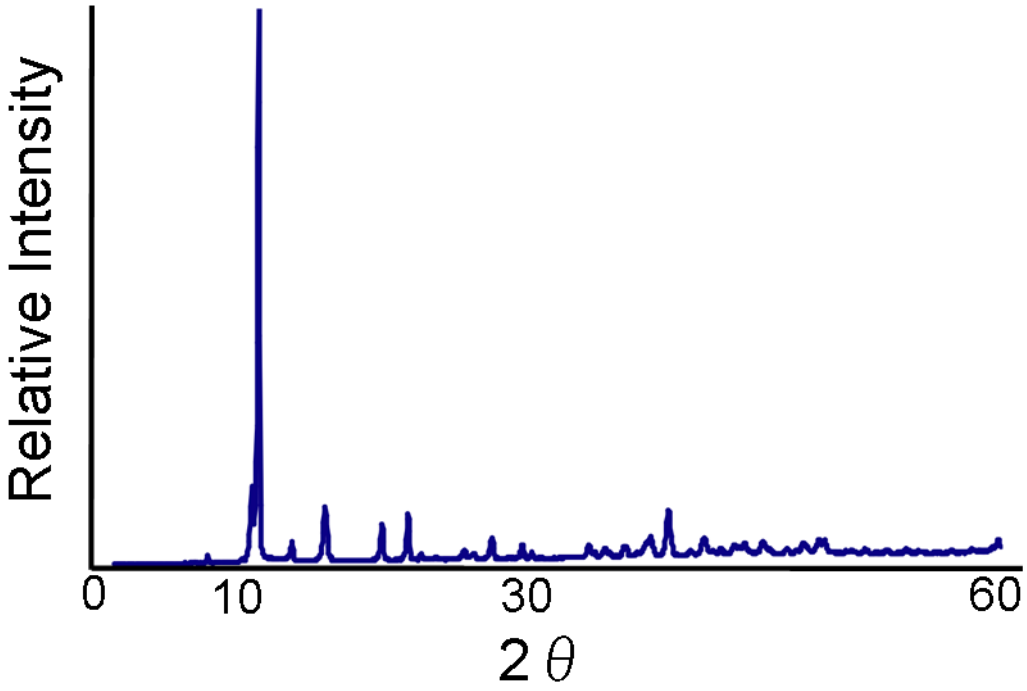

Figure A4. TP53i PXRD showed a new pattern but too small of crystals for structure solution.

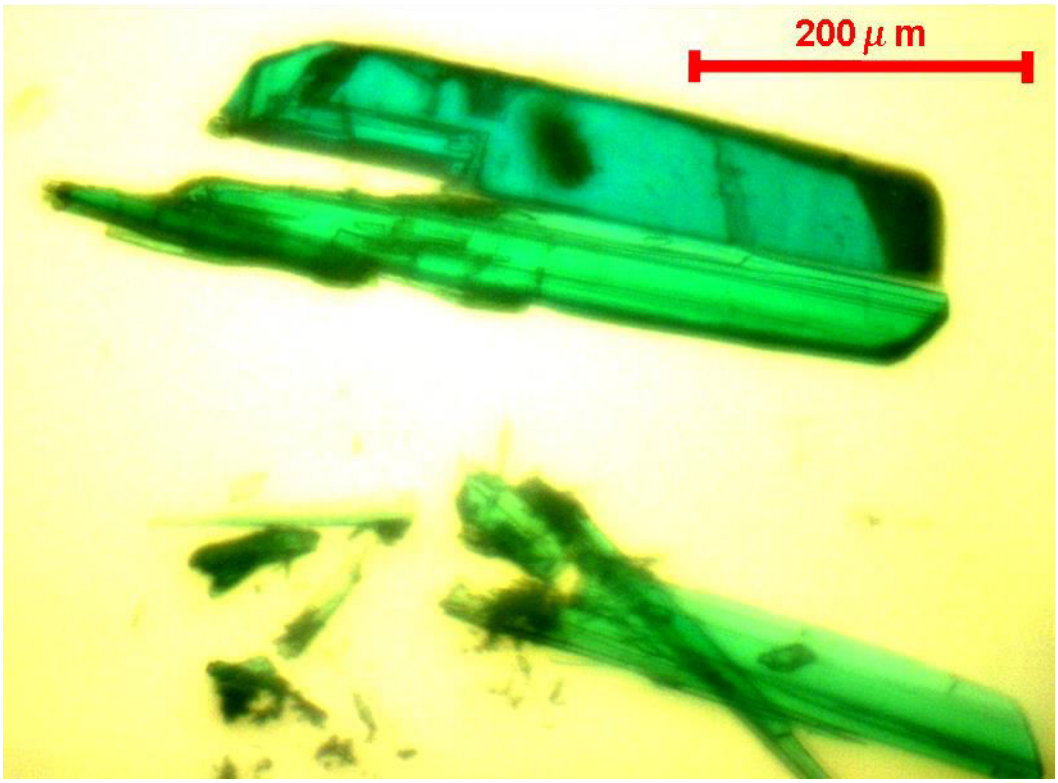

Figure A5. TP53i optical micrograph.